TREATMENT AND MODELING OF EPSTEIN-BARR VIRUS POST-TRANSPLANT LYMPHOPROLIFERATIVE DISORDER

TAN WEI JIAN
(*B.Sc. (Hons.), Nanyang Technological University*)

A THESIS SUBMITTED

FOR THE DEGREE OF DOCTOR OF PHILOSOPHY
DEPARTMENT OF MICROBIOLOGY AND IMMUNOLOGY
NATIONAL UNIVERSITY OF SINGAPORE

2016

DECLARATION

I hereby declare that this thesis is my original work and it has been written by me in its entirety. I duly acknowledged all the sources of information which have been used in the thesis.

This thesis has also not been submitted for any degree in any university previously.

_____

Tan Wei Jian
13 July 2016

Acknowledgements

I would like to express my heartfelt gratitude to my advisor Associate Professor Paul MacAry (Immunology Program, National University of Singapore) for his supervision in the past five years. I would also like to thank Paul for his understanding during the period when I am facing difficulties and his generosity in providing me employment as a research assistant so that I can complete my PhD. On a side note, it has been inspiring and encouraging to see Paul present during seminars; there was always something that I could benefit from these talks. I would also like to thank Professor Jianzhu Chen (Department of Biology, Massachusetts Institute of Technology) for his insightful thoughts, critical thinking, and scientific professionalism. Although I have not had the chance to work in Professor Chen's lab at MIT, the weekly video conferences, and individual Skype meetings have not only expanded my horizon across different research topics but also made me feel part of the whole collaborative effort. I would also like to thank my collaborators Emeritus Professor Soh Ha Chan (Department of Microbiology and Immunology, National University of Singapore) for providing cell lines and Dr. Brendon Hanson (Defense Science Organization, Singapore) for generating the antibody variant. To my mentor, Dr. Min Zin Oo, who imparted numerous experimental techniques required for EBV research. His helpful and humble attributes are characteristics that I have so much to learn from. To my ex-colleague at Singapore-MIT Alliance for Research and Technology,

Assistant Professor Qingfeng Chen (Institute of Molecular and Cell Biology, A* STAR), who provided precious human samples and motivation as a young and outstanding researcher. To labmate Ms. Sherlynn Chan, who had provided moral support in the juvenile years of my PhD. To labmate Ms. Junyun Lai, who not only assisted me experimentally, her enthusiasm at work provided me motivation, keeping me on pace. I am also very thankful to Ms. Lai for all the pleasant working experiences, constructive discussions and the synergisms we had when initiating a new project together. To my friends Ms. Lai Junyun and Ms. Joanna Choo who are my lunch and coffee partners, for bringing me fun and laughter after working hours. Compliments also go to Ms. Loo Hooi Linn and Ms. Fatimah Bte Mustafa for all the procurement processes and keeping the lab in order. To the very competent veterinary technician, Ms. Lan Xiang Wong, for her help with the mouse husbandry and the maintenance of the animal unit. I would like to thank all my family members for their support, especially to my parents for all their unwavering care and concern. Last but not least, to my wife Cheryl, who has always been there for me for the past 12 years. I would like to thank my wife for constantly accommodating to my schedule, her patience and understanding of the nature of my studies.

List of Poster Presentations

Yearly Singapore-MIT Alliance for Research and Technology symposium (2012-2015), Singapore

16th International Symposium on EBV and Associated Diseases (2014), Australia

Keystone Symposia: Cancer Immunotherapy - Immunity and Immunosuppression Meet Targeted Therapies (2016), Canada

List of Publications

Fenggang Yu, **Wei Jian Tan**, Yanan Lu, Paul A. MacAry and Thomas Loh. **The other side of the coin: Leveraging Epstein-Barr virus in research and therapy.** Oral Oncol. 2016 Sep;60:112-7. doi: 10.1016

Junyun Lai***, Wei Jian Tan***, Chien Tei Too, Joanna Ai Ling Choo, Lan Hiong Wong, Fatimah Bte Mustafa, Nalini Srinivasan, Angeline Pei Chiew Lim, Youjia Zhong, Nicholas R. J. Gascoigne, Brendon J. Hanson, Soh Ha Chan, Jianzhu Chen and Paul A. MacAry. **Targeting Epstein-Barr virus transformed B lymphoblastoid cells using antibodies with T cell receptor-like specificities.** Blood. 2016 Sep; 128(10):1396-40. doi: 10.1182 ***Co-first author**

Qingfeng Chen, Weijian Ye, **Wei Jian Tan**, Kylie Su Mei Yong, Min Liu, Shu Qi Tan, Eva Loh, Kenneth TE Chang, Thiam Chye Tan, Peter R Preiser & Jianzhu Chen. **Delineation of Natural Killer Cell Differentiation from Myeloid Progenitors in Human**. Sci Rep, 2015 Oct;5:15118. doi: 10.1038

Min Zin Oo*, **Wei Jian Tan***, Maroun Khoury, Jerry Chan, Jianzhu Chen and Paul A. MacAry. **Defining a causal role for Epstein-Barr virus in post-transplant lymphoproliferative disease and malignancy**. (Manuscript in preparation) ***Co-first author**

Table of Contents

Chapter 2: Materials and Methods

Chapter 3: Result (I)

Chapter 4: Result (II)

Chapter 5: Result (III)

Chapter 6: Discussion and Future Perspectives

Appendix

References

Summary

Epstein-Barr virus (EBV) is the etiological agent of infectious mononucleosis and is associated with various diseases such as Burkitt's lymphoma, nasopharyngeal carcinoma, and post-transplant lymphoproliferative disorder (PTLD). In all of these diseases, the expression of Epstein-Barr virus nuclear antigen 1 (EBNA-1) is common and therefore this viral protein represents a possible therapeutic target. Previous studies have intimated that EBNA-1 auto-inhibits its presentation to the immune system via the expression of a glycine-alanine rich domain that blocks proteasomal degradation. Thus to understand the expression of EBNA-1 and to evaluate the potential of targeting this viral antigen in the context of PTLD, we examined the role of glycine-alanine repeats (GAr) in EBNA-1 protein expression and further investigated the *in vivo* efficacy of an in-house produced α-EBNA-1 T cell receptor-like monoclonal antibody (α-EBNA-1 TCR-like mAb) using a mouse xenograft model of PTLD. With the aim of translating our findings into studies relevant to humans, we developed and optimized an autologous humanized mouse model for future preclinical evaluations of the antibody.

Here, we confirmed previously published data that the GAr within the EBNA-1 protein can indeed inhibit its synthesis, reducing its availability for presentation on MHC class I molecules. Despite this observation,

we were able to detect the presentation of EBNA-1 peptide on EBV-infected B lymphoblastoid cell lines (BLCL) using our in-house α-EBNA-1 TCR-like mAb. This antibody demonstrated *in vivo* efficacy in a mouse xenograft model engrafted with BLCL to model PTLD, conferring delayed weight loss and prolonged survival in treated mice. We further elucidated the mechanisms elicited by this antibody and showed that α-EBNA-1 TCR-like mAb could promote early apoptosis and phagocytosis *in vitro*.

We next established a humanized mouse model for the future testing of α-EBNA-1 TCR-like mAb. In this model, autologous BLCL was generated *in vitro* and injected into humanized mice reconstituted from the same donor. Using this approach, BLCL could be characterized and tested for binding to α-EBNA-1 TCR-like mAb *in vitro* prior to *in vivo* evaluations. With the employment of hydrodynamic injection of plasmids encoding human cytokines, we were able to augment NK cells reconstitution, thereby providing the option of investigating NK cell-mediated cytotoxicity. This autologous humanized mouse model not only provides the means to dissect the effector functions of α-EBNA-1 TCR-like mAb in the presence of reconstituted human immune cells, it can also serve as a platform for the testing of novel therapies.

List of Figures

List of Tables

List of Abbreviations

α	Anti
^{0}C	Degree Celsius
%	Percentage
µg	Microgram
µl	Microliter
µm	Micrometer
µM	Micromolar
M	Molar
min	Minute
7-AAD	7-Aminoactinomycin D
ACK	Ammonium-chloride-potassium
ADCC	Antibody-dependent cell-mediated cytotoxicity
APC	Allophycocyanin
BL	Burkitt's lymphoma
BLCL	B lymphoblastoid cell line
BLT	Bone marrow-liver-thymus
BSA	Bovine serum albumin
CD	Cluster of differentiation
CDC	Complement-dependent cytotoxicity
CFSE	Carboxyfluorescein succinimidyl ester
CTL	Cytotoxic T lymphocyte
Cy	Cyanine
DAPI	4', 6-diamidino-2-phenylindole
DNA	Deoxyribonucleic acid
DS	Dyad symmetry
EBNA	Epstein-Barr virus nuclear antigen
EBV	Epstein-Barr virus
EDTA	Ethylenediaminetetraacetic acid
ELISA	Enzyme-linked immunosorbent assay
FBS	Fetal bovine serum
Fc	Fragment, crystallizable
FcγR	Fc gamma receptor
FITC	Fluorescein isothiocyanate
FLT3L	FMS-like tyrosine kinase 3 ligand
FOV	Field of view
FR	Family of repeats
FSC	Forward scatter
g	Gram/gravitational force
GAPDH	Glyceraldehyde-3-phosphate dehydrogenase
GAr	Glycine-alanine repeat

GFP	Green fluorescent protein
H&E	Hematoxylin and eosin
HDI	Hydrodynamic injection
HEK	Human embryonic kidney
HER2	Human epidermal growth factor receptor 2
HL	Hodgkin's lymphoma
HLA	Human leukocyte antigen
HPC	Hematopoietic progenitor cell
HRP	Horseradish peroxidase
IgG	Immunoglobulin G
IL	Interleukin
IL2Rγ	Interleukin-2 receptor subunit gamma
IM	Infectious mononucleosis
K_D	Dissociation constant
kDa	Kilodalton
LMP	Latent membrane protein
MFI	Mean fluorescent intensity
MHC	Major histocompatibility complex
NK	Natural killer
nMFI	Normalized mean fluorescent intensity
NOD	Non-obese diabetic
NPC	Nasopharyngeal carcinoma
ns	Not significant
NSG	NOD/SCID/IL2Rγ$^{-/-}$
*ori*P	Origin of plasmid replication
PB	Pacific blue
PBMC	Peripheral blood mononuclear cell
PBS	Phosphate-buffered saline
PCR	Polymerase chain reaction
PE	Phycoerythrin
PerCP	Peridinin chlorophyll
PI	Phagocytic index
pMHC	Peptide-MHC complex
PS	Phosphatidylserine
PTLD	Post-transplant lymphoproliferative disorder
RIS	Reduction of immunosuppression
rpm	revolutions per minute
RPMI	Roswell park memorial institute
RT	Room temperature
s	Second
SCID	Severe combined immunodeficiency
SDS-PAGE	Sodium dodecyl sulfate-polyacrylamide gel electrophoresis

SSC	Side scatter
TCR	T cell receptor
TCR-like mAb	T cell receptor-like monoclonal antibody
WT	Wild type

Chapter 1: Introduction

1.1 EBV overview

EBV is a ubiquitous human gammaherpesvirus found in more than 90% of the human population [1]. EBV establishes life-long latent infection in humans and is estimated to have co-evolved with primates for millions of years [2]. The virus was discovered by Anthony Epstein, Yvonne Barr, and Burt Achong based on the employment of electron microscopy to observe virus particles in Burkitt's lymphoma (BL) biopsies [3]. Discovered in 1964, EBV was classified as the first human tumor virus by the World Health Organization in 1997 (International Agency for Research on Cancer Group I Carcinogens) [4].

EBV is a large, linear double-stranded deoxyribonucleic acid (DNA) virus (~172 kb) with a genome encoding more than 100 viral gene products [5]. The virus has a tropism for B cells and epithelial cells, and had been shown to transform human B cells *in vitro*, into immortalized BLCL [1, 6]. *In vivo*, primary EBV infection during childhood is often asymptomatic but can lead to the development of IM when infection occurs during adolescence [7]. To date, the virus is identified as the etiological agent of infectious mononucleosis (IM) and is associated with malignancies of both epithelial and lymphoid origins (**Table 1.1**).

Table 1.1: EBV latency programs and associated diseases

Latency program	EBNA-1	EBNA-2	EBNA-3	LMP-1	LMP-2	Disease
I	+	-	-	-	-	Burkitt's lymphoma Gastric carcinoma
II	+	-	-	+	+	Hodgkin's lymphoma Nasopharyngeal carcinoma
III	+	+	+	+	+	Post-transplant lymphoproliferative disorder B lymphoblastoid cell line (*in vitro*)

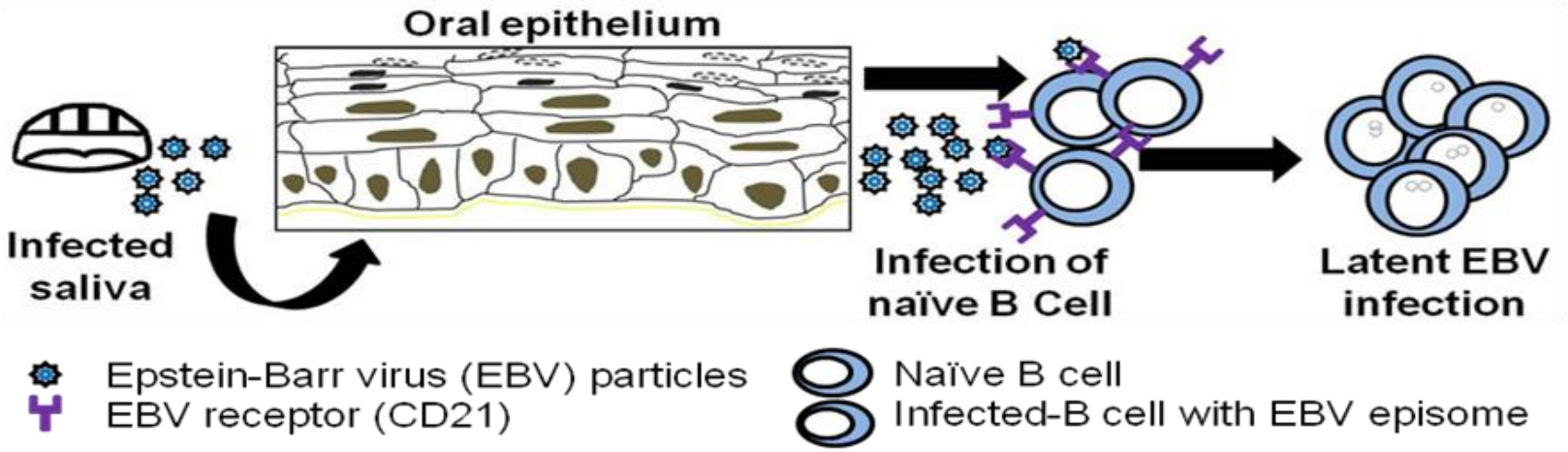

Figure 1.1: EBV life cycle. Virus particles from the saliva of infected individual pass through the oral epithelium and gain access to the B cells of a naïve individual. Using viral envelope glycoprotein (gp350), the virus binds to the receptor (CD21) to enter and infect the B cells. In the initial phase of infection, EBV-infected cells undergo lytic replication with the production of virus progenies. In healthy immunocompetent individuals, replication of the virus is kept in check by T cells (and NK cells), driving the virus into a quiescent state with the EBV genome maintained in the episomal form. In times of stress, reactivation of EBV infection can take place, resulting in the switch from latent to lytic replication (productive infection), with infectious virus particles budding off and shedding into the saliva.

1.1.1 EBV life cycle

The lymphocryptovirus EBV is transmitted through oral secretions of infected individuals, infecting B cells in the oropharynx [6] (**Figure 1.1**). The entry of EBV into the B cell is mediated through the binding of glycoprotein (gp350) on the viral envelope to the receptor - cluster of differentiation 21 (CD21) on the B cells. Upon infection, the linear EBV genome circularizes and forms an episomal genome, establishing latent infection in the memory B cell compartment (**Figure 1.2**) [8, 9]. In healthy adults, 1 to 50 EBV-infected cells per one million peripheral blood lymphocytes (PBL) can be found in the circulation [10]. Occasionally, these latently infected cells can undergo reactivation and lytic replication, leading to their recognition and elimination by cytotoxic T lymphocytes (CTLs).

1.1.2 EBV-associated diseases

Aside from IM, EBV infection is also associated with a spectrum of malignancies such as BL, Hodgkin's lymphoma (HL), nasopharyngeal carcinoma (NPC) and PTLD. The chronicity of EBV infection is based on the adaptation of different latency programs in various EBV-associated diseases; namely, latency I (in BL), latency II (in HL and NPC) and latency III (in IM and PTLD). While each latency program is characterized by a specific gene expression pattern as shown in **Table**

1.1, EBNA-1 is the only EBV latent protein which is expressed in all latency programs associated with EBV-linked malignancies.

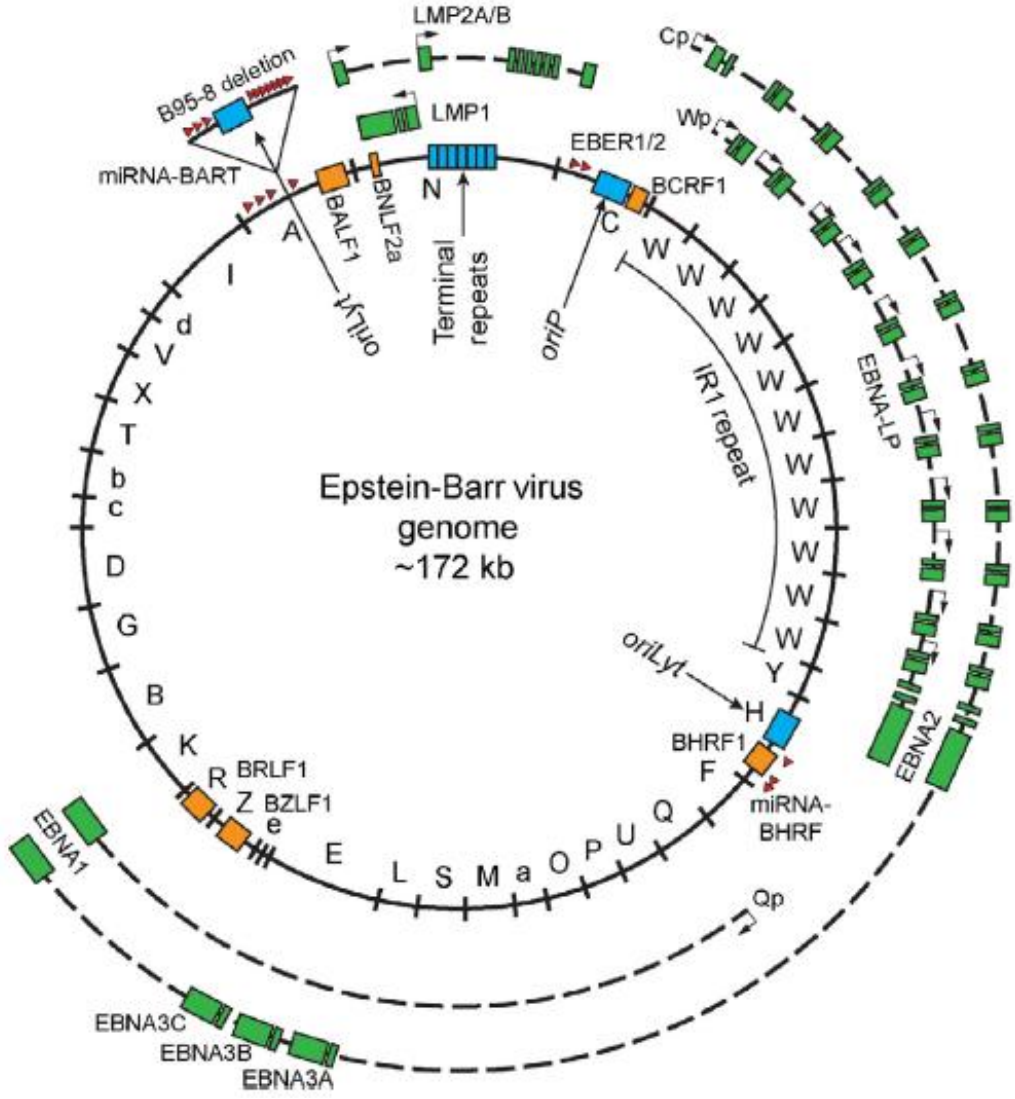

Figure 1.2: Schematic of the EBV episome. The genome of EBV is approximately 172 kb. *oriP* is required for the replication of plasmid while *oriLyt* are the two sites for lytic replication activation. All nine latent proteins are illustrated: EBNA-LP, EBNA-1, EBNA-2, EBNA-3 (A, B, and C), LMP1, and LMP2 (A and B). Image adapted from Alexander M. Price and Micah A. Luftig., 2014

1.2 EBNA-1 overview

The prototypic EBNA-1 protein is a 641 amino acids, 56 kDa protein that is expressed in both lytic and latent phases of EBV infection. EBNA-1 proteins from different geographical isolates of EBV are different in sizes due to the variation in the number of glycine-alanine, and thus far, five EBNA-1 subtypes have been classified based on the carboxy-terminus of the EBNA-1 protein [11-13].

Published findings on EBNA-1 reported its necessity in viral replication and maintenance of EBV episomal DNA via initiating DNA synthesis and tethering of EBV episome to the host chromosomes [14-16]. Subsequently, based on the lack of detection of EBNA-1-specific $CD8^+$ CTLs, EBNA-1 was proposed to play a role in immune processing and evasion [17-19]. In recent years, additional published evidence suggests that EBNA-1 also contributes to the oncogenic potential of EBV [20-23].

Given the multifaceted involvements of EBNA-1 in viral DNA replication, immunoevasion, and oncogenesis, it is anticipated that targeting EBNA-1 can abrogate viral replication, inhibit host cell transformation and enhance immune detection. As the protein is only expressed in EBV-infected cells, targeting EBNA-1 provides selectivity over the non-infected cells, justifying EBNA-1 as a therapeutic target.

1.2.1 Role of EBNA-1 in viral genome maintenance

EBNA-1 functions as a genome maintenance protein, mediating two critical processes: the initiation of viral DNA synthesis and episomal segregation [14-16]. As shown in **Figure 1.3**, the carboxy-terminus of EBNA-1 protein contains a DNA-binding domain which binds to two clusters within the *oriP* (origin of plasmid replication) of the viral episome; namely, dyad symmetry (DS) and family of repeats (FR). While DS serves as a site for the initiation of replication, FR functions as an anchor point for the binding of EBNA-1 protein to ensure equal partitioning of the viral episomes into daughter cells during cellular mitosis [24-26].

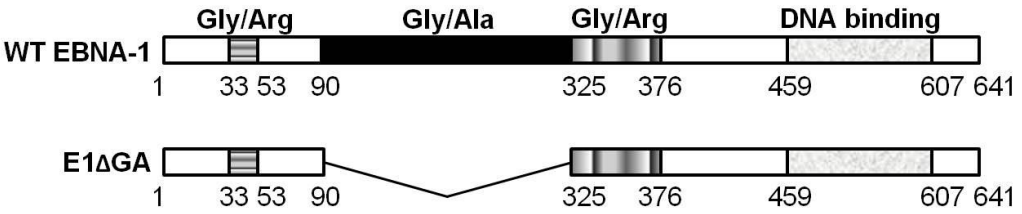

Figure 1.3: Schematic of WT EBNA-1 and its truncated variant (E1ΔGA). The WT EBNA-1 protein contains 641 amino acids (UniProt accession number: P03211). The C-terminal region contains the DNA binding domain for binding to the EBV episome. Within the WT protein, the GAr (solid black) occupies the positions 90 to 325 on the protein. A truncated variant with the deletion of GAr is denoted as E1ΔGA. Numbers indicated refer to the coordinates of the amino acids.

1.2.2 Role of EBNA-1 in EBV-oncogenesis

EBNA-1 is the only EBV protein that is expressed in all EBV-associated malignancies and this may suggest a common mechanism of EBNA-1-induced oncogenesis. As reported by Gahn et al., EBNA-1 was found to interact with the viral promoter that activates the transcription of EBV latent genes involved in cell immortalization and transformation [27, 28]. Moreover, EBNA-1 expression in 293T cells promoted serum independence, survival [20] and upregulated reactive oxygen species as well as genomic instability in BL cell lines [22, 23].

The protein is further implicated in the perturbation of TGF-β1 signaling in epithelial cells [29], dysregulating cellular functions such as cell proliferation and survival, all of which are the prerequisites of cancer development [30]. Moreover, the introduction of anti-sense EBNA-1 or EBNA-1-deficient viruses resulted in the failure of B cell immortalization [15, 31], whereas expression of EBNA-1 plasmids (in the absence of the whole virus) resulted in increased tumor formation and metastasis of murine cancer cells *in vivo* [32, 33]. While direct evidence of EBNA-1-induced oncogenesis has been forthcoming, these studies do provide indirect evidence of its oncogenic potential.

1.2.3 Role of EBNA-1 in immunoevasion

The classical major histocompatibility complex (MHC) class I antigen presentation pathway is intrinsic to all nucleated cells, where endogenous proteins destined for presentation are tagged with ubiquitin and targeted for degradation by the proteasome [34-36]. These degraded proteins, in the form of short peptides, are then transported into the endoplasmic reticulum via the transporter associated with antigen processing for subsequent loading onto nascent MHC class I molecules [37]. These peptide-MHC (pMHC) complexes are then trafficked via the secretory pathway onto the cell surface for presentation [38, 39]. In this regard, MHC class I antigen presentation is essential for immunosurveillance by presenting viral or tumor antigens as short peptides to $CD8^+$ CTLs to eliminate both virus-infected and malignant cells [40, 41].

In the early 1990s, the EBNA-1 protein was proposed to play a role in EBV immune evasion due to the inability of researchers to isolate EBNA-1-specific $CD8^+$ CTLs from EBV-seropositive individuals [19, 42, 43]. While EBNA-1-specific $CD4^+$ T cells and its memory subsets were detected [19, 44-48], it was intriguing that the endogenously expressed EBNA-1 protein was less recognized by the $CD8^+$ CTLs, and was less immunogenic compared to other EBV latent proteins such as latent membrane protein 1 (LMP1) and EBNA-3 [42, 49]. Furthermore, *in silico* prediction algorithms showed that the EBNA-1 protein expressed fewer binding motifs for MHC class I molecules, and this seemed to correlate with the lack of EBNA-1-specific $CD8^+$ CTLs detected [50].

With the failure to detect EBNA-1-specific $CD8^+$ CTLs in EBV-seropositive individuals, it was proposed that the GAr within the EBNA-1 protein was able to hinder the ubiquitin-proteasome proteolysis process, thereby leading to the inefficient presentation of EBNA-1 epitopes on MHC class I molecules [17, 51]. The role of GAr in proteasomal inhibition was further enforced when the removal of GAr restored the presentation of EBNA-1 epitopes to $CD8^+$ CTLs, while its insertion into other proteins inhibited their degradation and T cell recognition [17, 18, 52]. Additionally, it was reported that the degree of proteasomal inhibition is dependent on the length of GAr and that inhibition was observed with a minimal of eight GAr [53-55].

In 2004, three consecutive publications questioned the lack of detection for the EBNA-1-specific $CD8^+$ CTLs and reported that EBNA-1 protein could be presented via defective ribosomal products; in other words, EBNA-1 epitopes were generated through processes that involved its synthesis rather than a result of its degradation [56-58]. These observations altered the paradigm of GAr in the antigen presentation of EBNA-1. While the proposed mechanisms of GAr in inhibiting its own presentation are not mutually exclusive, accumulating evidence from the recent years supported the argument that presentation of EBNA-1 originates from its non-functional products of the protein translational machinery [59-63].

1.3 PTLD overview

PTLD is one of the EBV-associated diseases which arises in solid organ or allogeneic hematopoietic stem cell transplant recipients. As a heterogeneous group of diseases, the spectrum of PTLD ranges from B cell hyperplasia to B cell lymphoma (**Table 1.2**). The incidence of PTLD varies from 1% to 20%, depending on the type of the organ transplanted, recipient's age and the intensity of immunosuppressants administered [64-69]. Even though the overall incidence of PTLD is low, it is a potentially life-threatening disease with high mortality rates [70].

The association between PTLD and EBV was made based upon the observation that EBV-seronegative recipients who lacked EBV-specific immunity were more susceptible to PTLD development in comparison to EBV-seropositive recipients [71]. Evidence on EBV shedding preceding to PTLD development, and the elevated viral DNA load and proteins found in PTLD tissues further supported the involvement of EBV in PTLD development [72-74].

EBV-seropositive recipients are also at risk of developing PTLD because the administration of immunosuppressants to prevent graft rejection can lead to the suppression of T cell immunity, and this can consequently perturb the balance between T cell immunity and the latently EBV-infected B cells [75, 76]. As a result of immunosuppression, the unrestricted proliferation of EBV-infected B

cells accompanying the expression of a full repertoire of EBV latent proteins can be detected (**Table 1.1**: latency III program) [77, 78].

Even with the comprehensive classification of PTLD published by the World Health Organization in 2008 (**Table 1.2**), the diagnosis of PTLD can still be complicated with misdiagnosis of infection or graft rejection [79]. Furthermore, the design of a controlled randomized study with proper controls to compare the efficacy of current drugs in PTLD treatment is inherently difficult owing to the diverse range of organs transplanted, disease spectrum and age-related manifestations of the disease. Therefore, it is to no surprise that the small sample sizes of published trials from individual centers can be conflicting at times. Taken together, it is evident that there are still a number of hurdles to surmount in the treatment of PTLD.

Table 1.2: Classification of PTLD (based on 2008 WHO classification)

Histopathological Classification of PTLD	Frequency	EBV association
Early lesions	5%	100%
Plasmacytic hyperplasia		
Infectious mononucleosis-like PTLD		
Polymorphic PTLD	15-20%	<100%
Monomorphic PTLD	>70%	50%
Diffuse large B-cell lymphoma		
BL or Burkitt-like lymphoma		
Plasma cell myeloma		
Plasmacytoma		
Other types		
Classical HL and HL-like PTLD	<5%	100%

1.3.1 Host immunity in PTLD

The earliest indication of T cell immunity targeting EBV-infected B cells came from Rickinson et al., where donor-derived T cells were able to inhibit EBV-induced transformation *in vitro* [80-82]. Following the introduction of pMHC tetramer staining for EBV-specific $CD8^+$ CTLs, Callan et al. were the first to characterize EBV-specific T cell immunity and reported 44% of the $CD8^+$ T cells from the peripheral blood of an individual to be specific for the virus [83].

The responsiveness of T cell immunity to the virus was further highlighted by the massive expansion of EBV-specific T cells during primary EBV infection and the establishment of a T cell memory repertoire upon resolution of acute infection [84, 85]. The importance of T cell immunity in EBV-PTLD is well-illustrated in transplant recipients, where anti-thymocyte globulin conditioning regimen to prevent graft rejection confers an increased risk of PTLD development [86]. Consistently, in a longitudinal study of bone marrow transplant patients, the reduction of immunosuppression resulted in the recovery and expansion of $CD8^+$ T cells, driving the regression of PTLD [87, 88].

Humoral immunity, on the other hand, is crucial in preventing the spread of EBV via neutralization of the virus [89]. While the role of humoral immunity in PTLD is less clear, it is established that transplant recipients with EBV-specific humoral immunity prior to transplantation are protected from PTLD development [90, 91]. Indeed, Riddler et al. demonstrated that transplant recipients with deficient humoral responses against EBNA-proteins were predisposed to PTLD development, with disease development inversely correlating to the level of anti-EBNA-1 antibody [92].

1.4 Treatment of PTLD overview

Various treatment modalities are available for PTLD (**Table 1.3**). Yet, opinions differ on their utility due to the lack of comprehensive clinical trials to assess and compare the relative treatment efficacy of different therapeutics. In this section, the most commonly employed approaches to managing PTLD, namely the RIS, anti-B cell monoclonal antibody (rituximab), and T cell adoptive therapy are discussed (**Table 1.3**). The use of EBV-specific TCR-like mAb for PTLD treatment will also be explored.

Table 1.3: Management of PTLD

Management of PTLD
Reduction/or withdrawal of immunosuppression (RIS)
Anti-B cell monoclonal antibody
Surgery and radiation
Cytotoxic chemotherapy
Intravenous immunoglobulin
Antiviral therapy
Interferon and other cytokines
Cellular immunotherapy (Adoptive EBV-specific T cell therapy)

1.4.1 Reduction of immunosuppression (RIS)

Unlike other treatment approaches that involve the administration of therapeutics into transplant recipients, RIS is considered as PTLD management rather than treatment. RIS is achieved by decreasing the dosage of immunosuppressants to facilitate the recovery of host immunity against the EBV-infected B cells. Although RIS is the clinical mainstay in PTLD management, its practice can increase the risk of graft rejection. Thus, careful considerations have to be made in the case of heart transplant recipients, where organ replacement or substitution is almost not possible upon graft failure [93].

1.4.2 Anti-B cell monoclonal antibody

Rituximab is a therapeutic monoclonal antibody which binds and depletes CD20-expressing cells. The antibody is currently the best-selling oncology drug [94], and is used in the treatment of lymphoma [95], leukemia [96], rheumatoid arthritis [97] and lupus [98]. In the context of PTLD treatment, a number of groups expressed concern on the clinical employment of rituximab as the antibody's non-selective elimination of healthy B cells can have a dampening effect on humoral immunity, which is required for long-term protection against EBV [99]. In addition, the use of rituximab has been reported to increase the risk of opportunistic infections [100, 101], and the development of refractory $CD20^{-}$ lymphoma [102, 103]. Nonetheless, the therapeutic efficacy of rituximab under different transplantation settings has been demonstrated, either in the form of a single-agent or as a combinatory treatment with other drugs [104-110]. Evidently, the use of rituximab supports the feasibility of employing antibodies for PTLD treatment, while at the same time highlighting a need for therapeutics with better specificities to reduce adverse effects.

1.4.3 Adoptive T cell therapy

Adoptive T cell therapy involves the infusion of viral- or tumor-specific T cells into a patient to eradicate the diseased cells. The usage of EBV-specific T cells for adoptive T cell therapy came from the early observation by Rickinson et al., that T cells from EBV-seropositive donors could inhibit EBV infection *in vitro* [80]. In the 1990s, the first two human trials using adoptive T cell therapy were acclaimed for their successes in the treatment and prevention of PTLD in solid organ transplant and bone marrow transplant recipients [111-113].

Of note was the landmark human clinical trial conducted by Rooney et al., where 39 patients prophylactically infused with donor-derived EBV-specific T cells demonstrated protection against lymphoma development, while 7/61 patients in the control group developed the disease [112]. The same study also validated the safety aspects of EBV-specific T cell therapy, their potency as immunoprophylaxis and their feasibility in the treatment of established PTLD. Subsequently, many other human trials reported successes with EBV-specific T cell therapy, attesting to the employment of this approach in PTLD treatment [114-120].

In spite of the success with EBV-specific T cell therapy, it is not a readily available treatment option because the isolation and expansion of EBV-specific T cells from donors is a complex process that can span up to 12 weeks [121]. As this treatment modality requires human leukocyte antigen (HLA)-matching, the limited banking plus the time-consuming procedures in generating compatible EBV-specific T cell lines restrict its clinical utility. To overcome these limitations in producing EBV-specific T cells, Icheva et al. developed a rapid protocol for generating EBNA-1-specific T cell lines within 72 hours [122]. Notably, the authors reported that EBNA-1-specific T cells obtained from this rapid protocol could confer protective T cell immunity, preventing the development of PTLD. This study not only provides a methodology to enhance the production of EBV-specific T cells but also supports the feasibility of targeting EBNA-1 in PTLD treatment.

1.4.4 TCR-like mAbs

TCR-like mAbs are antibodies which exquisitely recognize a specific pMHC (**Figure 1.4**). The increasing interest in TCR-like mAbs is evident by the growing repertoire of TCR-like mAbs extending into areas of research, diagnostics, and therapies of cancers [123-125] and infectious diseases [126-128]. TCR-like mAbs are endowed with the specificity of a T cell receptor and have been employed for antigen presentation studies [127-131]. As shown in **Figure 1.5,** these antibodies have been reported to mediate the direct induction of apoptosis, complement-dependent cytotoxicity (CDC), and antibody-dependent cell-mediated cytotoxicity (ADCC) [123, 125, 132-135].

As a protein derivative, TCR-like mAbs have some advantages over effector T cells, in that they may be less susceptible to immunomodulatory cytokines in the tumor microenvironment which suppress anti-tumor functions [132]. More importantly, antibodies are stable and can be purified in large quantities for *in vivo* applications [136]. As the development of TCR-like mAbs is a relatively new phenomenon, efforts have been focused on establishing the groundwork for future application of these antibodies in the clinic [137, 138]. In the context of PTLD, our laboratory has previously suggested the potential utility of EBV-specific TCR-like mAbs for the treatment of EBV-associated diseases [129].

In this study, three EBV-specific TCR-like mAbs were utilized to delineate the antigen presentation hierarchy of EBV latent proteins EBNA-$1_{562-570}$, $LMP1_{125-133}$ and $LMP2A_{426-434}$ on HLA-A*0201 cells. Apart from the high binding affinities reported, these EBV-specific TCR-like mAbs were reported to be able to detect the endogenous presentation of these latent proteins in EBV-infected cell lines, with EBNA-1 epitope being the most abundantly presented. Importantly, this study has provided insights on the targeting of intracellular antigens which are often 'hidden', but made accessible upon surface presentation. As these antibodies were only used for the purpose of studying MHC class I antigen presentation, we proposed that it would be of interest to evaluate their *in vivo* efficacy.

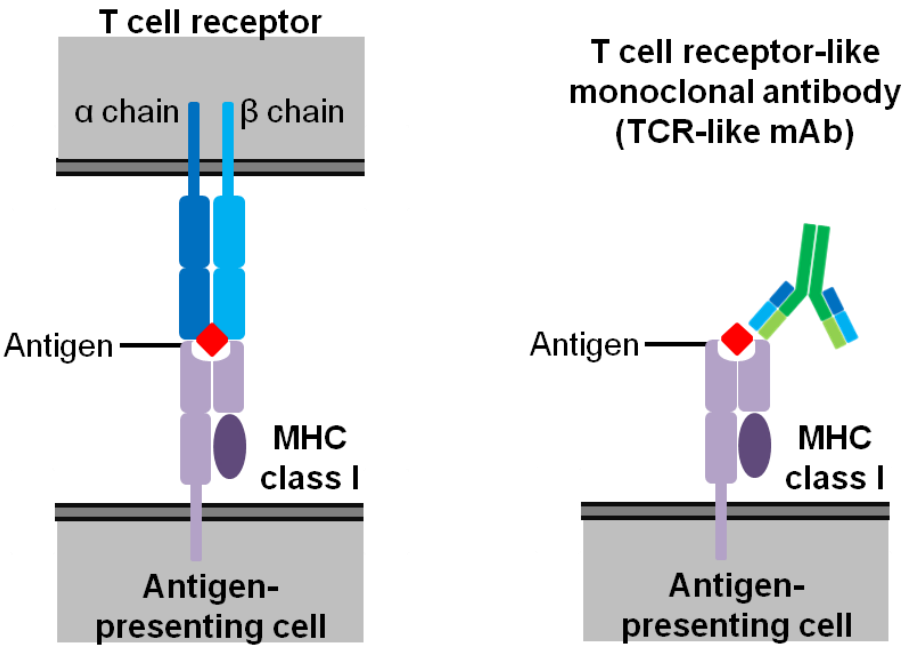

Figure 1.4: Schematic of pMHC binding to T cell receptor and TCR-like mAb. Left: T cell receptor is found on the surface of T cells, recognizing antigen/peptide presented on the MHC class I molecules. The destruction of tumor or virus-infected cells is based on TCR recognition. **Right**: TCR-like mAb is an antibody with specificity akin to that of a TCR, recognizing the surface presentation of pMHC.

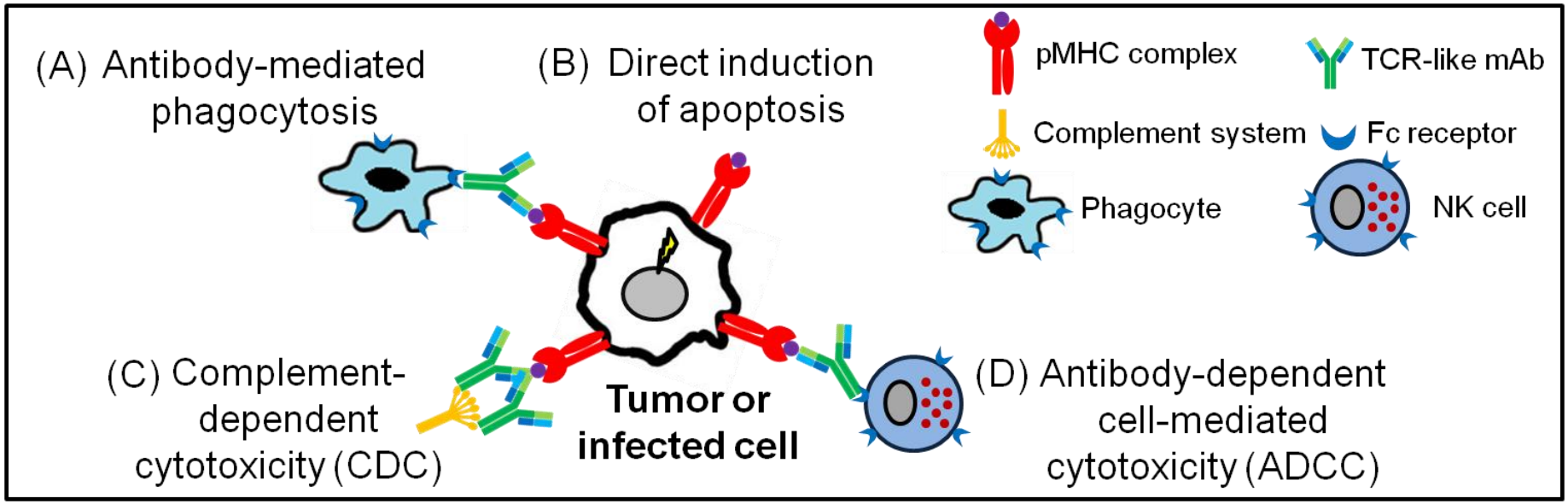

Figure 1.5: **Mechanisms of action of TCR-like monoclonal antibodies**. A collection of TCR-like mAbs specific for tumors and virus-infected cells generated over the years were reported to be capable of eliciting **(A)** antibody-mediated phagocytosis, **(B)** direct induction of apoptosis, **(C)** complement-dependent cytotoxicity and **(D)** antibody-dependent cell-mediated cytotoxicity [130].

1.5 *In vivo* models overview

Murine models play an important role in biomedical research and their usage has accelerated our understanding of numerous diseases. With regards to disease modeling and therapeutic testing, *in vivo* models are preferred over the use of cell lines as cells are often over-simplified in that they lack the physiological complexity of an organ system.

EBV as a gammaherpesvirus infects only humans and higher primates, and this consequently complicates the development of mouse models of EBV infection. While primates such as marmosets, cotton-top tamarins, and owl monkeys can be infected with the virus, they are either endangered or costly to maintain. Thus, there are limited animal model available for the establishment of EBV infection *in vivo*. To overcome the limitation of modeling EBV-associated disease in mice, Mosier et al. pioneered the injection of PBL from EBV-seropositive donors into severe combined immunodeficient (SCID) mice to simulate EBV-positive B cell lymphoma [139]. The methodology employed by Mosier et al. not only simulated the development of EBV-PTLD in bone marrow transplant recipients but also established the first mouse model reconstituted with a human hematolymphoid system.

The establishment of a mouse model with the human immune system by Mosier et al. opened up a new era of mouse modeling, now referred to as the humanized mice. With the advancements in genetic engineering and animal breeding, NOD/SCID/IL2Rγ$^{-/-}$ (NSG) mice were generated to better support human immune cells engraftment [140]. As these mice are highly immunodeficient, they are able to support the engraftment of human hematopoietic progenitor cells (HPCs), giving rise to the *de novo* generation of human B cells that are permissive to EBV infection *in vivo*.

The advent of humanized mice is in-line with the demand for an animal model which is relevant for modeling human diseases and possesses a high predictive value for therapeutics evaluation. The necessity of an animal model which can faithfully predict human responses to drug treatment is illustrated by one of the most catastrophic human trial of anti-CD28 antibody (TGN1412). In that particular clinical trial, all six healthy volunteers developed cytokine storm followed by multiorgan failure despite being administered with TGN1412 at a dosage which was 500 times lower than what was found to be safe in animal studies [141-143].

Owing to the species-specific, immunopharmacological differences between humans and animals, these tested animals failed to predict the development of a cytokine storm as the result of T cell activation in humans upon TGN1412 treatment [141]. This incident clearly exemplifies that the interaction between any therapeutic candidate in question and the human immune system should be thoroughly evaluated, and further highlights a need for a more robust animal model. In this regard, the humanized mice provide not only human immune cells for disease modeling; they are also amenable for predicting human immune responses to potential immunotherapeutics. Indeed, a recent publication by Weissmuller et al. demonstrated that the humanized mice are able to recapitulate the adverse effects as seen upon TGN1412 treatment in humans [144].

1.5.1 Mouse xenograft model

Xenograft modeling involves the transplantation of human tumor tissues or cells into immunodeficient mice. As these mice are devoid of a functional mouse immune system, human tissues/cells can be engrafted with minimal rejection. In the first mouse model of EBV-associated disease, Mosier et al. injected PBL from EBV-seropositive donors into immunodeficient C.B-17-SCID mice to simulate the development of EBV-positive B cell lymphoma in immunocompromised bone marrow transplant recipients [139]. When 5 X 10^7 PBL was injected into the immunodeficient C.B-17-SCID mice, B cell tumors were observed with histology similar to the lymphomas in EBV-PTLD patients [139, 145]. In contrast, no tumors were observed when 1 X 10^7 PBL was used.

The lack of B cell lymphoma development in mice injected with 1 X 10^7 PBL can be attributed to the low frequency of EBV-infected cells in the peripheral blood [146, 147]. However, it should be noted that although C.B-17-SCID mice are deficient in functional B and T cells, they have an intact innate immunity and that could impede the engraftment of EBV-infected B cells [148]. Due to the suboptimal reconstitution conditions provided by the C.B-17-SCID mice, as well as the low numbers and variability of EBV-infected B cells in the peripheral blood between donors, modeling EBV-PTLD with reproducibility and consistency is challenging.

To overcome the reproducibility issue, Rowe et al. injected BLCL as an alternative to PBL from EBV-seropositive donors to model EBV-PTLD (**Figure 1.6**) [149, 150]. The use of BLCL as a replacement of PBL was justified as the surface phenotype, karyotype, and viral gene expression of BLCL are analogous to the tumors in PBL-SCID mice. Using this approach, graft-versus-host disease as seen with the transfer of mature human T cells present in the PBL could be circumvented [151]. At the same time, this also ensured a more reliable development of B cell tumors in the mice. Consequently, the methodology of injecting BLCL into SCID mice became a basic model of EBV-PTLD and has since been used for the assessment of treatments such as adoptive T cell therapy [152-156].

As illustrated by the TGN1412 human trial, differences in the immunopharmacological characteristics between species could possibly be the reason why humans reacted differently from tested animals. In this regard, the lack of a human immune system in the mouse xenograft model of EBV-PTLD does not allow the assessment and prediction of human immune responses to therapeutics. As such, there is the need for an animal model that can recapitulate key features of EBV-PTLD and enable the examination of individualized human immune responses to treatments in order to provide a more accurate drug evaluation.

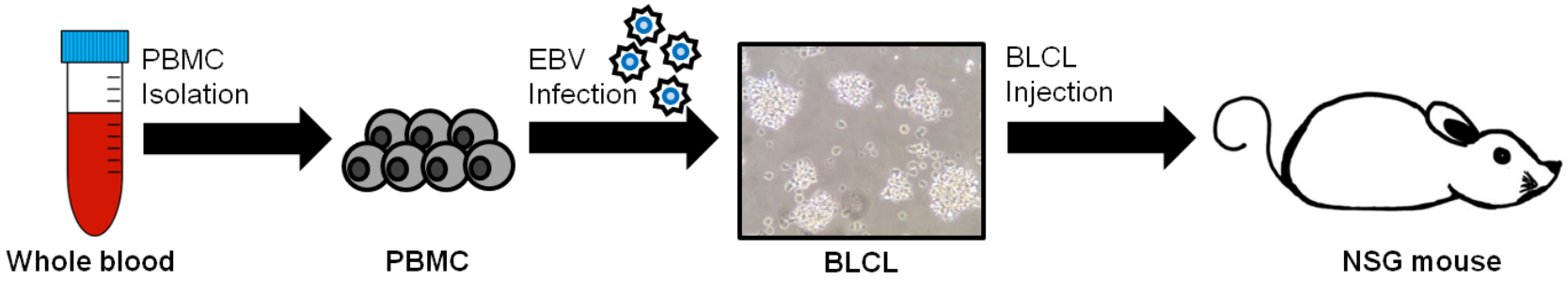

Figure 1.6: **Mouse xenograft model of EBV-PTLD**. EBV infects primates and humans but not mice. In order to model EBV-PTLD, BLCL is established from the *in vitro* infection of B cells and is injected into NSG mice. As these mice are immunodeficient, they are unable to reject and control the proliferation of BLCL, leading to the manifestation of B cell lymphoproliferative disorder and B cell lymphomas.

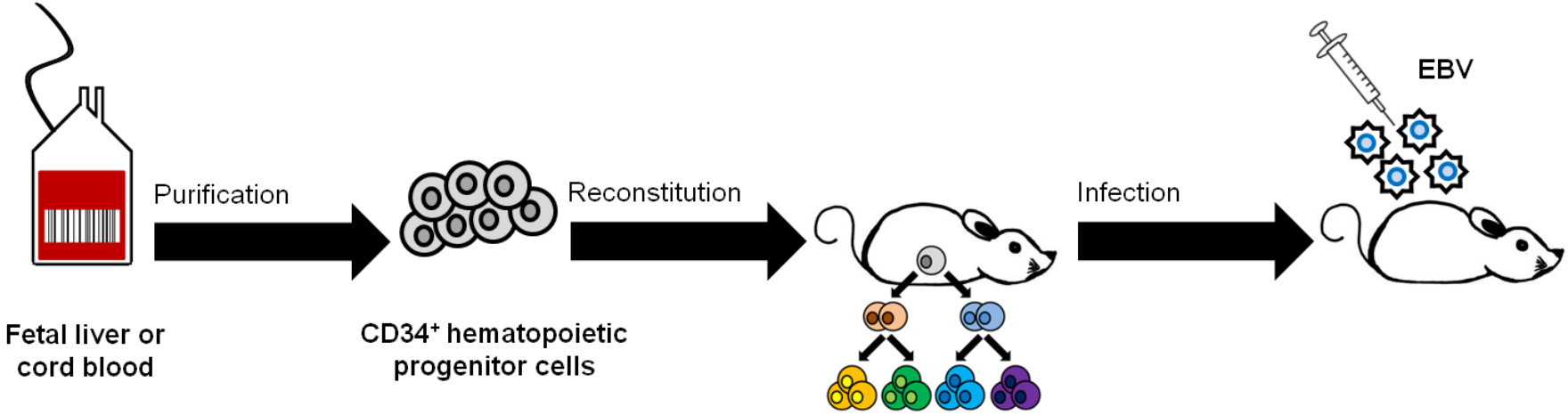

Figure 1.7: **Humanized mouse model of EBV infection**. The injection of human $CD34^+$ HPCs into NSG mice and their subsequent differentiation into B cells, T cells, NK cells, etc. permits the establishment of an *in vivo* model for human pathogens which have cellular tropism for these differentiated cells. Using the humanized mouse, *in vivo* modeling of B cell-tropic EBV can be performed for the study of EBV pathogenesis, immune responses as well as the testing of potential therapeutics.

1.6 Humanized mouse model overview

Humanized mice or more specifically human hematolymphoid system mice are commonly defined as immunodeficient mice which are engrafted with human immune cells (**Figure 1.7**). The generation of a humanized mouse is laborious due to the requirements of specialized housing and technical expertise in the delivering of $CD34^+$ HPCs during the reconstitution process. Two main factors can determine the success of generating a humanized mouse: the sources and quality of the human sample, as well as the strain of recipient mouse.

Human PBL, cord blood, and fetal liver are common sources of human cells used for the generation of humanized mice. The use of donor-derived cells in the humanized mice enables the construction of a mouse model which can reflect donor-specific disease heterogeneity and individualized responses to the tested therapeutics. In the first humanized mouse model, graft-versus-host disease was reported due to the presence of mature T cells in PBL that attacked the mouse tissues [139, 151]. However, such complication is avoided with the use of HPCs from the fetal liver [157] and cord blood [158]. Unlike circulating T cells which are committed to non-self recognition, HPCs are the blood precursor cells and thus do not mediate graft-versus-host disease. By far, *de novo* hematopoiesis of B cells, T cells, NK cells, monocytes, macrophages and dendritic cells have been observed after the engraftment of human HPCs in immunodeficient mice.

The choice of mouse strain is a key determinant in human immune cells reconstitution. Initially, the C.B-17-SCID mouse was used for the reconstitution of human immune cells but this system supported the engraftment poorly due to the presence of mouse innate immunity (**Table 1.4**) [139]. To improve the reconstitution of human immune cells in mice, Hesselton et al. generated the NOD-SCID mice which have reduced NK cell activity [159]. While the NOD-SCID mice was shown to better support human immune cells engraftment as compared to the C.B-17-SCID strain, they have shortened life span due to thymic lymphoma development, limiting their usage for long-term studies [160].

In 2002, Ito et al. crossed the NOD-SCID mouse with a mouse harboring a null mutation for interleukin-2 receptor subunit gamma ($IL2R_{\gamma}$) to giving rise to the NOD/SCID/γc^{null} mice which are defective in NK cell activity [161]. As $IL2R_{\gamma}$ is a common cytokine receptor subunit required for IL-2, IL-4, IL-7, IL-9, IL-15, and IL-21 receptors, the absence of $IL2R_{\gamma}$ in NOD/SCID/γc^{null} mice resulted in the blockage of NK cell development [161-163]. Further characterization by Shultz et al. revealed that these mice have severe defects in both their innate and adaptive immunity. However, unlike their parental NOD-SCID strain, NOD/SCID/γc^{null} mice do not develop thymic lymphoma and are better in supporting the engraftment of human immune cells [140]. At present, this strain of mouse is known as the NSG mouse and is one of the most popular mouse strains for humanized mouse modeling.

With the increasing demands for a humanized mouse model, newer strains of mice such as the BALB/c-Rag2$^{-/-}$IL2Rγ$^{-/-}$ mouse have been generated to enhance the maturation of reconstituted human B cells [164]; and the transgenic expression of human signal regulatory protein alpha in the Tg(hSIRPα)Rag2$^{-/-}$IL2Rγ$^{-/-}$ mouse strain improves the tolerance of murine macrophages towards engrafted human immune cells [165]. To date, the humanized mouse model has been employed to study a number of human pathogens with tropism for human immune cells such as EBV [164], *Salmonella typhi* [166], human cytomegalovirus [167], dengue virus [168], human immunodeficiency virus [169], Kaposi's sarcoma-associated herpesvirus [170], hepatitis B [171] and hepatitis C [172] viruses.

Table 1.4: History of the development of immunodeficient mice

Year	Mouse	Traits	References
1983	C.B-17-SCID	B and T cells deficiency Normal NK cells	Bosma et al., 1983 Nonoyama., 1993
1995	NOD-SCID	B and T cells deficiency Reduced NK cell activity	Hesselton et al., 1995 Shultz., 1995
2002	NOD SCID gamma (NSG)	Lacks B, T and NK cells	Ito et al., 2002 Shultz., 2005

1.6.1 Humanized mouse model of EBV-associated diseases

The engraftment of HPCs and their subsequent differentiation into B cells in the immunodeficient mice enables the establishment of an *in vivo* EBV infection model. Since the first described HPCs-engrafted humanized mouse model of EBV infection developed by Traggiai et al. in 2004 [164], the humanized mice platform has been used for the modeling of EBV-associated diseases such as lymphoproliferative disorder [173, 174], hemophagocytic lymphohistiocytosis [175], HL [176], diffuse large B cell lymphoma [177, 178] and rheumatoid arthritis [179]. The modeling of asymptomatic infection reminiscent of latent EBV infection in humans has also been reported in the humanized mice when the virus is inoculated at $<10^1$ 50% transforming dose [173].

B cell lymphoproliferative disorder and B cell lymphomas are the most commonly studied EBV-associated diseases in humanized mice. In the first humanized mouse model of EBV lymphoproliferative disorder, Yajima et al. were able to recapitulate salient features of EBV-PTLD in humans such as the detection of EBV viral DNA and the manifestation of lymphoproliferation in the spleens, livers and kidneys [173]. In addition, the observed disease phenotype, histology and the expression of latency III profile in the humanized mice were consistent with the disease presented in immunocompromised humans. Intriguingly, EBV-specific T cells and IgM antibody responses were

detected despite the development of both human B and T cells in the microenvironment of their murine recipients.

Based on the establishment of B cell lymphoproliferative disorder by Yajima et al., many research groups have since utilized this platform to study disease pathogenesis, immune responses and therapeutic approaches in the context of EBV-PTLD (**Table 1.5**). In particular, Ma et al. investigated the role of lytic cycle activator (BZLF1) in the humanized mice and demonstrated that BZLF1-defective EBV has an impaired ability in tumor formation *in vivo* [177]. Through this model, researchers have further uncovered an unexpected tumor suppressor role of EBNA-3B, in facilitating T cell-mediated killing of EBV-infected B cells [178]. Such a finding is intriguing, as the tumor suppressor role of EBNA-3B is incongruous to the oncogenic potential of EBV.

The use of humanized mice has also revealed the multifaceted roles of T cells in the pathogenesis of the EBV-associated lymphoproliferative disorder. The involvement of T cells in determining disease progression and pathogenesis was illustrated by Lee et al., where the disease outcome was dependent on the proportion of T cells in the humanized mice [176]. The importance of T cell immunity was also demonstrated in the humanized mice and exploited as a treatment modality, with the adoptive transfer of EBV-specific T cells reducing EBV viremia [180] and prolonging the lifespan [181] of treated mice. On the other hand, an alternate aspect of T cell functionality was observed with $CD4^+$ T

cells, where they were shown to downregulate the immunogenicity of EBV-infected B cells, diminishing their recognition by $CD8^+$ T cells [182].

In a recent report by Ma et al., human T cells within humanized mice were found to be inhibited by the expression of programmed cell death-ligand 1 on EBV-infected cells [183]. The inhibition of T cells could however be reversed upon the treatment with anti-PD-1 monoclonal antibody which has been approved by the FDA for the treatment of melanoma and squamous non-small cell lung cancer [184]. Despite the discrepancies in the reported T cell functions from different studies, these studies converge on the importance of T cells in shaping the outcome of the disease. Taken together, the humanized mouse model of EBV infection not only contributes to the understanding of disease pathogenesis, it also provides a platform for the evaluation of therapeutics.

Table 1.5: Utility of the humanized mouse model for modeling EBV-associated diseases in recent years

Mouse strain	HPCs source	Virus strain	Findings	References
NSG	Fetal liver	B95-8	EBV lytic gene (BZLF1) expression enhances lymphoma formation	Ma et al., 2011
NSG	Fetal liver	B95-8	EBNA-3B functions as a suppressor of lymphomagenesis	White et al., 2012
NOG	Cord blood	Akata	Modeling of EBV-PTLD and persistent infection	Yajima et al., 2008
NOG	Cord blood	Akata	T cell-mediated control of EBV infection	Yajima et al., 2009
NSG-A2	Cord blood	B95-8	HLA-A2-restricted and EBV-specific T cell responses	Shultz et al., 2010
NSG	Cord blood	B95-8	$CD4^+$ T cells modulate latency III expression in EBV-infected B cells	Heuts et al., 2014
NSG	Cord blood	B95-8	Development of EBV-induced lymphomas is immune cell composition-dependent	Lee et al., 2014
NSG	Fetal liver	B95-8	Adoptive transfer of EBV-specific $CD8^+$ T cells to control EBV infection	Antsiferova et al., 2014
NOG	Cord blood	B95-8	Treatment of EBV lymphoproliferative disorder with *ex vivo* expanded T cells	Matsuda et al., 2015
NSG	Fetal liver	B95-8	Checkpoint blockade of PD-1/CTLA-4 enhances T cells control of EBV-induced lymphomas	Ma et al., 2016

1.6.2 Improvements on the humanized mouse model

Since the introduction of humanized mouse technology 30 years ago, various efforts have focused on improving the specificity of T cells and engraftment of human innate cells in the humanized mice. The lack of specificity in the reconstituted T cells could be attributed to the suboptimal development and maturation processes involving the interactions between human T cells and pMHC on murine thymic epithelial cells [185]. To circumvent the lack of specificity, McCune et al. developed the BLT (bone marrow-liver-thymus) humanized mouse, which requires the co-implantation of fetal liver and fetal thymus, followed by the injection of autologous HPCs [157, 186].

The BLT mice are regarded as the gold standard of humanized mouse models as they provide a more extensive engraftment of human immune cells, with human immune cells reconstitution observed in the reproductive and gastrointestinal tract of mice, catering to the study of the mucosal transmission of HIV [187, 188]. Furthermore, due to the implantation of human thymic organoid, reconstituted human T cells are positively selected in the human leukocyte antigen milieu, giving rise to specific immune responses. In the context of EBV, Melkus et al. demonstrated that the reconstituted human T cells in BLT humanized mice were capable of mounting HLA-restricted EBV-specific responses [174, 189]. In spite of the advantages of BLT humanized mice, the limited availability of fetal samples and the requirement of surgical procedures restrict its widespread adoption and usage in laboratories.

The improvement of human innate cells reconstitution is another aspect which has gained significant attention in recent years. Although the use of immunodeficient mice has improved the engraftment of human immune cells, due to the lack of appropriate cytokine for differentiation and maintenance, the reconstitution of human innate cells and NK cells have remained low [190-192]. To enhance the reconstitution of these cells, many approaches such as cytokine transgene expression [193-195] and the injection of cytokines [196, 197] or vectors encoding these cytokines have been attempted [198, 199].

While these approaches are reliable in enhancing the reconstitution of human immune cells, each has their own disadvantages. The employment of cytokine transgene expression ensures constitutive gene expression. However, the development of transgenic mice is technically difficult and time-consuming. In the most sophisticated transgenic mice, Rongvaux et al. generated the MITRG (Human macrophage colony-stimulating factor, IL-3/granulocyte macrophage colony-stimulating factor and thrombopoietin transgenic $Rag2^{-/-}IL2R\gamma^{-/-}$ mice) and MITSRG (MITRG mice with human SIRPα transgene) mice to enhance the development and function of human innate cells and NK cells [200]. Reportedly, the reconstituted human NK cells and phagocytes in these transgenic humanized mice were capable of eliciting cytotoxicity and phagocytosis respectively. While these mice are available commercially, they are costly to acquire. A similar consideration of cost is ascribed to the use of cytokine injection. Due to the short-lived effects of cytokines, multiple maintenance injections are required to sustain their functions *in vivo*.

HDI of vectors encoding human cytokines is an alternative approach to improve the reconstitution of human immune cells. HDI is a technique introduced by Suda et al. in 2007, where a large volume of plasmids-containing solution is rapidly injected into a mouse, causing high pressure to the liver, forcing the uptake and subsequent expression of these plasmids by hepatocytes [201]. Such method has been demonstrated to be efficient and cost-effective, with the systemic distribution of the expressed human cytokines enhancing the differentiation of reconstituted human immune cells [198, 202, 203].

One major area that still requires more effort is the reconstitution of human epithelial cells for modeling oropharyngeal EBV infection *in vivo*. As the oropharyngeal site is an important niche for EBV infection, the lack of human epithelial cells restricts recapitulation of a complete EBV life cycle in the humanized mouse. Future endeavors on the humanized mouse modeling will have to strive towards the enhancement of human hematopoiesis and the development of more robust immune responses that bear a closer resemblance to that of humans. High cost, intensive technical skill and the need of controversial fetal samples are the challenges that have to be overcome.

Chapter 2:
Materials and Methods

2.1 Declarations

Human umbilical cord blood was obtained from the Singapore Cord Blood Bank. Human fetal tissues (livers, femurs, and spleens) were obtained from aborted fetuses from KK Women and Children Hospital, Singapore. All human samples were obtained with written informed consent from donors and in accordance with the institutional ethical guidelines stipulated by the Institutional Review Board. Animal experiments were performed under the provision of National University of Singapore Institutional Animal Care and Use Committee (protocol #122/11).

2.2 Cell lines

Human Embryonic Kidney (HEK) 293T (ATCC® CRL-3216), T2 (ATCC© CRL-1992™), and Raji (ATCC© CCL-86™) cells were purchased from ATCC©. C1R-A2 (C1R BLCL transduced with HLA-A*0201) cells were kind gift from Dr. Gan Shu Uin (National University of Singapore, Department of Surgery). BLCLs (**Table 2.1**) with determined HLA-A haplotype, BJAB, and B95-8 marmoset cell lines (B95-8 EBV) were kind gifts from Emeritus Professor Chan Soh Ha (WHO Immunology and Training Research Centre, Singapore). Primary macrophages were cultured in Dulbecco's Modified Eagle Medium (DMEM). Unless stated, all cells were cultured in Roswell Park

Memorial Institute (RPMI)-1640 medium. Both DMEM (Hyclone™) and RPMI-1640 (Biowest) culture medium were supplemented with 10% (v/v) fetal bovine serum (FBS) and 1% (v/v) penicillin/streptomycin (Gibco™). All cells were cultured at 37°C in 5% CO_2 incubator. For cryopreservation, cells were resuspended in 1 ml of freeze medium (90% FBS and 10% dimethyl sulfoxide v/v), transferred into a cryogenic vial and placed in a CoolCell® cell freezing container.

Table 2.1: HLA-A haplotype of BLCLs

BLCLs	HLA-A Haplotype	
AM001	0201	0201
AM002	0201	1101
CF508	0201	3303
CF522	3101	3303
CF884	0201	3303
CF888	1101	1101
CF893	0201	2402
CF986	0201	0201
CF990	0201	3303
CF1018	0201	0203
CF1059	0201	1101
CF1097	0201	0207
CM462	0201	3303
CM800	0201	0201
CM956	0203	0207

2.3 Peptides

All peptides were synthesized by Mimotopes with purity (>95%) determined by analytical high-performance liquid chromatography. (**Table 2.2**)

Table 2.2: List of peptides

Pathogen	Protein	Peptide Sequences
Epstein-Bar virus (B95-8 prototype)	EBNA-$1_{562-570}$	FMVFLQTHI
Epstein-Bar virus (B95-8 prototype)	LMP$1_{125-133}$	YLLEMLWRL
Epstein-Bar virus (B95-8 prototype)	LMP2A$_{426-434}$	CLGGLLTMV
Cytomegalovirus	Phosphoprotein $65_{495-503}$	NLVPMVATV
Influenza A virus	Matrix protein$_{58-66}$	GILGFVFTL

2.4 Peptide pulsing

2 X 10^6 cells were treated with 1 ml of citric acid medium (pH 3.0 in 1% bovine serum albumin (BSA) w/v) for 2 min at 4^{o}C to remove pre-existing surface pMHC complexes prior to peptide pulsing. Cells were washed twice with 1X phosphate-buffered saline (PBS), pulsed with the respective peptides as shown in **Table 2.2** and incubated for 3 h at 37^{o}C with 5% CO_2 incubator. Pulsed cells were then washed and stained with α-EBNA TCR-like mAb (refer to section **2.17.1** for details on using α-EBNA TCR-like mAb for the staining of surface EBNA-1 pMHC).

2.5 Antibodies

Unconjugated antibodies included both commercial and in-house produced α-EBV TCR-like mAbs (**Table 2.3**). Conjugated secondary antibodies, Alexa Flour® 488 goat α-mouse IgG (H+L) antibody (#A-11001), Alexa Fluor® 488 goat α-rat IgG (H+L) antibody (#A-11006), goat α-mouse IgG horseradish peroxidase (HRP) (#31430), and goat α-rabbit IgG HRP (#31460) were purchased from Thermo Fisher Scientific. Fluorophore-conjugated antibodies for flow cytometry application were purchased from BioLegend and BD Biosciences (**Table 2.4**).

HLA-A*02-restricted α-EBNA-1 TCR-like mAb was generated using the classical hybridoma technology and previously described in Ms. Eio Yating Michelle Master's Thesis (ScholarBank@NUS #4087). For flow cytometry application, purified antibodies were diluted with glycerol, aliquoted at 1 mg/ml and stored at -80^{o}C. Antibodies for phagocytosis assay and *in vivo* treatment were diluted in 1X PBS and sterile-filtered through a 0.22 µm filter.

2.6 Site-directed mutagenesis

α-EBNA-1 TCR-like mAb (FcγR-null binding variant) with D265A point mutation was generated by replacing aspartic acid at position 265 with alanine using the QuikChange Site-Directed Mutagenesis Kit (Stratagene), in accordance with the manufacturer's instructions.

Table 2.3: List of unconjugated antibodies

Target	Company	Catalogue Number
β2-microglobulin (Polyclonal)	Abcam	ab6608
EBNA-1 (Polyclonal)	Fitzgerald	20-EG46
EBNA-1 (0211)	Santa Cruz Biotechnology	sc-57719
α-EBNA-1 TCR-like mAb	In-house purified	-
EBNA-2 (PE2)	Abcam	ab90543
GAPDH (6C5)	Millipore	MAB374
GFP (FM264G)	BioLegend	338002
HLA-A2 (BB7.2)	In-house purified	-
α-LMP1 TCR-like mAb	In-house purified	-
Mouse IgG1 Isotype Control (MOPC-21)	BioLegend	400166

Fluorophores: allophycocyanin (APC), cyanine 5.5 (Cy5.5), cyanine 7 (Cy7), fluorescein isothiocyanate (FITC), phycoerythrin (PE), and peridinin chlorophyll (PerCP).

Table 2.4: List of conjugated antibodies

Target (clone)	Fluorophore	Company	Catalogue Number
CD3 (OKT3)	APC	BioLegend	300312
CD4 (OKT4)	APC	BioLegend	317416
CD10 (HI10a)	APC	BioLegend	312210
CD19 (HIB19)	APC	BioLegend	302212
CD27 (O323)	APC	BioLegend	302809
CD34 (561)	APC	BioLegend	343510
CD38 (HB-7)	APC	BioLegend	356606
CD40 (5C3)	APC	BioLegend	334310
CD56 (HCD56)	APC	BioLegend	318310
CD95 (DX2)	APC	BioLegend	305612
CD138 (DL-101)	APC	BioLegend	352308
IgM (MHM-88)	APC	BioLegend	314510
CD3 (SK7)	APC-Cy7	BioLegend	344818
hCD45 (HI30)	APC-Cy7	BioLegend	304014
CD4 (OKT4)	FITC	BioLegend	317408
CD10 (HI10a)	FITC	BioLegend	312208
CD14 (M5E2)	FITC	BioLegend	301804
CD21 (LT21)	FITC	BioLegend	315104
CD40 (G28.5)	FITC	BioLegend	303604
hCD45 (HI30)	FITC	BioLegend	304006
CD138 (1D4)	FITC	BioLegend	344404
Igκ (MHK-49)	FITC	BioLegend	316506

Target (clone)	Fluorophore	Company	Catalogue Number
CD5 (UCHT2)	PE	BioLegend	300608
CD11b (M1/70)	PE	BD Biosciences	553311
CD19 (HIB19)	PE	BioLegend	302208
CD20 (2H7)	PE	BioLegend	302306
CD69 (FN50)	PE	BioLegend	310906
CD86 (IT2.2)	PE	BioLegend	305405
HLA-A2 (BB7.2)	PE	BioLegend	343306
HLA-DR (L243)	PE	BioLegend	307606
Igλ (MHL-38)	PE	BioLegend	316608
IgD (IA6-2)	PE	BD Biosciences	557799
mCD45.1 (A20)	PE	BioLegend	110708
NKp46 (9E2)	PE	BioLegend	331908
CD10 (HI10a)	PE-Cy7	BioLegend	312214
CD19 (HIB19)	PE-Cy7	BioLegend	302216
hCD45 (HI30)	PE-Cy7	BioLegend	304016
CD80 (2D10)	PE-Cy7	BioLegend	305218
CD86 (IT2.2)	PE-Cy7	BioLegend	305422
mCD45.1 (A20)	PE-Cy7	BioLegend	110730
HLA-DR (L243)	PE-Cy7	BioLegend	307616
CD8 (SK1)	PerCP-Cy5.5	BioLegend	344710
CD11c (Bu15)	PerCP-Cy5.5	BioLegend	337210
CD23 (EBVCS-5)	PerCP-Cy5.5	BioLegend	338518
CD34 (581)	PerCP-Cy5.5	BioLegend	343522
CD38 (HB-7)	PerCP-Cy5.5	BioLegend	356614
hCD45 (HI30)	PerCP-Cy5.5	BioLegend	304028
CD138 (1D4)	PerCP-Cy5.5	BioLegend	344406
IgM (MHM-88)	PerCP-Cy5.5	BioLegend	314512

2.7 Plasmids construction

Both wild type (WT) EBNA-1 (1923 nucleotides) and E1ΔGA (1218 nucleotides) were cloned into pUC57 (GenScript). DNA fragments incorporating BamHI and XbaI restriction sites were amplified with AccuPrime™ *Pfx* DNA polymerase (Invitrogen) using sense primer sequence (5'-TTGGATCCACCATGTCTGACGAGGGGCCAGGTACA-3') and antisense primer sequence (5'-TTTCTAGACCCTCCTGCCCTTCCTCACCCTCATC-3'). Polymerase chain reaction (PCR) was performed in accordance to manufacturer's protocol (Invitrogen). PCR amplicons were then subjected to 1% gel electrophoresis, gel extracted with QIAquick® gel extraction kit (Qiagen) and cloned into the BamHI and XbaI restriction sites of pcDNA™3.1 V5-His-TOPO vector (Invitrogen). For the incorporation of green fluorescent protein (GFP)-2A into the 5' upstream of WT EBNA-1 and E1ΔGA (both constructs were in pcDNA™3.1 V5-His-TOPO vector as described above), DNA fragments incorporating flanking BamHI restriction sites were amplified with AccuPrime™ *Pfx* DNA polymerase using sense primer sequence (5'-GGATCCATGGTGAGCAAGGGC-3') and antisense primer sequence (5'- GGATCCGGGCCCAGGGTT-3'). All constructs were transformed into JM109 competent cells (Promega) and plated on ampicillin plate for selection. Sanger sequencing (1st BASE) was performed to verify clones prior to large-scale plasmid purification using Endofree Plasmid Maxi Kit (Qiagen).

2.8 Plasmid transfection

HEK293T cells were seeded at a density of 1 X 10^5 cells per well (in a 6-well plate) in penicillin-streptomycin-free culture medium on the day before transfection. Transfection was performed using plasmids encoding WT EBNA-1, E1ΔGA, GFP-2A WT EBNA-1, and GFP-2A E1ΔGA. 4 µg of each endotoxin-free plasmid was transfected into cells using Lipofectamine® 2000 Transfection Reagent (Invitrogen). Transfection was performed according to manufacturer's protocol. Cells were harvested at various time points for Western blot and flow cytometric analysis.

2.9 Western blot analysis

Cells were pelleted and lyzed with 1X radioimmunoprecipitation assay (RIPA) buffer (Millipore) containing ethylenediaminetetraacetic acid (EDTA)-free protease inhibitor (Roche) for 15 min on ice. Bradford protein quantification assay was performed and 40 µg of cell lysates were boiled (with SDS and β-mercaptoethanol) at 95^{o}C for 10 min. Samples were separated on 10% SDS-PAGE and transferred onto a polyvinylidene difluoride membrane. Membranes were blocked overnight at 4^{o}C with 5% (w/v) skimmed milk (Sigma-Aldrich) diluted in 1X PBST (0.1% Tween-20 in 1X PBS). Both primary and secondary antibodies were diluted with 3% (w/v) skimmed milk. Protein detection

was performed using Western Lightning Chemiluminescence (Perkin Elmer) and exposed onto a photographic film (GE Healthcare).

2.10 pMHC enzyme-linked immunosorbent assay (ELISA)

Biotinylated recombinant human HLA-A*0201 molecules (5 µM) with bounded UV-cleavable peptides were subjected to UV light for 15 min on ice to initiate peptide exchange. 500 µM of rescue peptides (EBNA-1 peptide, FMVFLQTHI) or control peptides from influenza A virus $M1_{58-66}$ were added and incubated at 37^{o}C for 1 h to facilitate the exchange. pMHC complexes with their respective exchanged peptides were added onto streptavidin-coated ELISA plate in quadruplicates and incubated for 1 h on ice to allow binding to the coated streptavidin. The plate was washed four times with 1X PBST prior to the addition of the 10X serially diluted α-EBNA-1 TCR-like mAb. The plate was incubated on ice for 90 min and washed four times with 1X PBST before adding 25 µl of HRP-conjugated goat α-mouse antibody (diluted in 1:10,000 with 2% BSA in 1X PBS). The reaction was incubated for another 30 min on ice and washed before adding 25 µl of 2, 2'-azino-bis (3-ethylbenzothiazoline-6-sulphonic acid) substrate solution (Invitrogen). The plate was incubated at room temperature (RT) for 15 to 20 min to allow the reactions to develop. 12.5 µl of stop buffer containing 1% sodium azide and 0.1 M citric acid was added to halt further colorimetric changes. Absorbance was measured on a spectrophotometer at 415 nm.

2.11 EBV production

The B95-8 marmoset cell line producing a prototypic B95-8 strain of EBV was cultured for virus production. Cells were seeded at a density of 1 X 10^6 cells/ml, and induced with 0.3 M of sodium butyrate and 200 ng/ml of 12-O-Tetradecanoylphorbol-13-acetate for 48 h. Thereafter, cells were washed with culture medium to remove inducer, re-seeded at a density of 1 X 10^6 cells/ml and further cultured another 14 days without passaging. After 14 days of starvation, the culture supernatant was then centrifuged and filtrated through a 0.45 µm syringe filter. Aliquots of 15 ml virus supernatant were stored at -80^{o}C.

2.12 BLCL generation

For *in vitro* EBV infection, cells were resuspended to a density of 2 X 10^6 cells/ml, with an equal volume of EBV supernatant added. The cell-virus mixture was then incubated at 37^{o}C with 5% CO_2 incubator for 2 h. After incubation, cells were washed, pelleted and resuspended to a density of 1 X 10^6 cells/ml using culture medium supplemented with 1 µg/ml cyclosporin A (Sigma-Aldrich). Cells were then aliquoted at 100 µl per well in a 48-well plate, and incubated for two to three weeks for the formation of macroscopic B cell clusters. Culture medium was supplemented with cyclosporin A for the first 14 days and removed thereafter.

2.13 Annexin V apoptosis assay

1.0 X 10^5 BLCL was resuspended in Opti-MEM® Reduced-Serum Medium (Gibco™) and seeded onto a 24-well plate. Cells were treated with 1 µg (or 10 µg) of α-EBNA-1 TCR-like mAb and incubated at 37°C with 5% CO_2 incubator. As a positive control, cells were treated with 1 µM camptothecin (anti-neoplastic alkaloid) to induce apoptosis. Mouse IgG1 isotype control antibody treatment was used as a negative control. Cells were harvested at 6 h and 24 h time points, pelleted and washed with 1 ml of 1X annexin binding buffer. A master mix constituting of 1 µl of 7-Aminoactinomycin D (7-AAD) (Sigma-Aldrich) and 2 µl annexin V Pacific Blue™ Conjugate (Thermo Fisher Scientific) per sample was prepared and added to each tube. Incubation was carried out at RT (in the dark) for 15 min. 200 µl of 1X annexin binding buffer was added to each sample prior to flow cytometry acquisition.

2.14 Cell isolation techniques

2.14.1 PBMC (peripheral blood mononuclear cells) isolation

Human peripheral blood was collected using BD Vacutainer® K2 EDTA (K2E) blood collection tube (BD Biosciences). The collected blood was mixed well with 1X sterile-filtered PBS (in 1:1 ratio). 30 ml of the blood mixture was then layered over 15 ml of Ficoll-Paque PLUS (GE Healthcare Life Sciences) in a 50 ml conical centrifuge tube (in the ratio of 2 ml of blood mixture: 1ml of ficoll). Cells were centrifuged at 400 X g for 30 min at RT (brake OFF). After centrifugation, PBMC was aspirated from the Ficoll-plasma interface using a 2 ml Pasteur pipette. Cells were then washed twice with 30 ml of 1X PBS and centrifuged at 300 X g for 5 min. Isolated PBMC was either utilized for the generation of BLCL or processed for the staining with α-EBNA-1 TCR-like mAb.

2.14.2 HPCs isolation

HPCs were isolated using EasySep^{TM} Human CD34 Positive Selection Kit (STEMCELL Technologies), in accordance with the manufacturer's protocol. An equal volume of 0.2 mM EDTA 1X PBS was added to the cord blood, mixed and gently layered onto Leucosep® Tubes (Greiner Bio-One) containing 15 ml of Ficoll-Paque PLUS. Blood fractionation to separate the buffy coat from the plasma and erythrocyte fractions was

conducted as per PBMC isolation. Several fractions of the buffy coat were pooled, pelleted and resuspended in 10 ml of ACK (ammonium-chloride-potassium) lysis buffer (Gibco^{TM}). Red blood cells were lyzed for 10 min at RT. 40 ml (4X volume of lysis buffer) of 0.2 mM EDTA 1X PBS was added to quench the lysis reaction prior to immunomagnetic cell separation. Automated cell separation was performed with a pre-programmed and customized $CD34^+$ selection protocol on the RoboSep™ machine. Cells were isolated under sterile condition, and both $CD34^+$ and negative $CD34^-$ fractions were collected and cryopreserved.

2.14.3 Human CD19 positive cells isolation

Immunomagnetic selection of human CD19 positive cells was performed using EasySep^{TM} Human CD19 Positive Selection Kit (STEMCELL Technologies), in accordance with the manufacturer's protocol. A single cell suspension of fetal liver $CD34^-$ fraction, fetal bone marrow, and fetal spleen were resuspended to the density of 2.5 X 10^6 cells/ml. Positive selection cocktail which contained a monoclonal antibody specific for CD19 was added to the cells and incubated at RT for 15 min. EasySep® Magnetic Nanoparticles were added to the cells, mixed and incubated at RT for 10 min. The mixture was inserted into a magnetic holder, followed by decanting the supernatant in a single continuous motion. The tube was then returned

to an upright position with CD19 positive cells magnetically attached to the tube. Cells were washed thrice with 3 ml of 1X PBS. Isolated cells were immunophenotyped via flow cytometry prior to *in vitro* EBV infection.

2.14.4 Murine macrophage isolation

To obtain macrophage progenitor cells, femurs of BALB/c mouse were harvested with both ends of the epiphysis partially cut to enable flushing of the bone marrow. Flushing of the bone marrow was performed using a 27-gauge needle. Single cell suspension was obtained by homogenizing the bone marrow and passing the sample through a 70 µm cell strainer (Corning®). ACK lysing buffer was used for the removal of red blood cell. Cells were washed twice with 1X PBS and cultured in DMEM supplemented with 10% FBS (v/v), 1% (v/v) penicillin-streptomycin and 20 ng/ml of recombinant murine macrophage colony-stimulating factor (R&D Systems). Macrophage progenitor cells were cultured for seven days to allow macrophage differentiation. Differentiated macrophages were harvested for phagocytosis assay.

2.15 *In vitro* phagocytosis assay

Murine bone marrow-derived macrophages were harvested from the femurs for phagocytosis assay. To determine the effect of α-EBNA-1 TCR-like mAb pre-incubation on phagocytosis, 10 µg of α-EBNA-1 TCR-like mAb was added to the BLCL and incubated for 24 h prior to phagocytosis. For phagocytosis assay, 0.5-1 X 10^6 macrophages were either seeded directly into a 12-well plate (for flow cytometry) or onto 18 mm coverslip within a 12-well plate (for microscopy). Macrophages were cultured in DMEM supplemented with 10% FBS (v/v) and 1% (v/v) penicillin-streptomycin and allowed to adhere overnight for at least 20 h. On the day of phagocytosis, the culture medium of the macrophages was removed and replaced with Opti-MEM® Reduced-Serum Medium. In parallel, 0.25 µl of carboxyfluorescein succinimidyl ester (CFSE) was added to 4 X 10^6 BLCL and incubated at RT (in the dark) for 10 min to label the BLCL. 5 µg of α-EBNA-1 TCR-like mAb (or mouse IgG1 isotype control antibody) was added to the labeled-BLCL and incubated for 3 h before co-culturing with the macrophages at the ratio of 1: 1 (macrophage: BLCL). Cells were co-cultured in a 37^{o}C with 5% CO_2 incubator for 4 h to allow phagocytosis to occur. Refer to section **2.17.3** and **2.19.1** for flow cytometry and fluorescent microscopy analysis of phagocytosis.

2.16 *In vivo* experiments

2.16.1 Mouse xenograft modeling and treatment regimen

2 X 10^6 BLCL was injected into 15 weeks old NSG mouse via the tail vein. Mice were then euthanized one week post-injection, with bone marrows, blood, brains, kidneys, livers, lungs, and spleens harvested to check for the infiltration of BLCL. In another separate batch, mice were kept for disease monitoring and euthanized when mice had more than 20% weight loss or found moribund. Flow cytometry staining for human pan-leukocyte marker CD45 (hCD45), mouse pan-leukocyte marker CD45 (mCD45), and human CD19 was conducted to determine the percentage of BLCL infiltration.

To evaluate the therapeutic effect of α-EBNA-1 TCR-like mAb, BLCL-injected mice were treated with a single weekly injection of 300 μg of α-EBNA-1 TCR-like mAb one week post-BLCL injection (on week 16). Mice treated with 300 μg of mouse IgG1 isotype control antibody (BioLegend) were used as a control. Criteria for euthanasia and flow cytometric analysis were adhered as abovementioned.

2.16.2 Autologous humanized mice

In-house bred NSG pups born within 48 h were sublethally irradiated with 100 cGy gamma irradiation. Frozen human cord blood $CD34^+$ HPCs were thawed and counted by trypan blue exclusion. 2 X 10^5 $CD34^+$ HPCs were injected into each of the NSG pups via the intracardiac route. At 12 weeks post-reconstitution, facial bleeding followed by flow cytometry staining with mCD45 versus hCD45 were used to determine the percentage chimerism.

To establish an autologous humanized mouse model, autologous BLCL was injected into humanized mice reconstituted with $CD34^+$ HPCs from the same donor. 8 X 10^6 autologous BLCL was injected intravenously via the tail vein into matching humanized mice and monitored for 18 weeks (30 weeks old). Humanized mice injected with control medium were used as a control. Mice were monitored for their body weight and bled weekly for flow cytometric analysis of peripheral blood lymphocytes.

2.16.3 Hydrodynamic injection (HDI)

pcDNA3.1 (+) vectors (Invitrogen) encoding human IL-15 and FMS-like tyrosine kinase 3 ligand (FLT3L) gene were purified separately using PureYield™ Plasmid Maxiprep Kit (Promega). A single intravenous injection of IL-15 and FLT3L plasmids (50 µg each) in 1.8 ml of 1X PBS was performed on 13 weeks old, fetal liver $CD34^+$ HPCs-reconstituted humanized mice within 7 s using a 27-gauge needle. Mice were checked for their chimerism on week 12 and HDI was performed on week 13. Mice were injected with autologous BLCL generated from the fetal spleen at week 14 and bled weekly from week 14 to 17 for flow cytometric analysis of human immune cells reconstitution.

2.17 Flow cytometry acquisition and analysis

Flow cytometry buffer solution contained 0.2% BSA (w/v) and 0.05% (v/v) sodium azide in 1X PBS. For live/dead staining, samples were resuspended with 300 µl of flow cytometry buffer before the acquisition. All samples were acquired on BD LSRFortessa™ (Becton Dickinson). Dead cells were excluded by DAPI (4', 6-diamidino-2-phenylindole) staining and data was analyzed using FlowJo software v 7.6.5 (TreeStar).

2.17.1 Surface staining (EBV pMHC)

3 X 10^5 HLA-A*02 BLCL was harvested and resuspended in 100 µl of flow cytometry buffer. Cells were stained with 5 µl of 1 mg/ml α-EBV TCR-like mAb (α-EBNA-1 TCR-like mAb or α-LMP1 TCR-like mAb) and incubated for 3 h before staining with Alexa Flour® 488 goat α-mouse IgG (H+L) secondary antibody for 1 h. Non-HLA-A*02 BLCL and HEK293T cells were used as the control cell lines, while mouse IgG1 isotype antibody was used as a staining control. The α-HLA-A2 antibody was used as a positive control. nMFI was calculated by taking the MFI of an antibody staining divided by the MFI of its respective isotype control.

2.17.2 Surface staining (immunophenotyping)

Immunophenotyping of BLCLs, human PBMC, human fetal tissues (livers, femurs, and spleens) and the peripheral blood of humanized mice was conducted. All primary cells (except BLCLs) were lyzed with ACK lysis buffer for 5 to 10 min at RT, washed and stained with a cocktail of different fluorophore-conjugated antibodies (**Table 2.4**). Staining was incubated at 4^{o}C for 30 min, washed twice with flow cytometry buffer solution prior to acquisition.

2.17.3 Surface staining (phagocytosis assay)

Cells from phagocytosis assay (in a 12-well plate) were trypsinized, washed and stained with PE rat α-mouse CD11b. Staining was incubated for 30 min and washed twice prior to flow cytometry acquisition. Phagocytosis was defined by the $CFSE^{+}$ $CD11b^{+}$ cells in the second quadrant (Q2) of the CFSE (BLCL) versus CD11b (macrophage) plot.

2.17.4 Intracellular staining

3 X 10^5 cells were permeabilized by resuspending in 250 µl of BD Cytofix/Cytoperm solution (BD Biosciences) and incubated at 4^oC for 20 min. Permeabilized cells were washed twice with 1 ml of BD Perm/Wash buffer, stained with 5 µl of 1 mg/ml commercial α-EBNA-1 antibody and incubated at 4^oC for 1 h. Staining with mouse IgG1 isotype control antibody was used as a negative control. Subsequently, cells were washed and stained with Alexa Flour® 488 goat α-mouse IgG (H+L) secondary antibody for 1 h before flow cytometry acquisition.

2.18 Histology

2.18.1 Tissue processing and sectioning

Fresh mouse organs were harvested and fixed in 10% neutral buffered formalin (Sigma-Aldrich) overnight. Fixed samples were then transferred to a semi-enclosed benchtop tissue processor (Leica Biosystems) and processed on a preset protocol with programmed ethanol dehydration gradient of 50%, 70%, 80%, 90% and then twice in 100%, for 1 h at each step. Subsequently, samples were incubated in xylene: ethanol (50%: 50%) followed by immersing twice in 100% xylene for 1 h before transferring to molten paraffin and embedded onto histology cassettes. Formalin-fixed paraffin-embedded samples

were stored at RT, sectioned to 4 µm thickness using microtome (Leica Biosystems) and mounted on SuperFrost Plus charged slides (Fisher Scientific).

2.18.2 Hematoxylin and eosin (H&E) staining

Formalin-fixed, paraffin-embedded sections were rehydrated by immersing in gradient ethanol in the reverse order of dehydration, for 1 min at each step. Slides were then immersed in filtered-hematoxylin for 5 min, followed by 0.25% HCl for 3 s. After which, slides were rinsed gently in running water for 3 min and then stained with 0.5% aqueous eosin for 30 to 40 s. Thereafter, slides were rinsed in distilled water before adding slide mounting medium (Sigma-Aldrich).

2.19 Imaging

2.19.1 Fluorescent microscopy

Cells from phagocytosis assay (on the coverslip in the 12-well plate) were fixed with 0.8 ml of 4% paraformaldehyde at RT for 10 min. After fixation, 1.0 ml of 1X PBS (supplemented with 3% FBS, 0.5% mouse serum and 0.5% rat serum) was added and blocked overnight. Macrophages were stained with PE rat α-mouse CD11b for 1 h at RT in a humidified chamber, then washed and stained with Hoechst dye before mounted onto a glass slide with ProLong® Antifade reagent (Thermo Fisher Scientific). Phagocytosis was imaged using Olympus IX81 inverted fluorescence microscope with MetaMorph® software (at 40X objective). Successful phagocytosis was indicated by the colocalization of $CFSE^+$ BLCL and $CD11b^+$ macrophage. $CFSE^+$ $CD11b^+$ cells were counted over three field of view (FOV) and phagocytic index (PI) was computed based on: (% macrophage with at least one BLCL) X (average number of BLCL per phagocytic cell). At least 200 macrophages were counted for each sample.

2.19.2 Confocal microscopy

BLCL was cultured overnight on 18 mm poly-L-lysine coated coverslip. Cells were then fixed with 4% paraformaldehyde at RT for 10 min before staining with α-EBNA TCR-like mAb and rabbit α-β2-microglobulin antibody for 2 h at RT in a humidified chamber. Cells were stained with polyclonal goat α-mouse IgG RPE (Dako) and polyclonal goat α-rabbit IgG Alexa Fluor® 488 (Life Technologies) for 1 h prior to nuclear staining with Hoechst dye. ProLong® Gold Antifade mountant was added and images (512 X 512 resolution) were acquired at 63X (with oil immersion) using Zeiss LSM 510 confocal microscope software v2.5 SP2. Images were subsequently processed using Adobe Photoshop CS6.

2.19.3 Digital slide scanner

Slides were scanned using MIRAX MIDI slide scanner (Carl Zeiss). H&E slides were scanned in brightfield while slides from phagocytosis assay were scanned in the fluorescent channel, with constant gain and exposure. Scanned images were analyzed using Pannoramic Viewer (3DHISTECH).

2.20 Statistical analysis

Statistical analysis including Student's *t*-test, Kaplan-Meier survival analysis, and Log-rank test was performed using GraphPad Prism. $p < 0.05$ was considered statistically significant.

Chapter 3:
Result (I)

3.1 Synopsis

EBNA-1 protein is expressed in all EBV-associated malignancies, and thus has been proposed as a good target for therapeutic development. Initially, protein degradation was thought to be the determinant of EBNA-1 antigen presentation, with studies reporting the presence of GAr within the protein auto-inhibiting its proteasomal degradation, thereby reducing EBNA-1 presentation [18, 51, 53-55]. However, subsequent studies detailed EBNA-1 protein synthesis as the principal determinant that underlies the generation of EBNA-1 peptides for antigen presentation [56-58].

In this chapter, we determined the effects of GAr on EBNA-1 protein translation by comparing EBNA-1 expression in HEK293T cells transfected with plasmids encoding full-length EBNA-1 or its GAr-deleted variant (E1ΔGA). Additionally, we used GFP as a surrogate marker for EBNA-1 expression to elucidate the role of GAr in EBNA-1 protein expression. To test whether EBNA-1 was indeed processed and presented on MHC class I molecules, we employed our in-house α-EBNA-1 TCR-like mAb to detect surface EBNA-1 pMHC complexes. We evaluated the specificity of α-EBNA-1 TCR-like mAb to bind to surface EBNA-1 pMHC via peptide pulsing of exogenous peptide and conducted staining of EBV-infected BLCL with the antibody to detect endogenously derived EBNA-1 pMHC.

3.2 Establishing an experimental workflow for EBNA-1 protein expression

To determine the role of GAr in EBNA-1 protein expression, plasmids encoding the full-length WT EBNA-1 (UniProt accession number: P03211) and E1ΔGA$_{90\text{-}325}$ (truncated variant deleted of the GAr) sequences were synthesized (**Figure 3.1** and **Appendix A**). Owing to the high guanine-cytosine content nature of the nucleotide sequence encoding the GAr region, a series of optimization was performed to obtain amplicons containing the correct number of GAr (**Figure 3.2A**). As shown in **Figure 3.2B**, larger bands (in lane 2 and 3) from the PCR corresponded to the WT EBNA-1 amplicons, while smaller bands observed in lane 4 and 5 corresponded to the E1ΔGA amplicons (lane 3 and 5 were diluted amplicons reflective of their actual size).

To allow the expression of plasmids encoding either WT EBNA-1 or E1ΔGA construct in the mammalian system (HEK293T), BamHI and XbaI restriction sites were incorporated into the 5' and 3' ends of each construct respectively for cloning into the multiple cloning site of the pcDNA™ 3.1 V5-His-TOPO vector. The sequence of WT EBNA-1 and E1ΔGA within the pcDNA™ 3.1 V5-His-TOPO vector were verified using Sanger sequencing prior to transfection. HEK293T cells were transfected with plasmids encoding either WT EBNA-1 or E1ΔGA and harvested at 4 h, day 1, 2, 3 and 5 to check for protein expression via Western blot analysis. As shown in **Figure 3.2C**, the onset of protein

expression was different in HEK293T transfected with the two constructs. In E1ΔGA-transfected cells, a band (between 55 to 70 kDa) corresponding to the truncated EBNA-1 ($E1\Delta GA_{90\text{-}325}$) protein was detected as early as day one post-transfection.

In contrast, a band (between 70 to 100 kDa) corresponding to the full-length WT EBNA-1 protein was detectable at day 3 post-transfection. Besides delayed protein expression, the amount of protein expressed by the WT EBNA-1-transfected cells was also relatively lower as compared to the E1ΔGA-transfected cells. This observation was in agreement with an earlier report by Yin et al., which showed that the presence of GAr sequence in the WT EBNA-1 protein inhibits its synthesis [204]. Furthermore, in WT EBNA-1-transfected cells, a single band corresponding to the full-length protein was observed. This is in contrast to the multiple smaller bands observed in E1ΔGA-transfected cells, suggesting possible degradation of the truncated protein, corresponding to the reported function of GAr in inhibiting proteasomal-dependent protein degradation [18, 51].

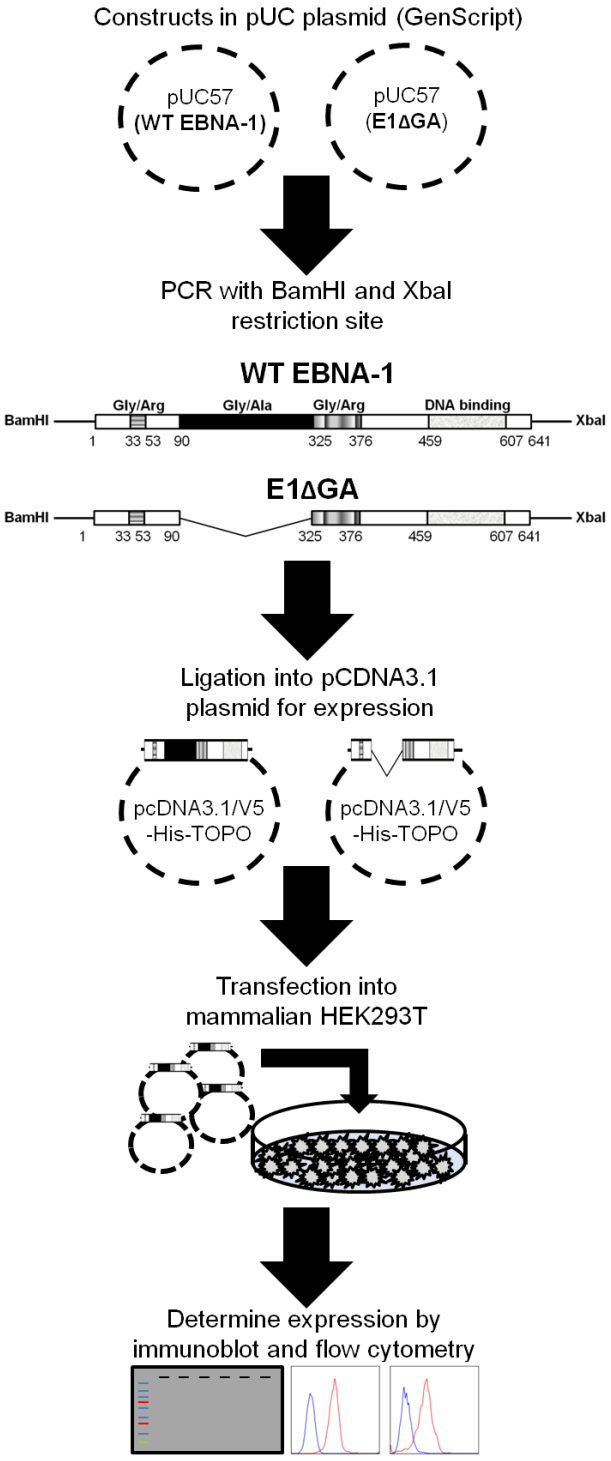

Figure 3.1: **Experimental workflow of EBNA-1 protein expression.** Constructs encoding full-length WT EBNA-1 and its truncated variant deleted of its GAr (E1ΔGA$_{90\text{-}325}$) were abbreviated as WT EBNA-1 and E1ΔGA respectively. Sequences encoding WT EBNA-1 and E1ΔGA were synthesized by GenScript and subcloned into pcDNA™ 3.1 V5-His-TOPO vector to enable cytomegalovirus promoter-driven translation upon transfection into mammalian HEK293T cells. Transfected cells were harvested at various time points to check for their protein expression using Western blot and flow cytometry.

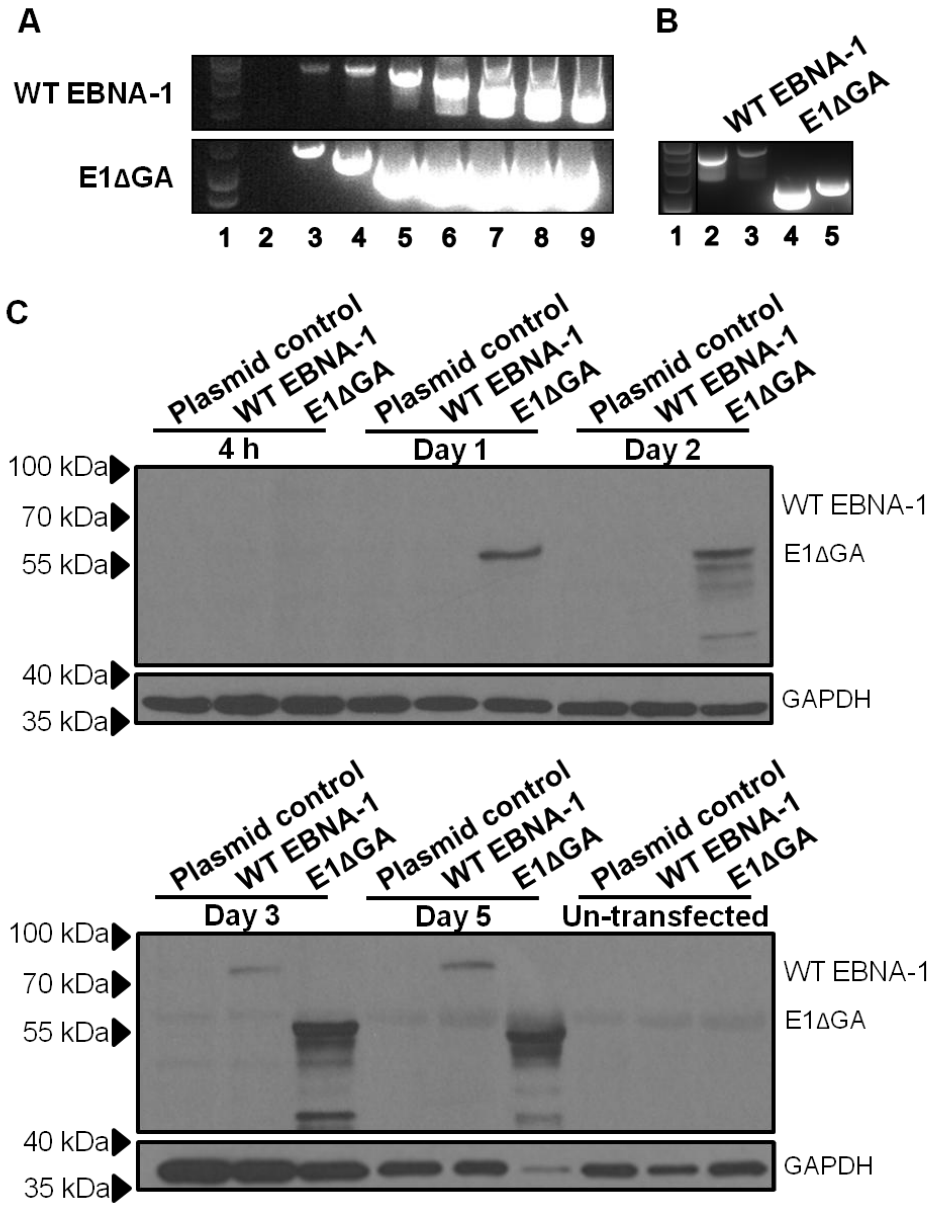

Figure 3.2: Cloning and expression of plasmids encoding WT EBNA-1 and E1ΔGA. (A) As the GAr within the WT EBNA-1 is guanine-cytosine-rich, numerous optimizations were required for its amplification. **(B)** WT EBNA-1 and E1ΔGA amplicons with BamHI and XbaI restriction sites were cloned into the pCDNA3.1/V5-His-TOPO vector. The size differences between WT EBNA-1 (lane 2 and 3) and E1ΔGA (lane 4 and 5) as observed on a 1% agarose gel, was due to the truncation (removal) of the GAr sequence in the E1ΔGA construct. **(C)** HEK293T cells were transfected with plasmids encoding WT EBNA-1 or E1ΔGA and harvested (at 4 h, day 1, 2, 3 and 5) for SDS-PAGE and Western blot. Protein expression was observed in E1ΔGA-transfected cells as early as day 1 post-transfection, as compared to day 3 post-transfection in the WT EBNA-1-transfectants. While a single band (between 70 to 100 kDa ladders) was detected in the whole cell lysates of WT EBNA-1-transfected cells, multiple smaller bands were observed in E1ΔGA-transfectants. Glyceraldehyde-3-phosphate dehydrogenase (GAPDH) was used as a loading control.

3.3 Employment of GFP-2A sequence as a surrogate marker for protein expression

GFP is a widely used reporter of gene expression in cell and molecular biology [205]. However, GFP has also been suggested to affect the function and degradation of fusion protein [206]. To overcome the issue of direct tagging with GFP, we employed the autocatalytic 2A peptide. Derived from the *Picornaviridae* family, the 2A peptide mediates a breakage between the glycine (G) and proline (P) residues via the mechanism known as 'ribosome skipping' (**Figure 3.3A**). Specifically, the autocatalytic activity is a result of steric hindrance between these two residues during peptide bond formation [207, 208]. The insertion of GFP-2A into the 5' ends of WT EBNA-1 and E1ΔGA respectively (abbreviated as GFP-2A WT EBNA-1 and GFP-2A E1ΔGA) permits the usage of GFP as a reporter for gene expression without hindering the translation of WT EBNA-1 and E1ΔGA proteins (**Figure 3.3B**). Importantly, GFP is co-translated as an individual protein and expressed at an equimolar concentration with WT EBNA-1 or E1ΔGA. To confirm that GFP was cloned into the correct reading frame, HEK293T cells were transfected with plasmids encoding either GFP-2A WT EBNA-1 or GFP-2A E1ΔGA and harvested 24 h post-transfection for readout via flow cytometry. As shown in **Figure 3.3C**, GFP expression was detected in cells transfected with both constructs, but not in the cells transfected with their non-GFP parental plasmids.

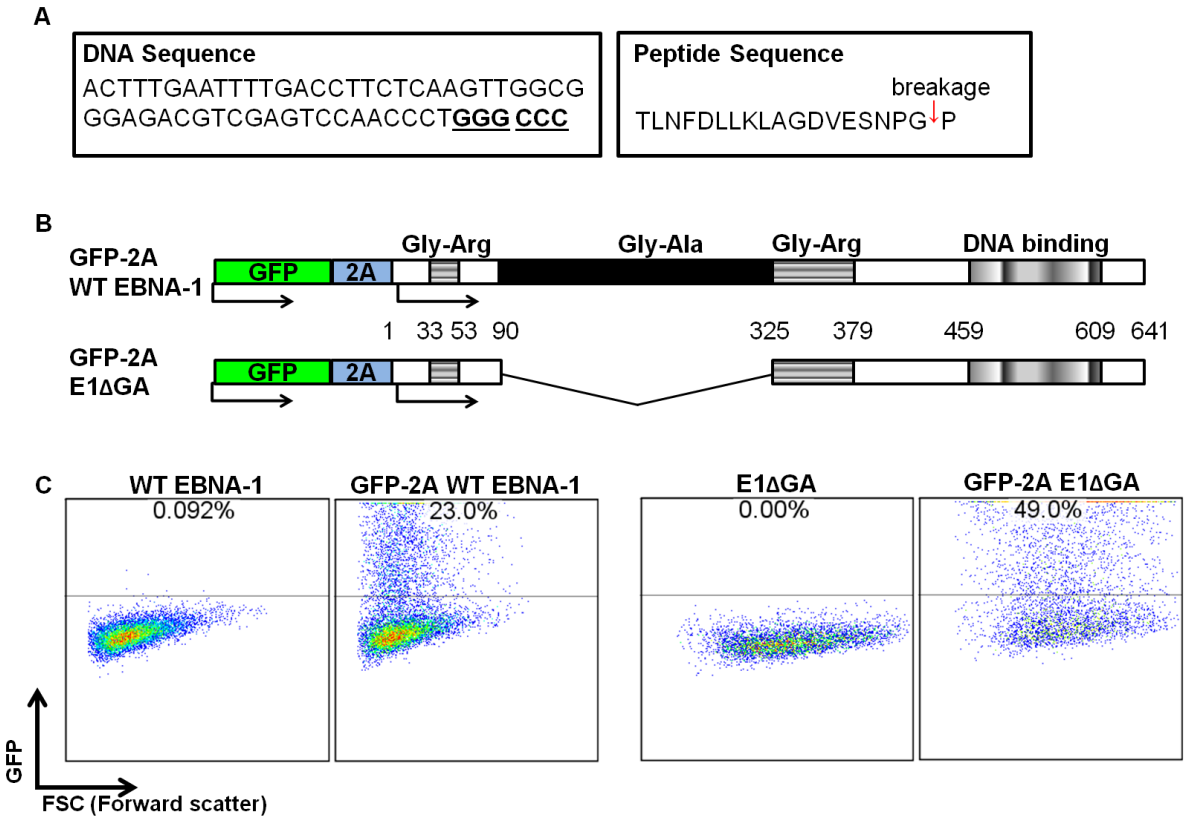

Figure 3.3: **Cloning and expression of plasmids encoding GFP-2A WT EBNA-1 and GFP-2A E1ΔGA. (A)** DNA and peptide sequences of the 2A peptide from foot-and-mouth disease virus (family: *Picornaviridae*). The DNA sequence encodes for a 19 amino acids, with GGG CCC (underlined) coding for glycine (G) and proline (P). The red arrow between glycine and proline indicates the site of 'ribosome skipping' and breakage. The utility of the 2A peptide enables the translation of individual proteins flanking the 2A sequence, in equimolar concentrations. **(B)** Schematic illustration of the cloning of GFP-2A into plasmid containing WT EBNA-1 (GFP-2A WT EBNA-1) and E1ΔGAr (GFP-2A E1ΔGA). The utilization of 2A peptide enabled equimolar co-translation of GFP and WT EBNA-1 or E1ΔGA, circumventing the potential inference of GFP in the translation, folding, trafficking or degradation of EBNA-1. **(C)** HEK293T cells were transfected with either the GFP-2A WT EBNA-1 or GFP-2A E1ΔGA plasmids, and harvested 24 h post-transfection. GFP expression was detected in both GFP-2A WT EBNA-1 and GFP-2A E1ΔGA-transfected cells as compared to their respective non-GFP control plasmids.

3.4 Elucidating the role of GAr in EBNA-1 expression

With the introduction of GFP into WT EBNA-1 and E1ΔGA constructs, we next assessed whether GFP expression could function as a surrogate marker for EBNA-1 protein expression. To this end, HEK293T cells were transiently transfected with either GFP-2A WT EBNA-1 or GFP-2A E1ΔGA plasmids and harvested over a time course of four days for the detection of GFP signal via flow cytometry. Transfected cells were additionally processed for intracellular detection of EBNA-1 protein.

GAr has been reported to reduce the availability of their fusion partner [52, 53, 55]. Consistent with these reports, lower GFP and EBNA-1 protein expression were observed in cells transfected with GFP-2A WT EBNA-1 across all time points in comparison to the GFP-2A E1ΔGA-transfectants (**Figure 3.4A and B**). Additionally, GFP and EBNA-1 displayed a similar trend in expression, suggesting that both proteins were co-translated and that GFP could be utilized as a marker for EBNA-1 protein expression (**Figure 3.4C**). These observations of reduced GFP and EBNA-1 expression provide support to the earlier findings that GAr within the WT EBNA-1 protein could function as an independent *cis*-inhibitory component, inhibiting protein synthesis in general.

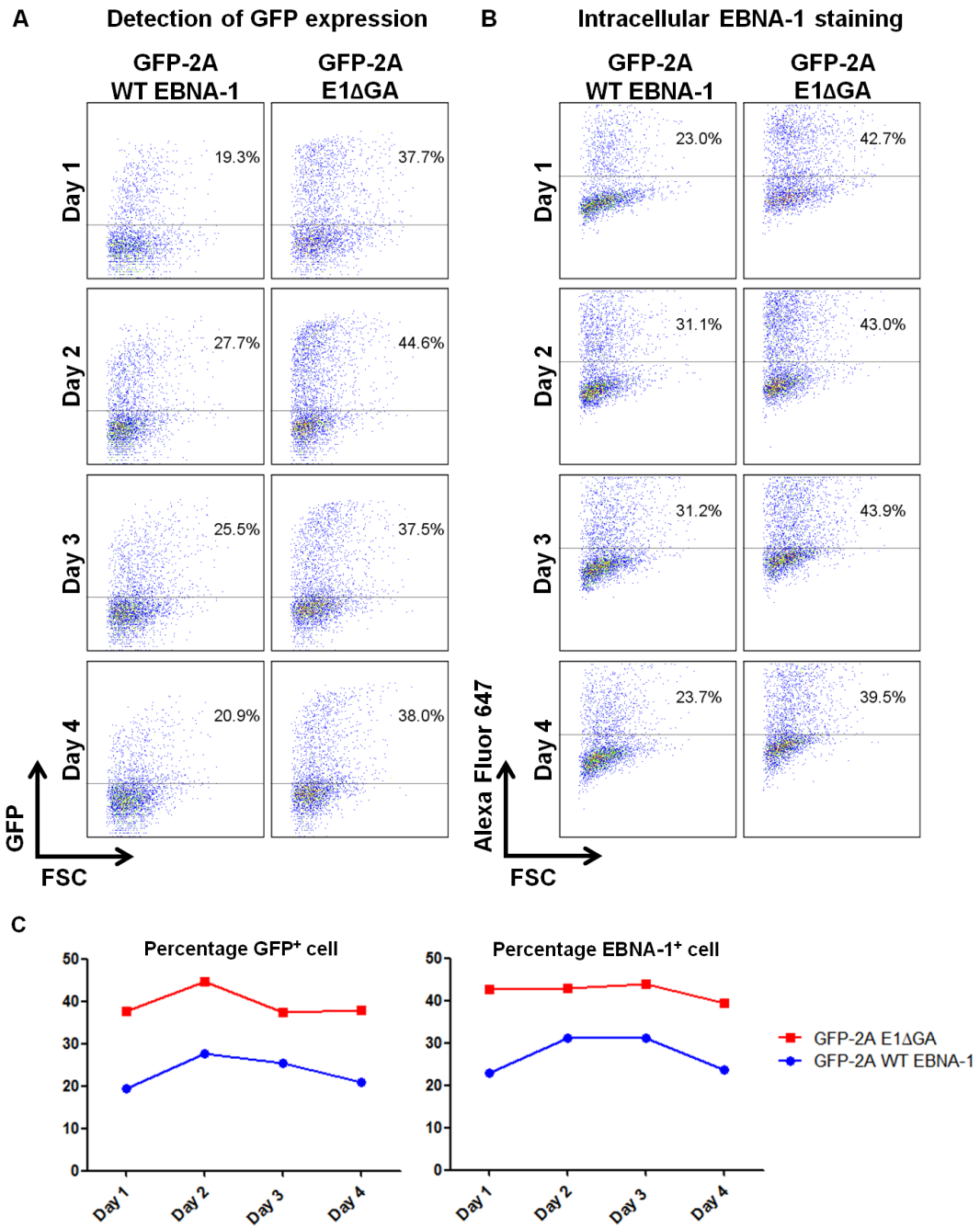

Figure 3.4: Reduced GFP and EBNA-1 expression in GFP-2A WT EBNA-1-transfected cells. HEK293T cells were transfected with plasmids encoding either GFP-2A WT EBNA-1 or GFP-2A E1ΔGA, and harvested to check for their **(A)** GFP expression and **(B)** intracellular EBNA-1 expression. **(C)** Percentages of GFP$^+$ and EBNA-1$^+$ cells were plotted to compare the protein expression between GFP-2A WT EBNA-1 and GFP-2A E1ΔGA-transfected cells. Cells transfected with the plasmid encoding GFP-2A WT EBNA-1 (with the presence of GAr) displayed lower GFP and EBNA-1 expression as compared to E1ΔGA-transfectants. Data is representative of three independent experiments.

3.5 Detection of surface EBNA-1 presentation using α-EBNA-1 TCR-like mAb

To determine whether the presence of GAr could impact the antigen presentation of EBNA-1 protein, we employed an in-house produced α-EBNA-1 TCR-like mAb to detect surface pMHC on GFP-2A WT EBNA-1 and GFP-2A E1ΔGA-transfected cells. Details on the generation of α-EBNA-1 TCR-like mAb, which targets HLA-A*0201-associated EBNA-1 peptide (FMVFLQTHI) [50] found at the C-terminus region of EBNA-1 protein, were as previously described (Eio Yating Michelle, Master's thesis). Briefly, mice were immunized with refolded HLA-A*0201/EBNA-1 (FMVFLQTHI) monomers, and splenocytes were magnetically enriched for target-specific, antibody-secreting cells prior to hybridoma generation and subsequent obtainment of the monoclonal antibody.

HEK293T cells were transfected with either GFP-2A WT EBNA-1 or GFP-2A E1ΔGA encoding plasmids and were harvested for surface EBNA-1 pMHC staining with α-EBNA-1 TCR-like mAb. As seen in **Figure 3.5**, no surface EBNA-1 pMHC staining could be seen in both transfectants. The lack of surface EBNA-1 pMHC detection was not due to the absence of EBNA-1 synthesis and expression, as intracellular EBNA-1 staining was observed in both transfected cells, with consistently higher protein expression detected in GFP-2A E1ΔGA-transfectants as compared to GFP-2A WT EBNA-1.

Despite further attempts to stain for surface antigen presentation using an alternative transfection cell line HeLa-A2, we were unsuccessful in detecting any surface EBNA-1 pMHC with α-EBNA-1 TCR-like mAb (data not shown). As such, it remains to be determined whether the lack of surface staining was due to the absence of surface EBNA-1 pMHC presentation or the inability of the α-EBNA-1 TCR-like mAb to detect its respective pMHC.

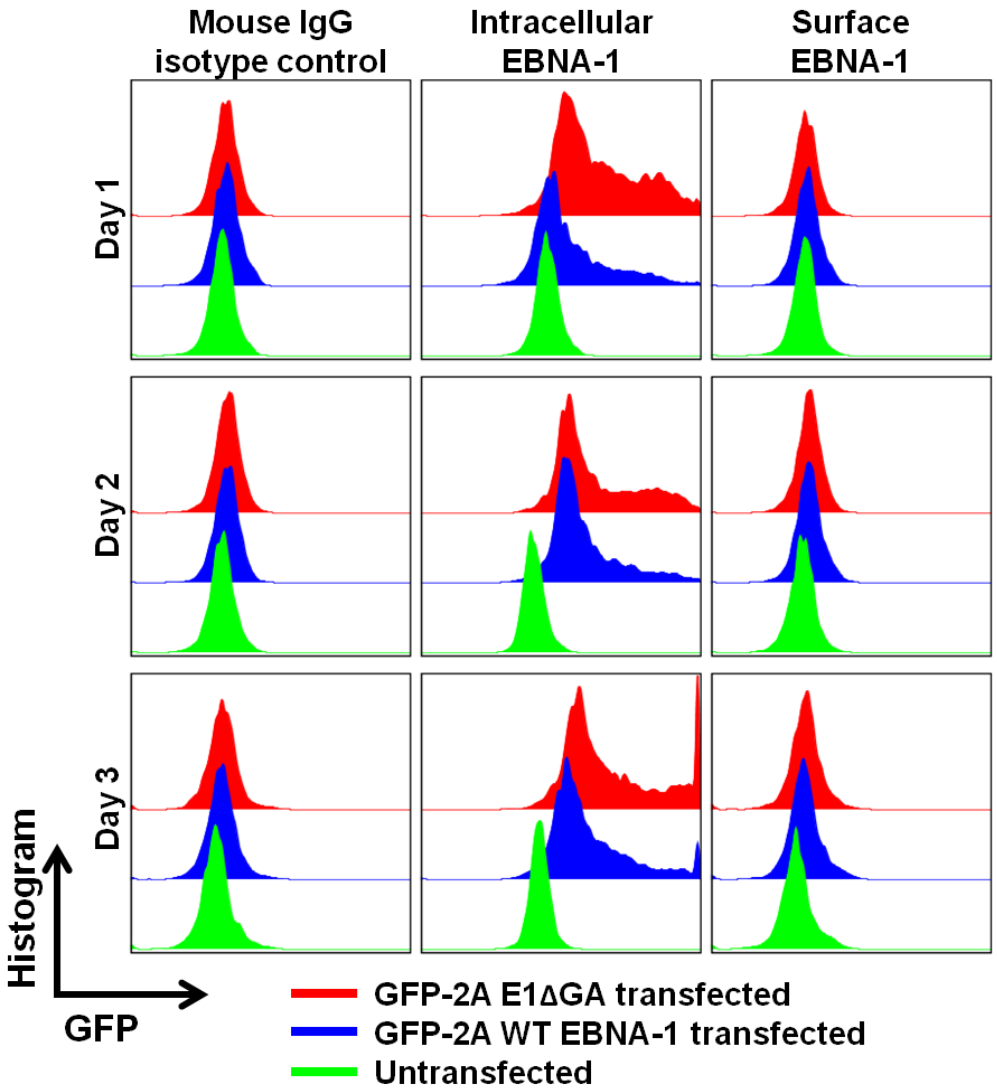

Figure 3.5: **Utility of α-EBNA-1 TCR-like mAb for the detection of surface EBNA-1 pMHC.** HEK293T cells were transfected with either GFP-2A WT or GFP-2A ΔGAr EBNA-1, and harvested on day 1, 2, and 3 for flow cytometric analysis. Untransfected cells were included as a control. Harvested cells were stained for intracellular EBNA-1 and surface EBNA-1 pMHC. Cells were stained with mouse IgG1 isotype antibody as an additional negative control. While intracellular EBNA-1 proteins were detected in both GFP-2A WT and GFP-2A ΔGAr EBNA-1-transfectants, no staining for surface EBNA-1 pMHC was observed. Data is representative of three independent experiments.

3.6 Analyzing the binding activity of α-EBNA-1 TCR-like mAb for its pMHC

To ensure that the lack of binding to transfected HEK293T cells as observed in **Figure 3.5** was not due to the inability of α-EBNA-1 TCR-like mAb in detecting surface presentation of its cognate EBNA-1 pMHC, we performed pMHC ELISA and peptide pulsing experiments to determine the specificity of the antibody for its target. For pMHC ELISA, EBNA-1 peptide (FMVFLQTHI)-bound HLA-A*0201 molecules were coated onto ELISA plate prior to the addition of the serially diluted α-EBNA-1 TCR-like mAb (with influenza A M1 peptide GILGFVFTL as control). α-EBNA-1 TCR-like mAb displayed antibody concentration-dependent binding to the wells coated with EBNA-1 pMHC monomers, while no binding was observed in those wells coated with the influenza A M1 pMHC monomers (**Figure 3.6A**). Data was plotted on GraphPad Prism and a K_D value of 3.98 nM was obtained, which was consistent with surface plasmon resonance data as reported previously by our laboratory [129].

To further verify the specificity of α-EBNA-1 TCR-like mAb, we determined its binding to exogenously derived peptides on HLA-A*0201 cells. C1R-A2 cells were treated with citric acid to remove pre-existing surface peptides prior to peptide pulsing with various HLA-A*02-restricted, pathogen-derived peptides [209]. As shown in **Figure 3.6B**, staining was only observed when C1R-A2 cells were pulsed with EBNA-1 peptide, but not with other peptides from EBV, cytomegalovirus, and influenza A virus, demonstrating that α-EBNA-1 TCR-like mAb was capable of distinguishing its cognate peptide (FMVFLQTHI) from other irrelevant peptides.

We additionally performed pulsing experiments using serially diluted peptides with HLA-A*0201, transporter associated with antigen processing-deficient T2 cells as a test of the sensitivity of α-EBNA-1 TCR-like mAb in detecting varying amounts of exogenously loaded peptides. Although T2 cells are positive for EBV, their deficiency in processing endogenously derived antigens made them suitable for studying the presentation of exogenously derived peptides. As seen in **Figure 3.6C** (left histogram), staining was observed when cells were pulsed with 1 μM of the EBNA-1 peptide (FMVFLQTHI), and concentration-dependent binding was seen with increasing amount of FMVFLQTHI pulsed. In contrast, no staining was observed when cells were pulsed with the peptide control (NLVPMVATV) from cytomegalovirus $pp65_{495\text{-}503}$ (**Figure 3.6C**, right histogram).

Immunofluorescent staining was performed to visualize the binding of α-EBNA-1 TCR-like mAb to surface EBNA-1 pMHC. In brief, T2 cells were pulsed with either EBNA-1 (FMVFLQTHI) or M1 (GILGFVFTL) peptide before staining with α-EBNA-1 TCR-like mAb, followed by staining with the fluorescent conjugated secondary antibody. As shown in **Figure 3.7**, staining was observed when cells were pulsed with EBNA-1 peptide (FMVFLQTHI), with co-localizing staining with β2-microglobulin (a subunit of MHC class I). In contrast, staining was not observed when cells were pulsed with control peptide GILGFVFTL from influenza A M1 protein. Taken together, these data from pMHC ELISA and peptide pulsing demonstrated the specificity of α-EBNA-1 TCR-like mAb for its peptide FMVFLQTHI presented on HLA-A*0201 molecules, reinforcing the notion that α-EBNA-1 TCR-like mAb recognizes pMHC complex similar to a TCR.

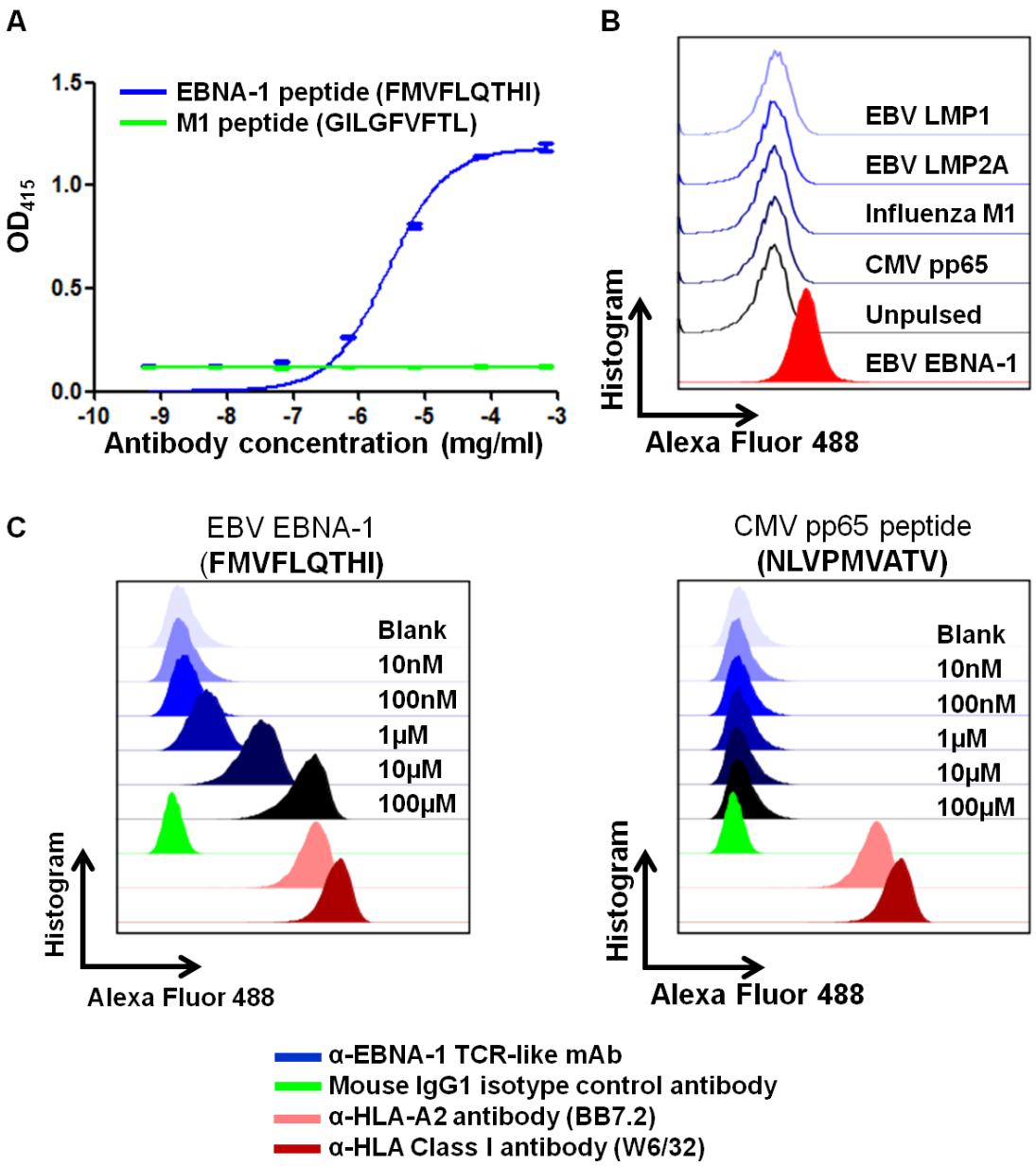

Figure 3.6: **Analyzing the binding activity of α-EBNA-1 TCR-like mAb for its pMHC. (A)** pMHC ELISA was performed to determine the binding avidity of α-EBNA-1 TCR-like mAb to its cognate peptide (FMVFLQTHI) in association with HLA-A*0201. Antibody concentration-dependent binding was observed with EBNA-1 pMHC but not with control peptide GILGFVFTL monomers. Readings were measured on a spectrophotometer (at 415 nm) and K_D (3.987 nM) was determined using GraphPad Prism. **(B)** C1R-A2 cells were acid-stripped to remove pre-existing surface presentation before being pulsed with HLA-A*02-restricted peptides. Binding was only observed when cells were pulsed with EBNA-1 peptide (FMVFLQTHI), but not with other irrelevant peptides. **(C)** TAP-deficient T2 cells were pulsed with 10X serially diluted EBNA-1 peptide (FMVFLQTHI) or control CMV pp65 peptide (NLVPMVATV) before staining with α-EBNA-1 TCR-like mAb. Increased staining was observed on T2 cells when higher amounts of FMVFLQTHI peptides were pulsed.

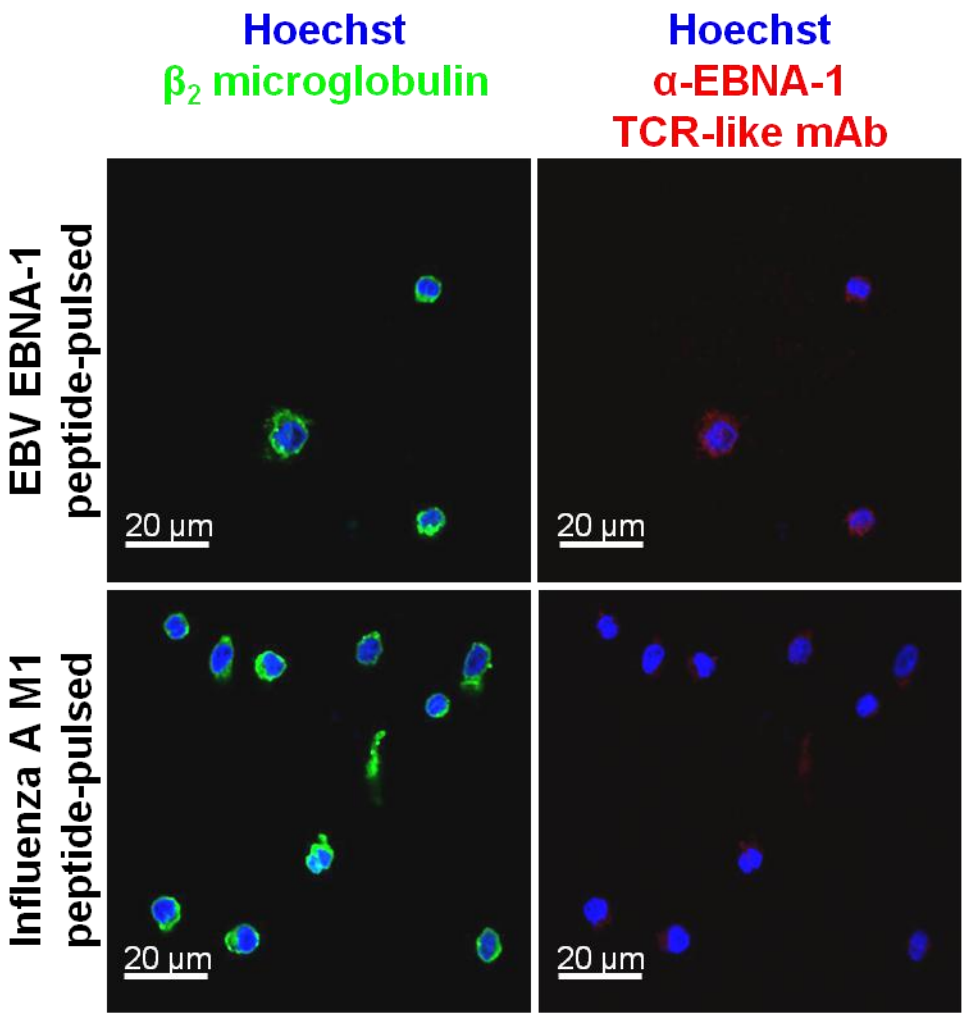

Figure 3.7: **The employment of α-EBNA-1 TCR-like mAb to detect surface EBNA-1 pMHC on pulsed T2 cells.** Hoechst dye and α-β2-microglobulin antibody staining were performed to respectively visualize cell nucleus and MHC class I (with β2-microglobulin as a subunit). T2 cells were pulsed with either FMVFLQTHI (EBNA-1 peptide) or GILGFVFTL (influenza A M1) and stained with α-EBNA-1 TCR-like mAb. Staining was observed when cells were pulsed with the relevant FMVFLQTHI peptide, but not with the control peptide GILGFVFTL. α-EBNA-1 TCR-like mAb staining displayed co-localization with β2-microglobulin. **Scale bar**: 20 µm. Images (512 X 512 pixels) were acquired on Zeiss LSM 510 confocal microscope software version 2.5 SP2 under 63X oil immersion objective. Images were overlayed using Adobe Photoshop CS6. **Blue**: nuclear staining with Hoechst dye; **Red**: goat α-mouse IgG RPE (detects α-EBNA-1 TCR-like mAb); **Green**: goat α-rabbit IgG Alexa Fluor® 488 (detects β2-microglobulin).

3.7 Detection of endogenously derived EBNA-1 pMHC using α-EBNA-1 TCR-like mAb

Given that EBV is prevalent in the humans, we investigated if α-EBNA-1 TCR-like mAb is capable of detecting surface EBNA-1 pMHC in EBV-seropositive individuals. Peripheral blood samples were collected from HLA-A*0201 EBV-seropositive donors (HLA haplotype and EBV serostatus were determined by in-house polymerase chain reaction methodology and commercial sequencing). PBMC were obtained by Ficoll gradient separation for staining with α-EBNA-1 TCR-like mAb.

We first investigated the staining profiles of α-EBNA-1 TCR-like mAb on granulocytes, monocytes, and lymphocytes in the PBMC of a HLA-A*0201 donor (AM002) (**Figure 3.8A**). However, none of the three immune subsets displayed positive staining with the antibody (**Figure 3.8B**). Nonetheless, it should be noted that the frequency of EBV-infected cell in the peripheral blood can be as low as 1 in 10 million peripheral blood lymphocytes [147, 210, 211]. Moreover, taking the immunoevasive properties of EBNA-1 into consideration, it should not be surprising that no staining was observed with α-EBNA-1 TCR-like mAb. This observation is substantiated by an earlier report from Wagner et al., which characterized that healthy individuals who were latently infected with EBV had no detectable expression of the EBNA-1 protein [212].

Next, we questioned whether our antibody would be capable of detecting the presentation of EBNA-1 pMHC on cells naturally infected with EBV. Here, we selected BLCL to assess the staining of α-EBNA-1 TCR-like mAb, as these cells are the *in vitro* counterpart of EBV-infected B cells in humans, expressing all of the EBV latent products, including EBNA-1 (**Table 1.1**, latency III program). To start, HLA-A*0201 PBMC from the same individual (AM002) was isolated and immortalized *in vitro* to generate BLCL. Briefly, B95-8 EBV supernatant was added to the PBMC, and macroscopic cell clumps were observed two weeks post-infection.

With the establishment of a stable BLCL after 30 days of culture, we proceeded to stain the newly generated cell line (AM002 BLCL) with our α-EBNA-1 TCR-like mAb. In contrast to the lack of staining with PBMC (**Figure 3.8B**), positive staining was observed with α-EBNA-1 TCR-like mAb on AM002 BLCL generated from the same PBMC (**Figure 3.8C**). As peptide pulsing was not utilized, the detection of surface EBNA-1 pMHC with α-EBNA-1 TCR-like mAb demonstrated the existence of endogenously derived EBNA-1 pMHC on BLCL, and that α-EBNA-1 TCR-like mAb could differentiate BLCL from the PBMC which they were derived.

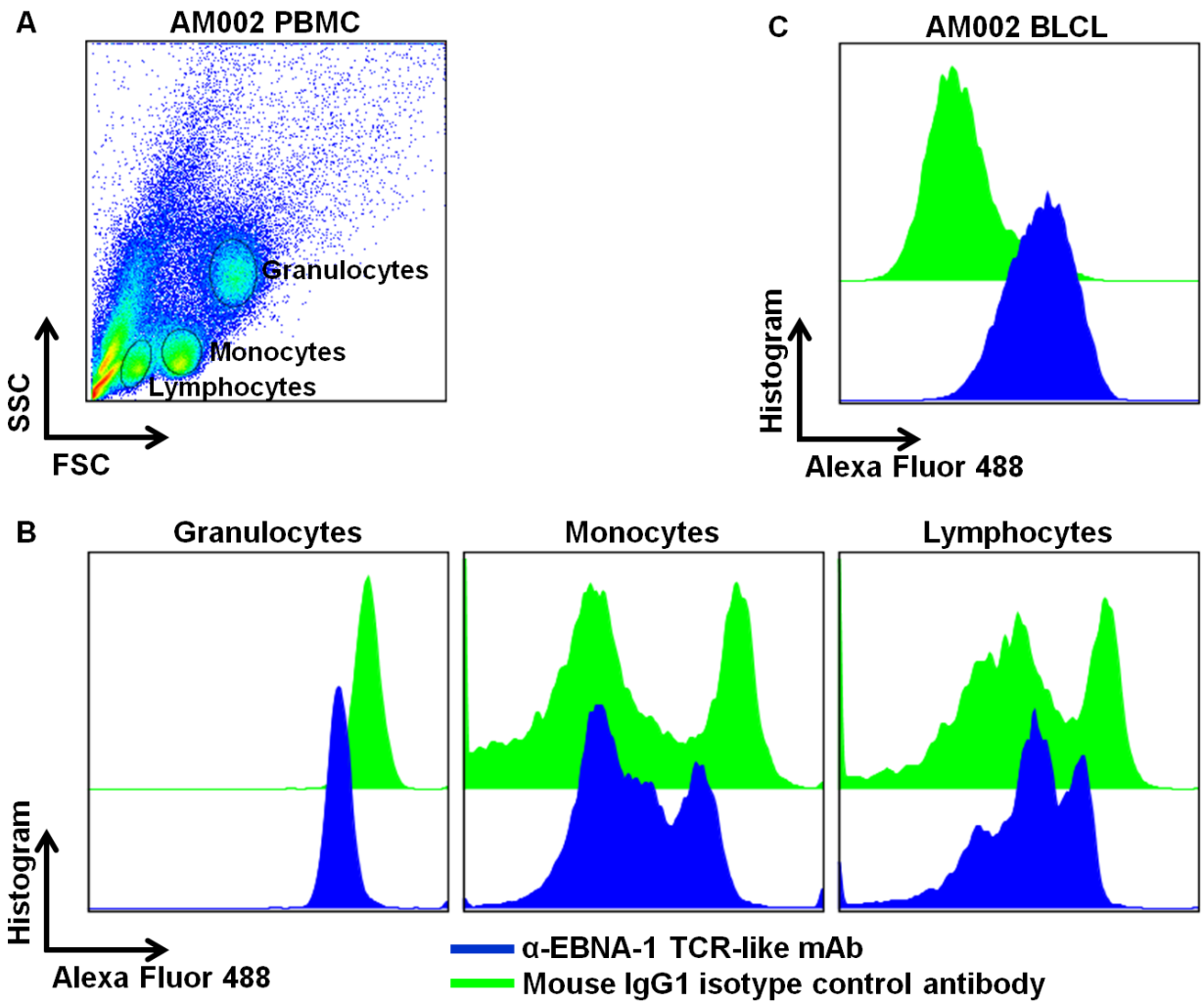

Figure 3.8: **Staining of surface EBNA-1 pMHC was observed on BLCL but not on matching PBMC.** PBMC was obtained from HLA-A*0201 donor and stained with α-EBNA-1 TCR-like mAb. **(A)** Cells were plotted on FSC versus SSC to differentiate granulocytes, monocytes and lymphocytes. **(B and C)** While no staining was observed on the different immune subsets (based on parent gates in **Figure 3.8A**), a distinct staining for surface EBNA-1 pMHC was observed on BLCL generated from EBV *in vitro* infection of the PBMC. HLA-A haplotype of BLCLs was determined using in-house polymerase chain reaction methodology and commercial

3.8 Restriction and specificity of α-EBNA-1 TCR-like mAb

With the validation on the capability of α-EBNA-1 TCR-like mAb to detect endogenously derived EBNA-1 pMHC, we further verified the restriction of the antibody for HLA-A*0201 and its specificity for EBV. As shown in **Figure 3.9**, staining was observed with EBV-infected, HLA-A*0201 BLCL (CF986) but not with non-HLA-A*0201 BLCL (CF888), illustrating that the recognition of surface EBNA-1 pMHC by α-EBNA-1 TCR-like mAb was only relevant in the context of HLA-A*0201 (HLA-A*0201-restricted).

To demonstrate the specificity of α-EBNA-1 TCR-like mAb for EBV, we stained EBV^- HLA-A*0201 HEK293T cells with α-EBNA-1 TCR-like mAb. In contrast to EBV^+ CF986 BLCL, HEK293T are EBV^- and do not express EBNA-1, and thus these cells were not stained positive for surface EBNA-1 pMHC (**Appendix B** - intracellular EBNA-1 staining was performed to verify the presence of EBV in HEK293T and CF986). Similarly, no staining was observed with EBV^- and non-HLA-A*0201 BL cell line (Ramos). Altogether, our data demonstrated HLA-A*0201-restriction and EBV-specific characteristics of α-EBNA-1 TCR-like mAb for its surface target.

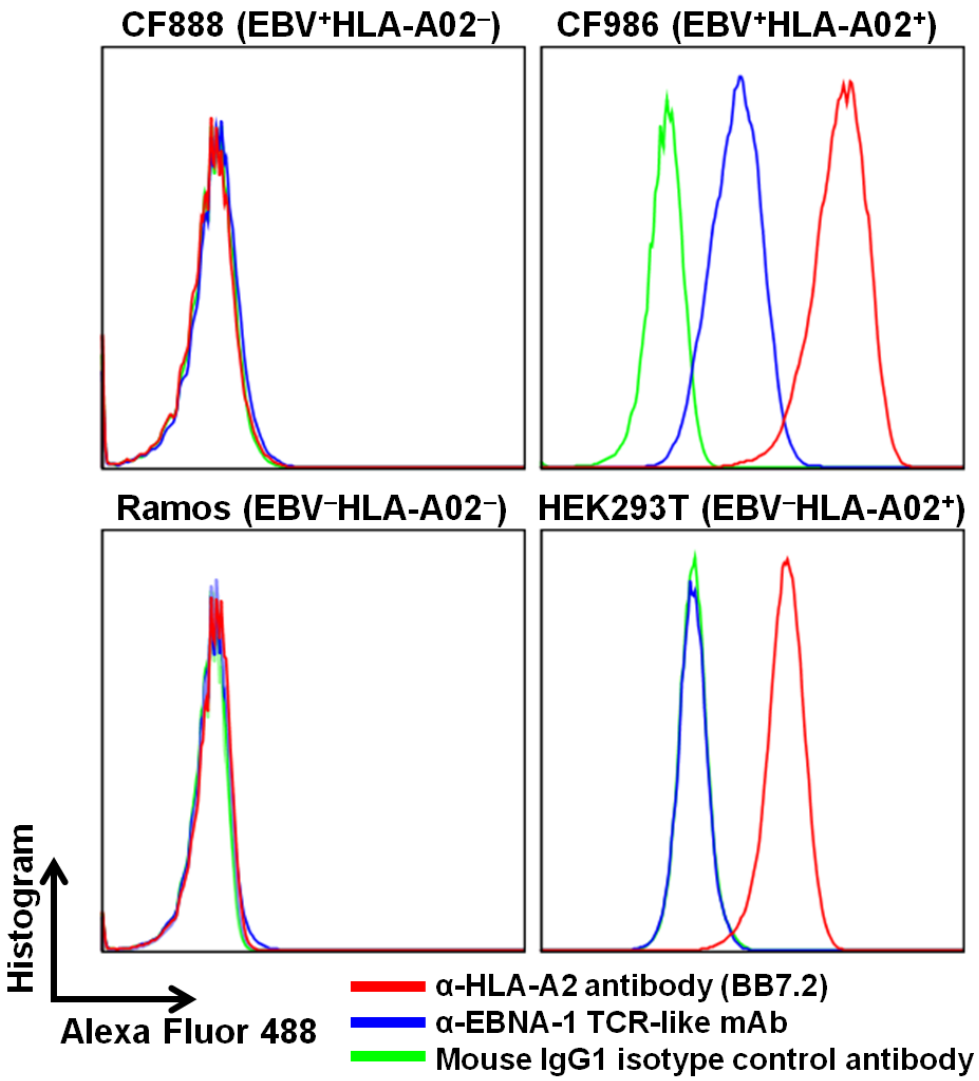

Figure 3.9: **α-EBNA-1 TCR-like mAb can detect endogenously derived, surface EBNA-1 pMHC on HLA-A*0201 BLCL.** Staining with α-EBNA-1 TCR-like mAb was observed on HLA-A*0201 and EBV^+ BLCL (CF986), but not on EBV^- HEK293T, HLA-A*02^- CF888 and EBV^-HLA-A*02^- Ramos. Mouse IgG1 isotype antibody was used as a negative control. In addition, intracellular EBNA-1 staining was conducted to verify the presence of EBV in HEK293T and CF986 (**Appendix B**).

We next visualized the staining of endogenously derived EBNA-1 on BLCL via confocal microscopy. Staining for surface EBNA-1 pMHC was observed with α-EBNA-1 TCR-like mAb on BLCL in comparison to isotype control antibody, with co-localization of EBNA-1 pMHC with β2-microglobulin staining (**Figure 3.10**). Taken together, the use of α-EBNA-1 TCR-like mAb enabled the discernment of BLCL versus PBMC from which they were derived. More importantly, the employment of α-EBNA-1 TCR-like mAb permitted the detection of both exogenously-pulsed and endogenously derived peptides, highlighting its capability of binding to surface EBNA-1 pMHC in the context of HLA-A*0201.

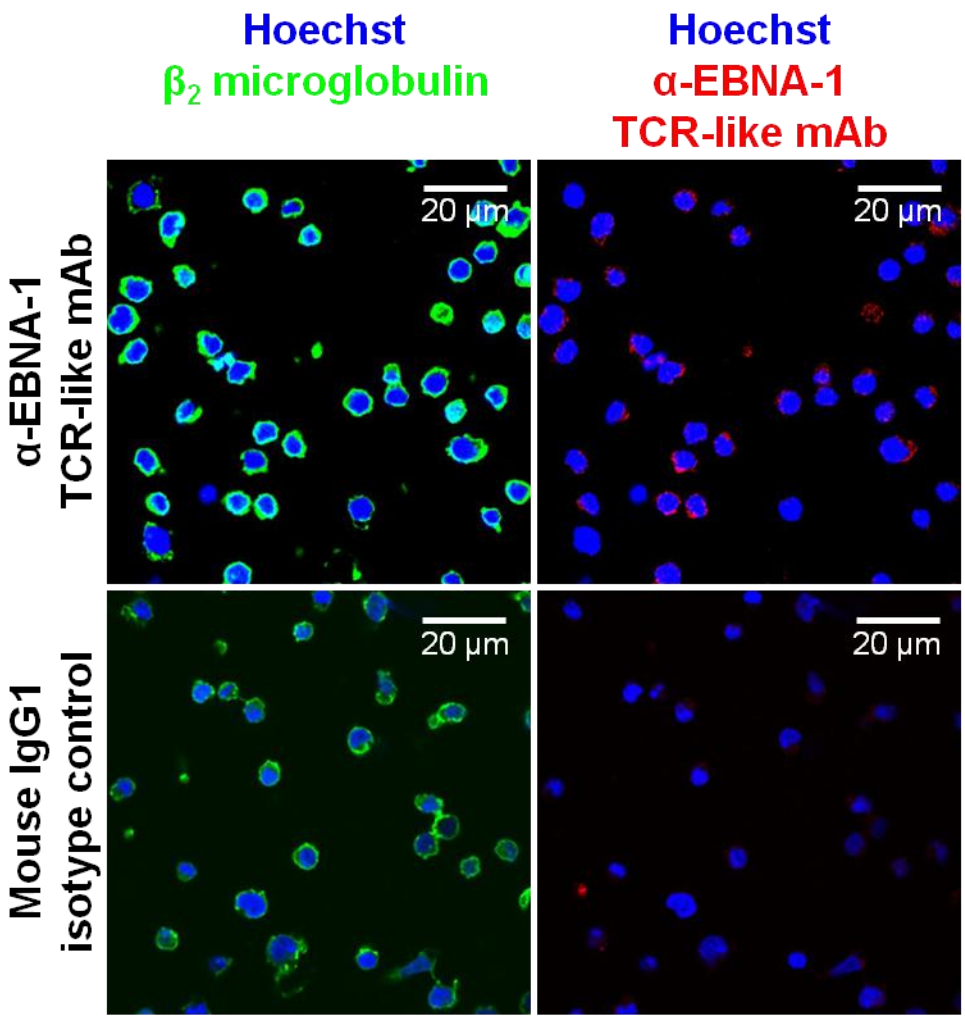

Figure 3.10: Immunofluorescent staining revealed surface EBNA-1 pMHC of endogenous origin. HLA-A*0201 BLCL was fixed onto coverslip and stained with α-EBNA-1 TCR-like mAb and α-β2-microglobulin antibody. Staining of endogenous EBNA-1 pMHC was observed with the α-EBNA-1 TCR-like mAb, co-localizing with the β2-microglobulin. Mouse IgG1 isotype antibody was used as a negative control. **Scale bar**: 20 μm. Images (512 X 512 pixels) were acquired on Zeiss LSM 510 confocal microscope software version 2.5 SP2 under 63X oil immersion objective. Images were overlayed using Adobe Photoshop CS6. **Blue**: nuclear staining with Hoechst dye; **Red**: goat α-mouse IgG RPE (detects α-EBNA-1 TCR-like mAb); **Green**: goat α-rabbit IgG Alexa Fluor® 488 (detects β2-microglobulin).

3.9 α-EBNA-1 TCR-like mAb can bind to BLCLs despite their intrinsic heterogeneity

BLCLs are EBV-infected B cells which are heterogeneous with respect to their size, morphology, and immunophenotype. Using AM001 BLCL and CF986 BLCL as examples, we could observe apparent differences in terms of size under the microscope (**Figure 3.11A**), as well as forward scatter (FSC, size) and side scatter (SSC, granularity) profiles via flow cytometry (**Figure 3.11B**). Both AM001 and CF986 exhibited villous membrane projections, which are characteristic of BLCL, as compared to a more rounded morphology of Raji (B lymphoma cell line) [213]. In order to further characterize these BLCLs, multicolor flow cytometry was employed to determine their immunophenotypes (**Table 3.1**).

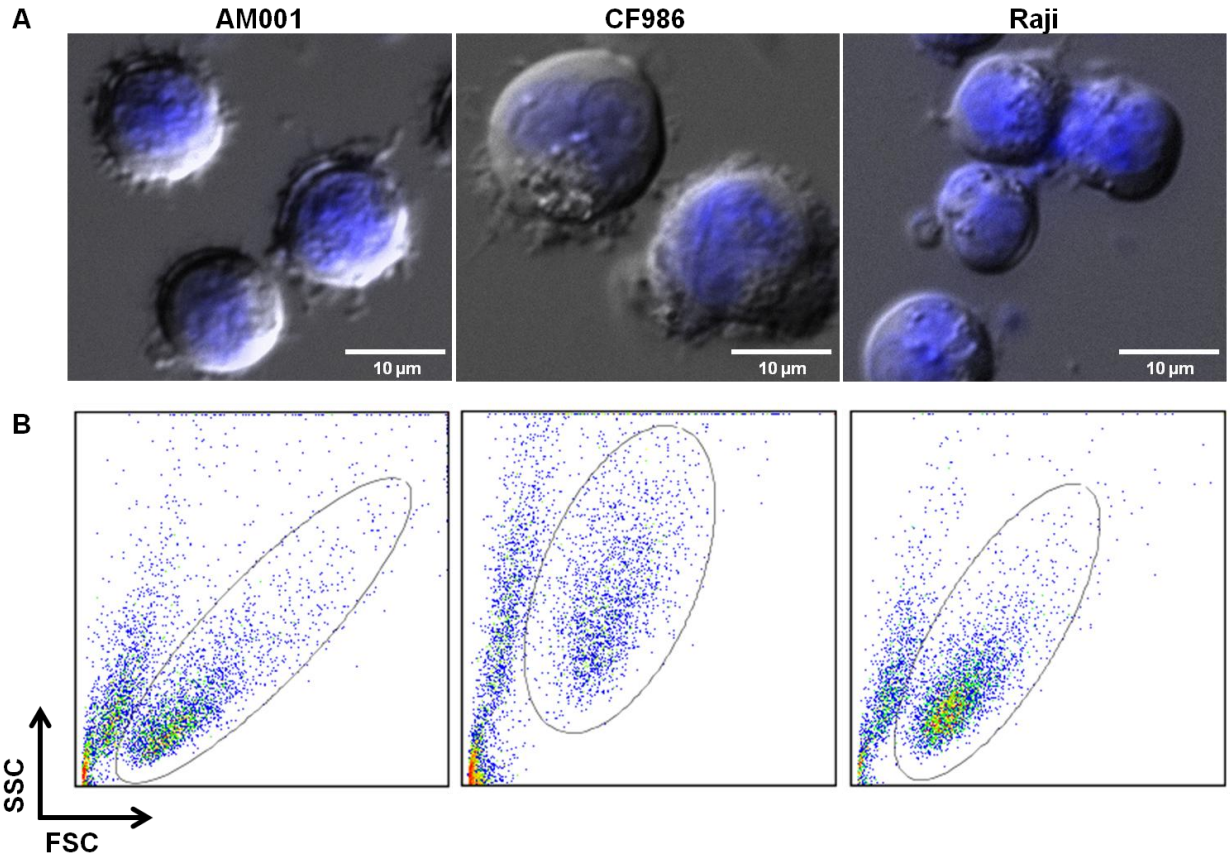

Figure 3.11: Morphological heterogeneity in BLCLs. (A) Fluorescent microscopy of BLCLs (AM001 and CF986) and BL cell line (Raji). Cells were stained with Hoechst dye (Blue) for nuclear staining. Villous membrane projections, as observed in both AM001 and CF986, are characteristic of the immunoblastic and activated status of the BLCLs. In comparison, Raji cells displayed a more rounded morphology (Images were courtesy of Ms. Lai Junyun). **(B)** Forward (FSC) and side (SSC) scatter plot on a flow cytometer also revealed differences in the size and granularity between AM001 and CF986 BLCL).

Table 3.1: Immunophenotypic heterogeneity in BLCLs.

BLCLs	CD3	CD34	CD56	HLA-A2	CD10	CD138	CD19	CD20	CD23	CD27	CD38	CD40	CD86	CD95	IgM	IgD
AM001	-	-	-	+++	-	-	++	++	+	+	++	++	++	++	++	-
AM002	-	-	-	+++	-	-	++	++	+	+	++	++	+	++	-	-
CF508	-	-	-	+++	-	-	++	++	++	-	++	++	++	++	+	-
CF522	-	-	-	-	-	-	++	++	+	-	++	++	++	++	+	+
CF884	-	-	-	+++	-	-	++	++	++	-	+	++	++	++	-	-
CF893	-	-	-	+++	-	-	++	++	++	-	++	++	++	++	++	+
CF990	-	-	-	+++	-	-	++	++	++	-	+	++	++	++	++	+
CF1018	-	-	-	+++	-	-	++	++	++	-	++	++	++	++	++	-
CF1059	-	-	-	+++	-	-	++	++	++	+	++	++	++	++	++	++
CF1097	-	-	-	+++	-	-	++	++	++	+	++	++	++	++	++	-
CM462	-	-	-	+++	-	-	++	++	++	+	+	++	++	++	+	+
CM800	-	-	-	+++	-	-	++	++	++	+	++	++	++	++	++	-
CM956	-	-	-	+++	-	-	++	++	++	-	++	++	++	++	++	++

nMFI values were calculated by taking the MFI of an antibody stain divided by the MFI of its respective isotype control. nMFI values were categorized into: negative value to <2 (-), 2 to <6 (+), 6 to <100 (++) and 100 to <1000 (+++).

As shown in **Table 3.1**, all BLCLs were found to be negative for non-B cell markers such as CD3 (T cells), CD34 (hematopoietic progenitor cells), and CD56 (NK cells). While the expression of CD10 (early B cell marker) and CD138 (plasma cell marker) was not detected, the expression of B cell lineage markers such as CD19, CD20, and CD23 was observed in all the BLCLs. In addition, the expression of co-stimulatory molecules (CD40 and CD86) and activated markers (CD38) were also found in all BLCLs tested. However, markers such as CD27, IgM, and IgD varied in their expression, highlighting the heterogeneity between BLCLs. Notably, the expression of prototypic death receptor (CD95) was detected, consistent with the reported upregulation of CD95 upon EBV infection [214-216].

Despite the observed morphological and immunophenotypic heterogeneity between BLCLs, the fact that all BLCLs are latently infected with EBV indicates a common feature among these cells. To show the similarity between the BLCLs, immunoblotting for EBV latent proteins was conducted. As shown in **Figure 3.12,** the expression of EBNA-1, LMP1, and EBNA-2, though at varying levels, were observed in all the BLCLs, but not in EBV^- BL cell line (BJAB). In particular, the expression of EBNA-2 which defines EBV latency III gene expression profile was found in all the BLCLs, consistent with previous reports [217, 218].

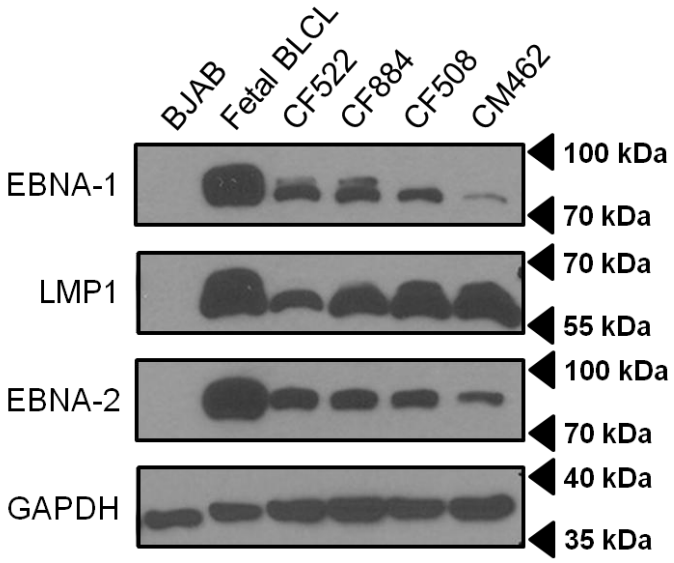

Figure 3.12: Immunoblot detection of EBV latent proteins in BLCLs. Immunoblotting was performed to determine the latency profile of BLCLs. The expression of EBNA-1, LMP1 and EBNA-2 were detected in all the BLCLs. All cells displayed latency III profile based on the characteristic expression of EBNA-2. Housekeeping gene GAPDH was used as a loading control. EBV^- human BL cell line (BJAB) was used as a negative control.

With the expression of EBV latent proteins shown in the heterogeneous BLCLs, we next assessed whether α-EBNA-1 TCR-like mAb could detect its surface target on a panel of different donor-derived HLA-A*0201 BLCLs. For comparison purposes, we included addition staining with another in-house produced antibody (α-LMP1 TCR-like mAb) which recognizes surface EBV LMP1 pMHC presented on HLA-A*0201 molecules. As shown in **Figure 3.13A**, a significant higher staining was observed with α-EBNA-1 TCR-like mAb as compared to α-LMP1 TCR-like mAb (**Appendix C**), and this observation was consistent within individual BLCL (**Figure 3.13B**).

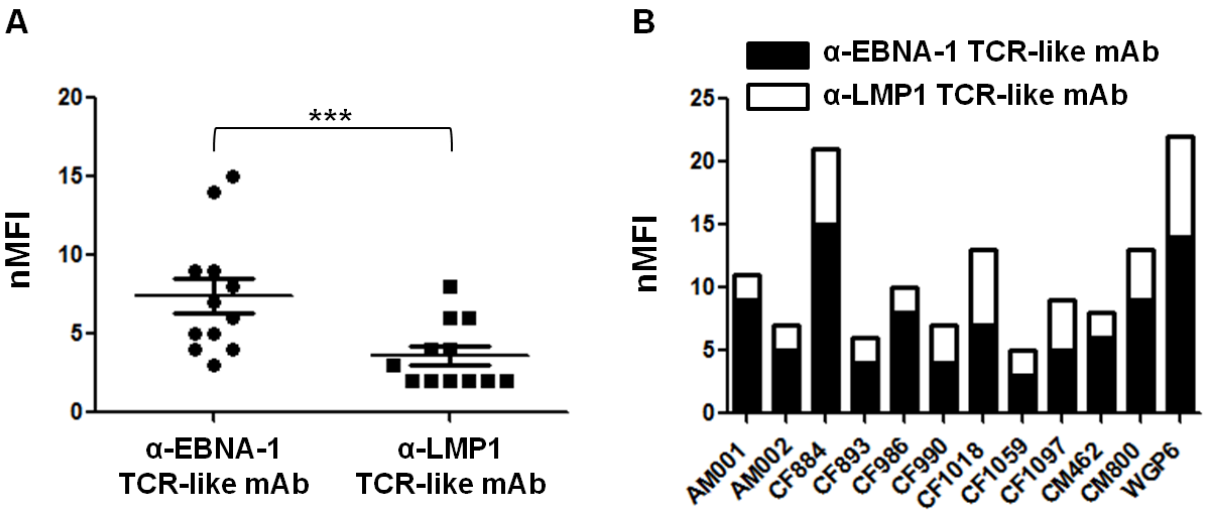

Figure 3.13: α-EBNA-1 TCR-like mAb detects endogenous surface EBNA-1 pMHC between different donor-derived HLA-A*0201 BLCLs despite their heterogeneity. (A) A collection of HLA-A*0201 PBMC-derived BLCLs was obtained from different donors, harvested and stained with α-EBNA-1 TCR-like mAb and α-LMP1 TCR-like mAb (another in-house produced antibody specific for EBV surface LMP1 pMHC). Mouse IgG1 isotype control and α-HLA-A2 were used as the negative and positive control respectively (**Appendix C**). Despite the heterogeneity between BLCLs, endogenously derived surface EBNA-1 and LMP1 pMHC were observed, with a general trend of higher surface EBNA-1 pMHC staining detected in all HLA-A*0201 BLCLs (p = 0.0005). **(B)** Graphical representation of surface EBNA-1: LMP1 pMHC staining of each BLCL presented in **Figure 3.13A**. Higher nMFI values were consistently observed with α-EBNA-1 TCR-like mAb (as compared to α-LMP1 TCR-like mAb) in each of the HLA-A*0201 BLCLs. nMFI values were obtained by dividing α-EBNA-1 (or LMP1) TCR-like mAb MFI readings by its respective mouse IgG1 isotype control MFI. Values are expressed as mean ± SD.

3.10 Constitutive surface presentation of EBNA-1 pMHC on BLCLs

Previously, α-EBNA-1 TCR-like mAb was employed to study the antigen presentation of EBNA-1 but its therapeutic application was left unexplored. Before assessing the therapeutic potential of α-EBNA-1 TCR-like mAb, it is important to validate the availability of surface EBNA-1 pMHC on BLCLs, as that will impact the accessibility of the antibody to target the BLCLs. To understand the kinetics of EBNA-1 pMHC surface presentation on HLA-A*0201 BLCLs, we evaluated α-EBNA-1 TCR-like mAb staining on BLCLs daily, for up to seven days. As shown in **Figure 3.14A**, EBNA-1 pMHC was consistently detected on CM462 BLCL during all of the assessed time points. We expanded our kinetic study to include a panel of HLA-A*0201 BLCLs; despite fluctuations in surface presentation (**Figure 3.14B**), surface EBNA-1 pMHC was detected in all of the tested BLCLs (**Appendix D**). Furthermore, surface EBNA-1 pMHC was detected repeatedly on BLCLs despite multiple freeze-thaw cycles (data not shown). Based on the constitutive presentation of surface EBNA-1 pMHC on BLCLs and the capability of α-EBNA-1 TCR-like mAb to detect endogenous EBNA-1 pMHC, our data suggested on the potential utility of α-EBNA-1 TCR-like mAb for therapeutic purposes.

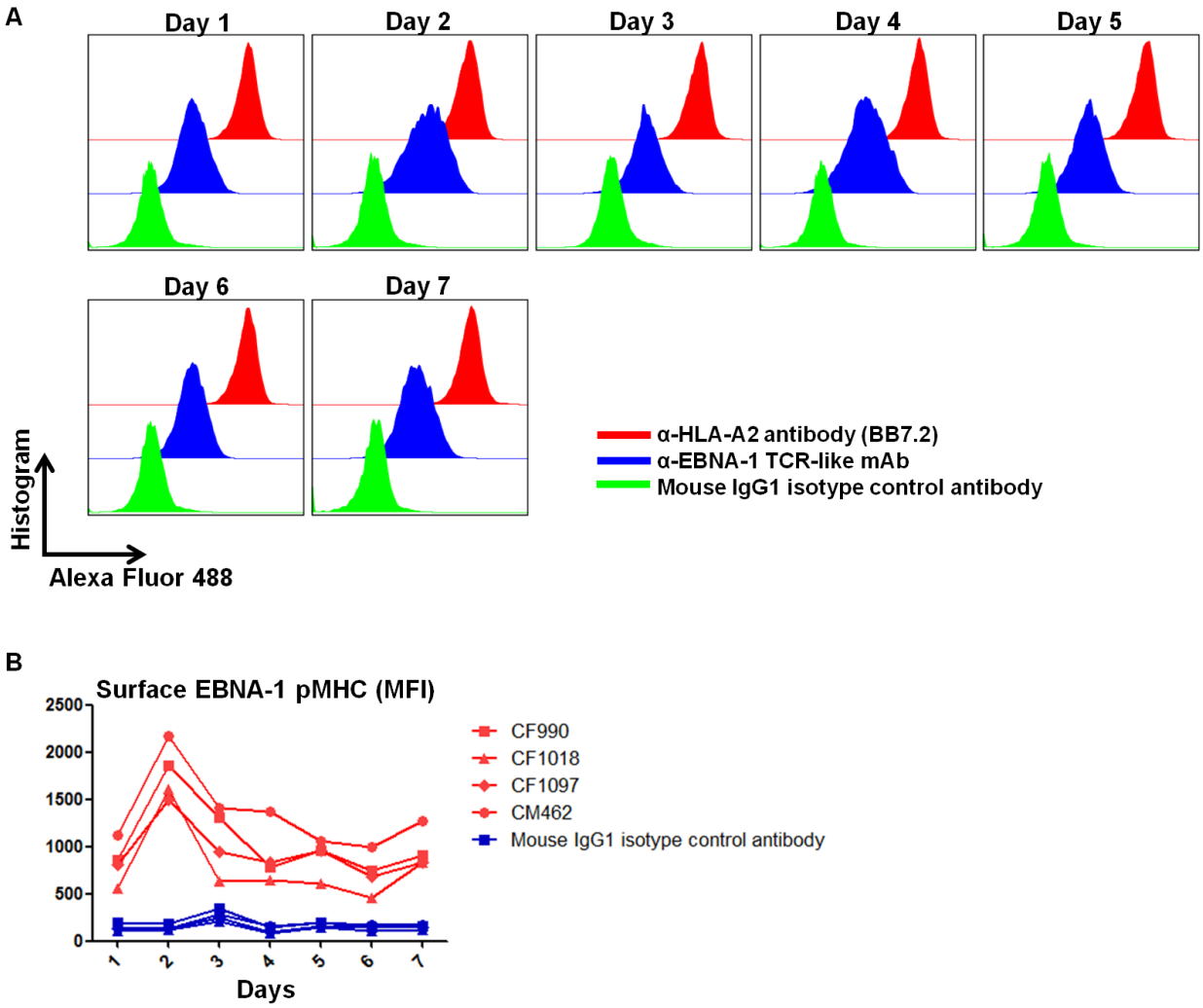

Figure 3.14: Constitutive surface presentation of EBNA-1 on HLA-A*0201 BLCLs. HLA-A*0201 BLCLs were stained with α-EBNA-1 TCR-like mAb daily, for up to one week. **(A)** Using CM462 (HLA-A*0201 BLCL) as an illustration, surface EBNA-1 pMHC was constitutively detected in all seven days. **(B)** Despite fluctuations in the staining profiles of the assessed BLCLs, their levels of surface EBNA-1 pMHC were consistently observed and well-separated from their respective mouse IgG1 isotype control.

Chapter 4:
Result (II)

4.1 Synopsis

EBV-associated B cell lymphoproliferative disorders like PTLD occur in immunosuppressed transplant recipients when immunological suppression of EBV is weakened due to the suppression of T cell immunity. To assess the therapeutic potential of α-EBNA-1 TCR-like mAb in a context relevant to PTLD, we employed NSG mice to simulate immunosuppressed individuals with B cell lymphoproliferation. Having an immunodeficient background, NSG mice can support the engraftment of BLCL, permitting uncontrolled B cell lymphoproliferation as observed in PTLD patients. In this chapter, we assessed the weekly administration of α-EBNA-1 TCR-like mAb on disease manifestations (B cell lymphoproliferation) in various organs of the mice. Furthermore, we performed apoptosis assay and phagocytosis assay to dissect the *in vitro* effects of α-EBNA-1 TCR-like mAb on EBV-infected B cells. In addition, we generated a FcγR-null binding variant of the antibody to further verify whether α-EBNA-1 TCR-like mAb-mediated phagocytosis is Fc-dependent mechanism.

4.2 Determining a treatment regimen for α-EBNA-1 TCR-like mAb

In order to define the treatment regimen, a batch of BLCL-injected NSG mice was euthanized one week post-BLCL injection, while others were set aside for the monitoring of disease progression. While no abnormal

pathology was observed in the organs of the mice that were euthanized one week post-BLCL injection (**Figure 4.1**), flow cytometric analysis revealed the presence of $hCD45^+$ cells in the bone marrows, peripheral blood, kidneys, livers, lungs, and spleens of these mice one week post-BLCL injection (**Figure 4.2A**). These cells were further confirmed to express CD19, indicating successful BLCL engraftment (**Figure 4.2B**).

In a separate batch of mice that were kept for disease monitoring, signs of terminal disease were observed at day 21. Upon euthanasia, mass lesions were seen in the spleens and livers, in addition to splenomegaly and pale kidneys (**Figure 4.3**). Importantly, these observations were similar to several of the clinical manifestations found in PTLD patients, suggesting that this mouse xenograft model is capable of recapitulating some features of the disease. No disease manifestation was observed in mice injected with control media. With the defined disease progression and pathological manifestations, we next proceeded to test the *in vivo* therapeutic efficacy of α-EBNA-1 TCR-like mAb (**Figure 4.4**).

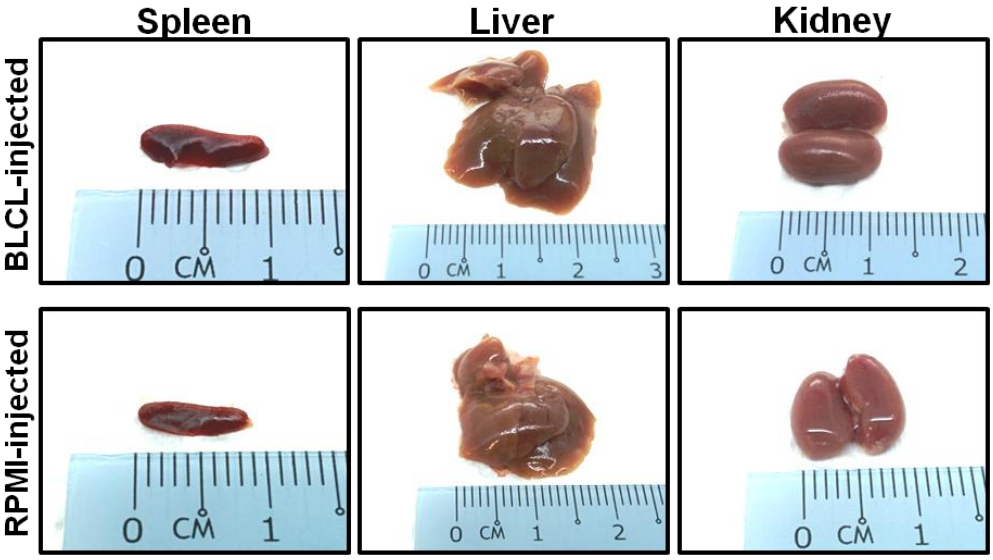

Figure 4.1: **No abnormal pathology was observed in day 7 BLCL-injected mouse xenograft model.** Immunodeficient NSG mice were injected with 2 X 10^6 BLCL (or control media), and euthanized 7 days thereafter. Compared to RPMI-injected mice (n=2), no observable disease manifestation was seen in BLCL-injected mice (n=3). Images illustrated above are representative of their respective group.

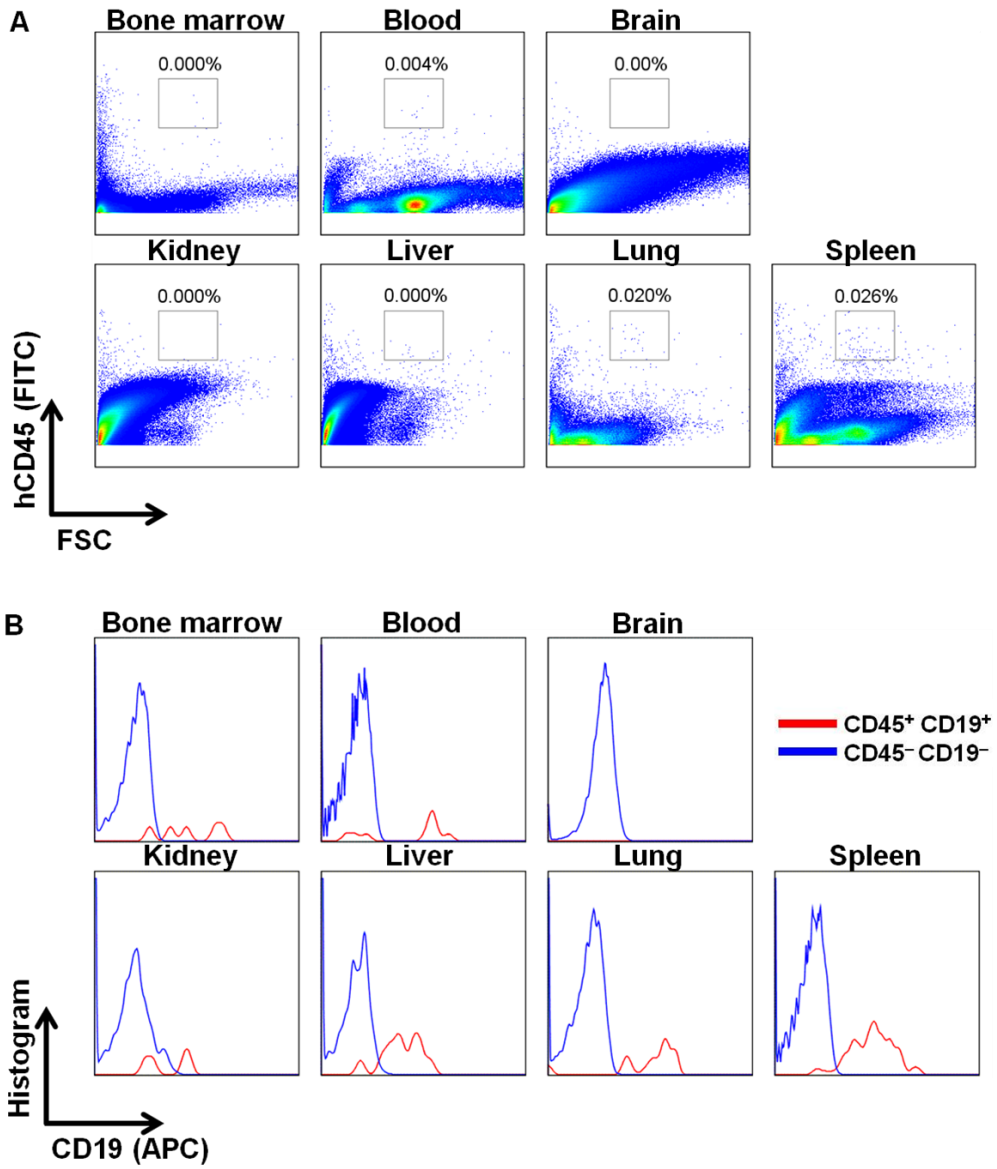

Figure 4.2: Detection of BLCL in the various organs at day 7 BLCL-injected mice. On top of gross anatomy examination, organs of BLCL-injected mice were processed and stained for hCD45 and CD19 prior to flow cytometric analysis. **(A)** Based on hCD45 vs FSC plot, the presence of hCD45 cells, though at very low percentages were detected in the peripheral bloods, livers, lungs, and spleens. **(B)** When these cells were subsequently checked for CD19 expression, staining was observed in all organs (except brain).

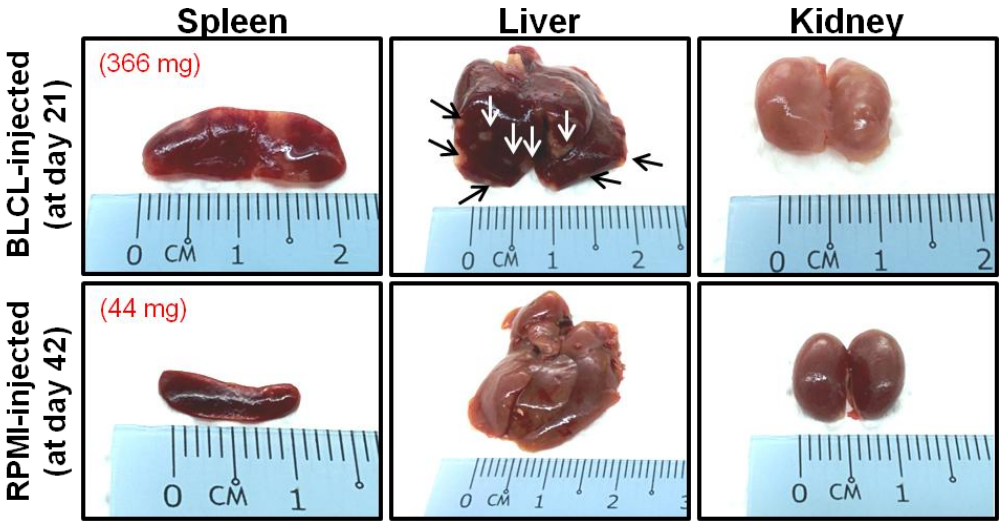

Figure 4.3: Disease manifestations were observed in BLCL-injected mouse xenograft model. Pathological manifestations in the spleen, liver and kidney were observed in mice 3 weeks post-BLCL injection (n=4). Mass lesions (tumor spots) were present in the spleen, liver and kidney. In addition, splenomegaly (the enlargement of the spleen) and pale kidneys were observed in the BLCL-injected mice (**Top panel**), displaying some of the clinical features PTLD in transplant recipients. Arrows indicate the mass lesions observed on the liver.

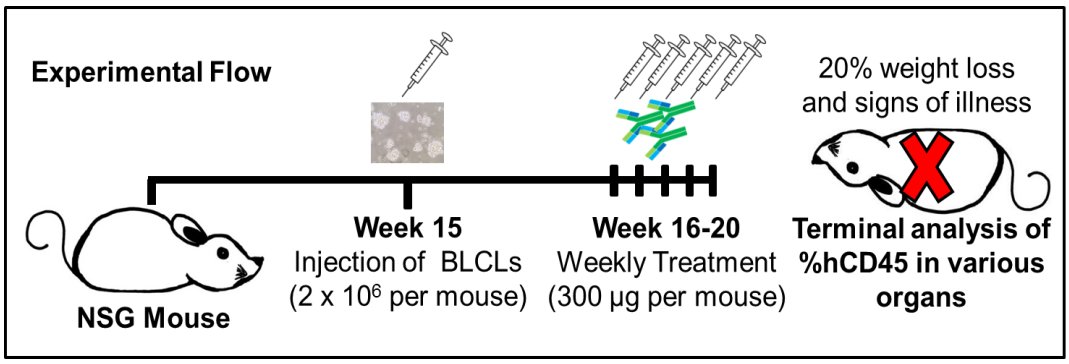

Figure 4.4: Schematic illustration of α-EBNA-1 TCR-like mAb treatment regimen. Two million (2 X 10^6) BLCL was injected into 15 weeks old NSG mice via the tail vein. Mice were treated weekly, with either a single dose of α-EBNA-1 TCR-like mAb (300 µg/injection) or isotype control antibody from week 16 onwards. Euthanasia was performed when weight loss of 20% or signs of disease were observed. Organs were then harvested for flow cytometric analysis and H&E staining.

4.3 α-EBNA-1 TCR-like mAb treatment ameliorates disease *in vivo*

As shown in **Figure 4.5A**, despite the fluctuations in the body weight of mice treated with α-EBNA-1 TCR-like mAb, they exhibited a delayed weight loss as compared to mice treated with mouse IgG1 isotype control antibody. Mice treated with another in-house produced TCR-like mAb specific for EBV LMP1 (α-LMP1 TCR-like mAb) did not exhibit any delayed weight loss. Based on Kaplan-Meier analysis, α-EBNA-1 TCR-like mAb treatment (p = 0.0098) significantly prolonged the survival of treated mice (**Figure 4.5B**). In contrast, all mice that were treated with the mouse IgG1 isotype control antibody or α-LMP1 TCR-like mAb displayed signs of disease (20% weight loss and/or moribund) and had to be euthanized by day 28.

Based on gross anatomy, no obvious disease manifestation was observed in the α-EBNA-1 TCR-like mAb-treated mice, while mass lesions were seen in the spleens of the isotype control antibody-treated mice (**Figure 4.6A** and **Appendix E**). Furthermore, H&E staining revealed a uniform appearance in the spleen histology of α-EBNA-1 TCR-like mAb-treated mouse, and this is in contrast to the regions of irregularity shown in the spleen of the isotype control antibody-treated mouse (**Figure 4.6B**). To assess the treatment effect in a more quantitative manner, we analyzed the percentages of $hCD45^+$ infiltration within organs via flow cytometry. As seen in **Figure 4.6C** and **Appendix E**, a stark decrease in BLCL infiltration was observed in the

spleen of α-EBNA-1 TCR-like mAb-treated mice as compared to that of the isotype control antibody-treated mice.

The amelioration of disease manifestations was also evident in the liver of the α-EBNA-1 TCR-like mAb-treated mice (**Figure 4.7A** and **Appendix E**). In mice treated with the isotype control antibody, multiple mass lesions were observed all over the liver. Consistent with the gross anatomy, H&E staining revealed the infiltration of small, round and monomorphic cells with hyperchromatic staining (**Figure 4.7B**). Digitally-highlighted image of the liver histology further revealed the severe disruption of the liver parenchymal architecture in the isotype control antibody-treated mice, but in the α-EBNA-1 TCR-like mAb-treated mice, the tissue morphology was well-preserved. Coherently, flow cytometric analysis of the liver showed that treatment with the α-EBNA-1 TCR-like mAb resulted in a reduction of $hCD45^+$ cells infiltration (6.51% versus 1.49%) when compared to isotype control antibody-treated mice (**Figure 4.7C** and **Appendix E**).

Despite the improvements in disease outcome in the spleens and livers of α-EBNA-1 TCR-like mAb-treated mice, such effect was not observed in the kidneys. Based on the staining for CD45 and CD19, a comparable percentage of kidney infiltration (11.7% versus 10.3%) was observed regardless of antibody treatment (**Figure 4.8A and B**). Furthermore, in mice which were euthanized at day 22, 33, and 44, an increasing amount of BLCL infiltration into the kidneys was observed (**Figure 4.8C**)

Taken together, our data demonstrated that the administration of a single dose of α-EBNA-1 TCR-like mAb weekly can decrease tumor burden and bring about therapeutic effects in the spleen and liver, providing a possible explanation for the observed delayed weight loss and prolonged survival in α-EBNA-1 TCR-like mAb-treated mice.

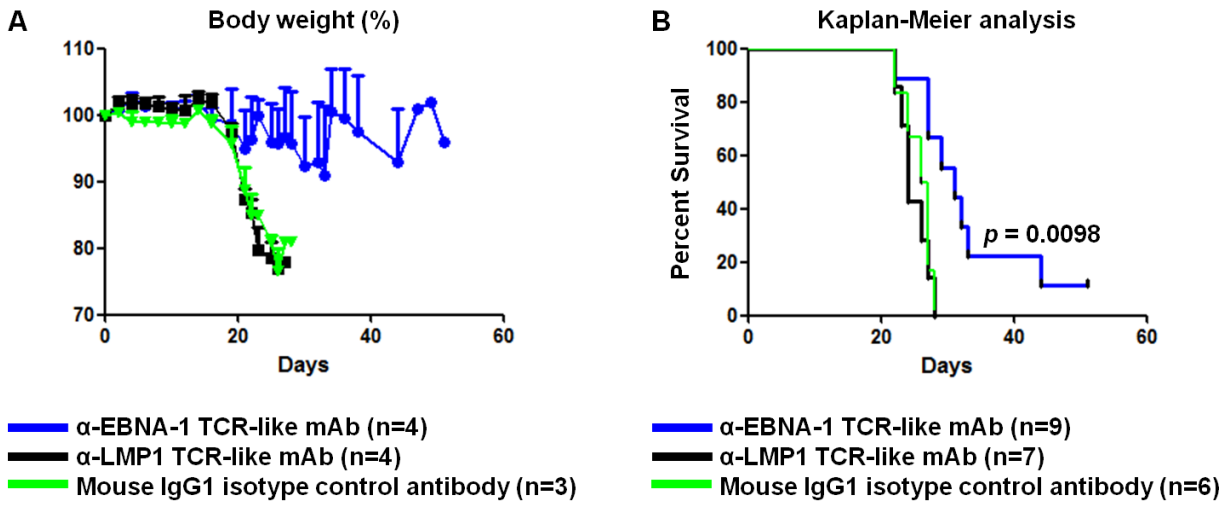

Figure 4.5: α-EBNA-1 TCR-like mAb treatment delayed weight loss and prolonged survival in treated mice. (A) Body weight and **(B)** Kaplan-Meier survival analysis of mice treated with α-EBNA-1 TCR-like mAb or mouse IgG1 isotype control antibody. Treatment with another in-house produced α-EBV TCR-like mAb (α-LMP1 TCR-like mAb) was included for comparison. Although an overall reduction in body weight was observed in the α-EBNA-1 TCR-like mAb-treated mice, the extent of weight loss was much lesser than mouse IgG1 isotype control antibody and α-LMP1 TCR-like mAb-treated counterparts. In addition, Kaplan-Meier survival plot also demonstrated that α-EBNA-1 TCR-like mAb-treated mice exhibited prolonged survival (Log-rank (Mantel-Cox) test $^{**}p = 0.0098$). Data is representative of two independent experiments.

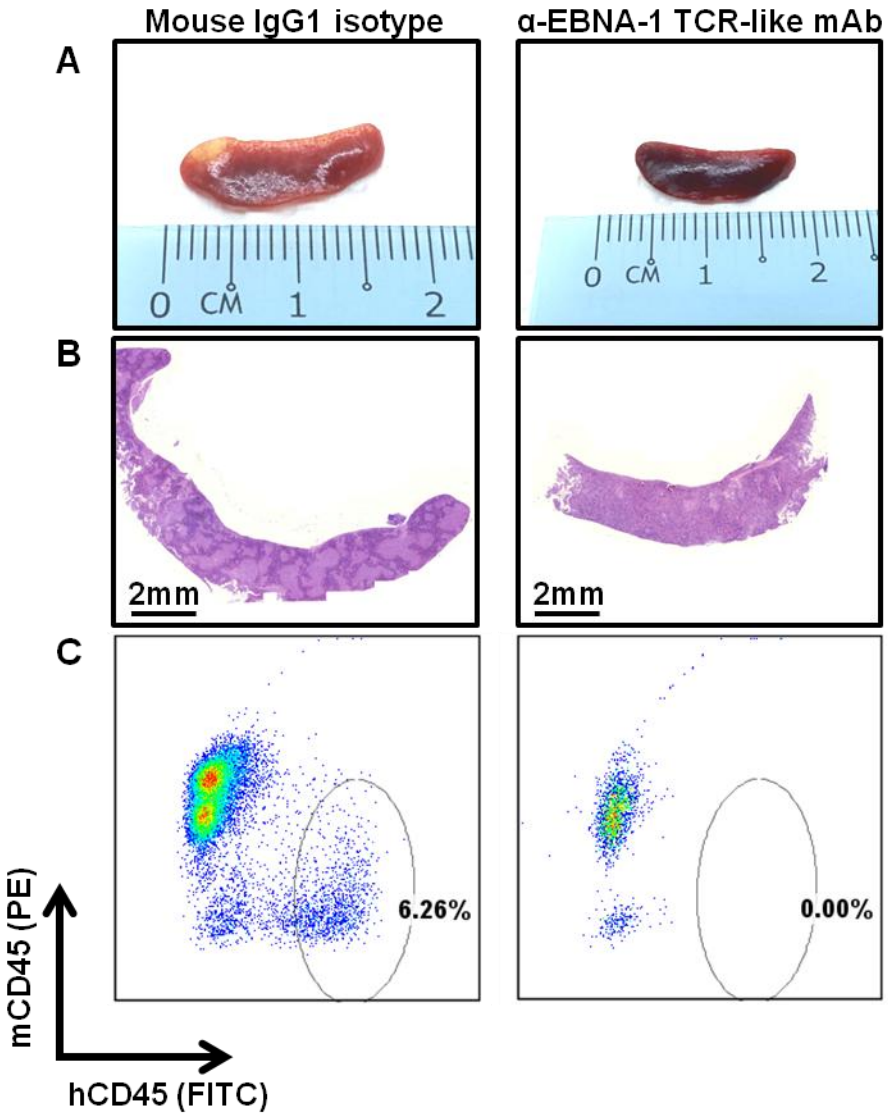

Figure 4.6: α-EBNA-1 TCR-like mAb ameliorated disease manifestation in the spleens of treated mice. Representative **(A)** gross anatomy, **(B)** H&E staining, and **(C)** flow cytometry profiles of spleens harvested from treated mice. Mass lesions were observed in the spleen of mouse IgG1 isotype control antibody-treated mice (n=3), but not that of the α-EBNA-1 TCR-like mAb-treated mice (n=4). H&E staining showed regions of irregularity in the spleen sections of the isotype control antibody-treated mice, which was in contrast to the uniform appearance seen in the α-EBNA-1 TCR-like mAb-treated mice. Furthermore, flow cytometric analysis showed no infiltration of hCD45 cells in the spleen of the α-EBNA-1 TCR-like mAb-treated mouse, while mouse treated with the IgG1 isotype control antibody had an approximately 6.26% of BLCL infiltration.

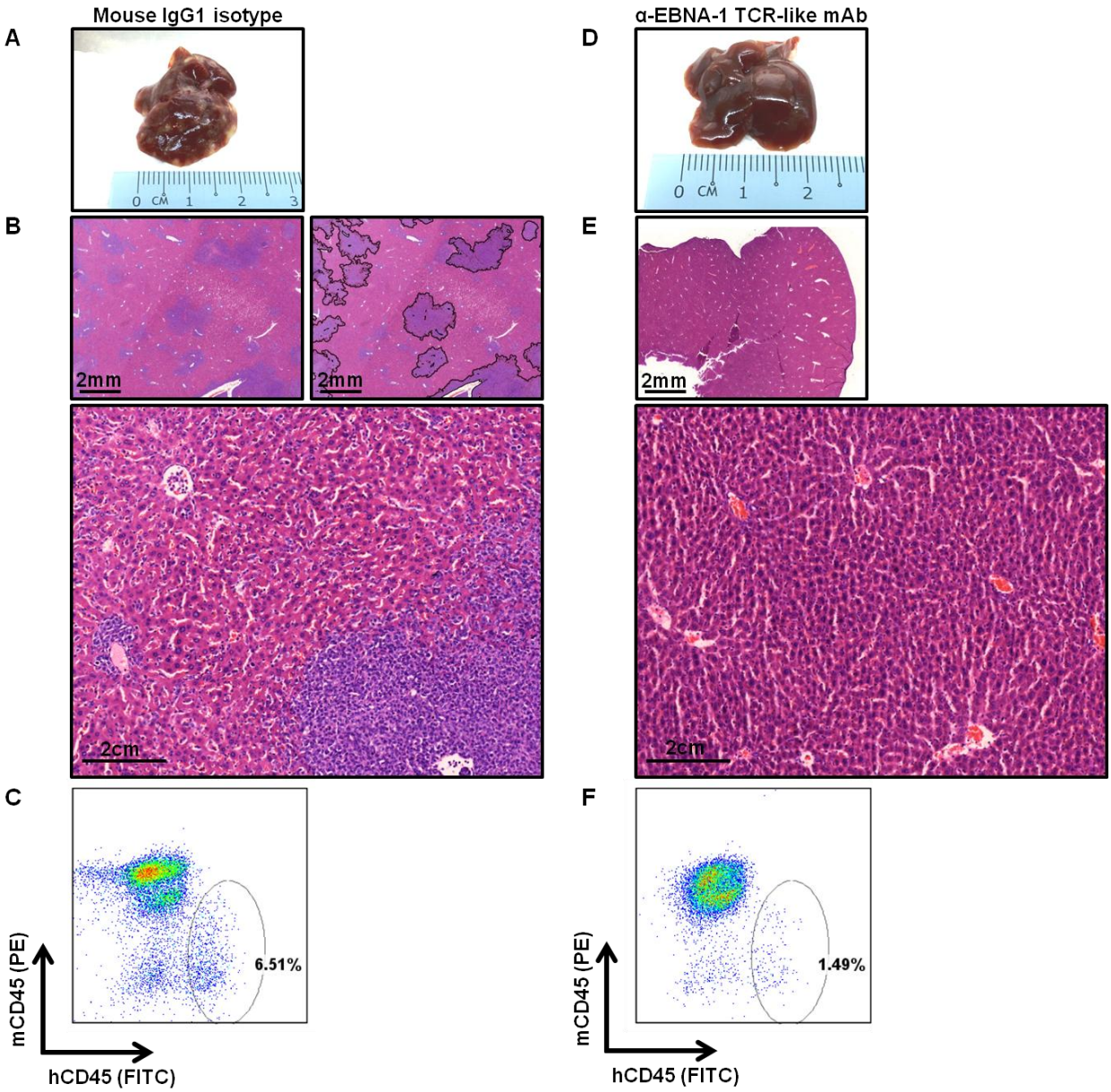

Figure 4.7: **α-EBNA-1 TCR-like mAb ameliorated disease manifestation in the livers of treated mice. (A and D)** In terms of gross anatomy, multiple mass lesions were observed in the liver of IgG1 isotype control-treated mice (n=3), but not the mice treated with α-EBNA-1 TCR-like mAb (n=4). **(B and E)** Consistent with the gross anatomy observation, H&E staining on the liver section of IgG1 isotype control-treated mice revealed the infiltration of small, round and monomorphic cells with hyperchromatic nuclear staining. Mass lesions were digitally highlighted using Adobe Photoshop CS6, and a 10X magnification of the liver section together illustrated the disruption of the liver parenchymal architecture. On the other hand, no obvious pathology was observed in α-EBNA-1 TCR-like mAb-treated mice. Coherently, flow cytometry plot of hCD45 versus mCD45 dot plot also showed higher percentage of hCD45 infiltration in IgG1 isotype control-treated mouse **(C, 6.51%)**, while reduced BLCL infiltration was observed in α-EBNA-1 TCR-like mAb-treated mouse **(F, 1.49%)**. **Scale bar**: 2 mm and 200 µm.

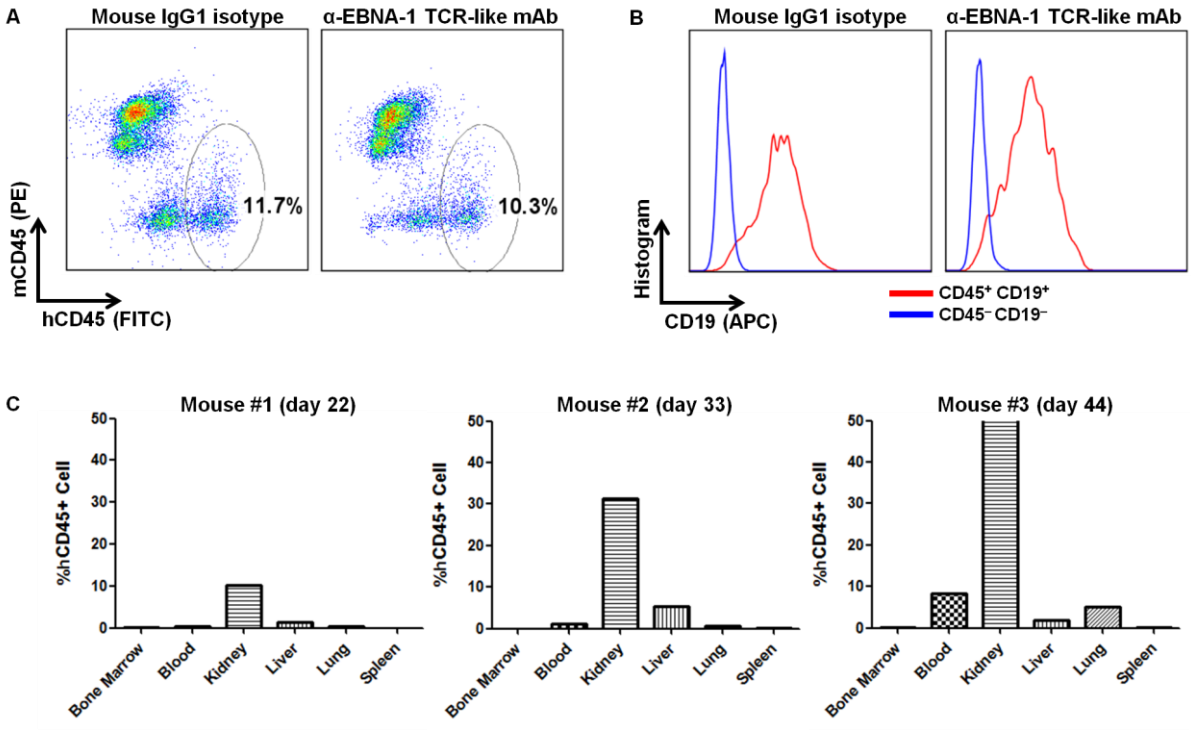

Figure 4.8: Infiltration of BLCL into the kidneys was observed regardless of the treatment. (A) Flow cytometric illustration of hCD45 (human leukocyte marker) versus mCD45.1 (mouse CD45 marker) dot plot showed similar percentage of BLCL infiltration into the kidneys of mice treated with mouse IgG1 isotype control antibody or α-EBNA-1 TCR-like mAb. **(B)** Based on the parent gating in **Figure 4.8A**, gated cells were confirmed to be of B cell lineage, expressing the surface marker CD19. **(C)** α-EBNA-1 TCR-like mAb-treated mice were euthanized at day 22, 33, and 44 to check for the percentage of BLCL infiltration into various organs. An increasing severity of BLCL infiltration into the kidneys was observed in mice euthanized at later time points. Days post-injection of BLCL were as per indicated.

4.4 α-EBNA-1 TCR-like mAb induces early apoptosis in BLCL

Unconjugated antibodies can engender a number of effector functions such as CDC, ADCC, antibody-mediated phagocytosis and the direct induction of apoptosis [123, 125, 132-135]. As mice treated with the α-EBNA-1 TCR-like mAb displayed delayed weight loss and prolonged survival, we next sought to examine the underlying mechanism(s) for this observed therapeutic effect.

As NSG mice are devoid of B cells, T cells, NK cells and the hemolytic complement system [160], the mechanisms of which the α-EBNA-1 TCR-like mAb could elicit were narrowed down to the direct induction of apoptosis and antibody-mediated phagocytosis. To test if the treatment of α-EBNA-1 TCR-like mAb can induce the apoptosis *in vitro*, BLCL was incubated with the antibody and checked for features of apoptosis.

Exposed phosphatidylserine (PS) on the outer leaflet of the cell membrane is an indicator of early stage apoptosis. As such, we assessed the amount of surface PS on BLCL via the preferentially binding of annexin V to exposed PS. Staining with fluorescent-conjugated annexin V showed that treatment with the α-EBNA-1 TCR-like mAb upregulated the expression of PS at 6 h and 24 h, with a greater upregulation of PS when 10 µg of α-EBNA-1 TCR-like mAb was added (**Figure 4.9A**).

In late apoptotic cells, the integrity of the cell membrane is compromised and no longer able to exclude DNA-binding dye. We thus used the DNA-binding dye 7-AAD as an indicator of late stage apoptosis. As shown in **Figure 4.9B**, no staining with 7-AAD was observed in BLCL treated with α-EBNA-1 TCR-like mAb. These data demonstrated that α-EBNA-1 TCR-like mAb treatment could directly trigger early but not late stage apoptosis at the assessed time points.

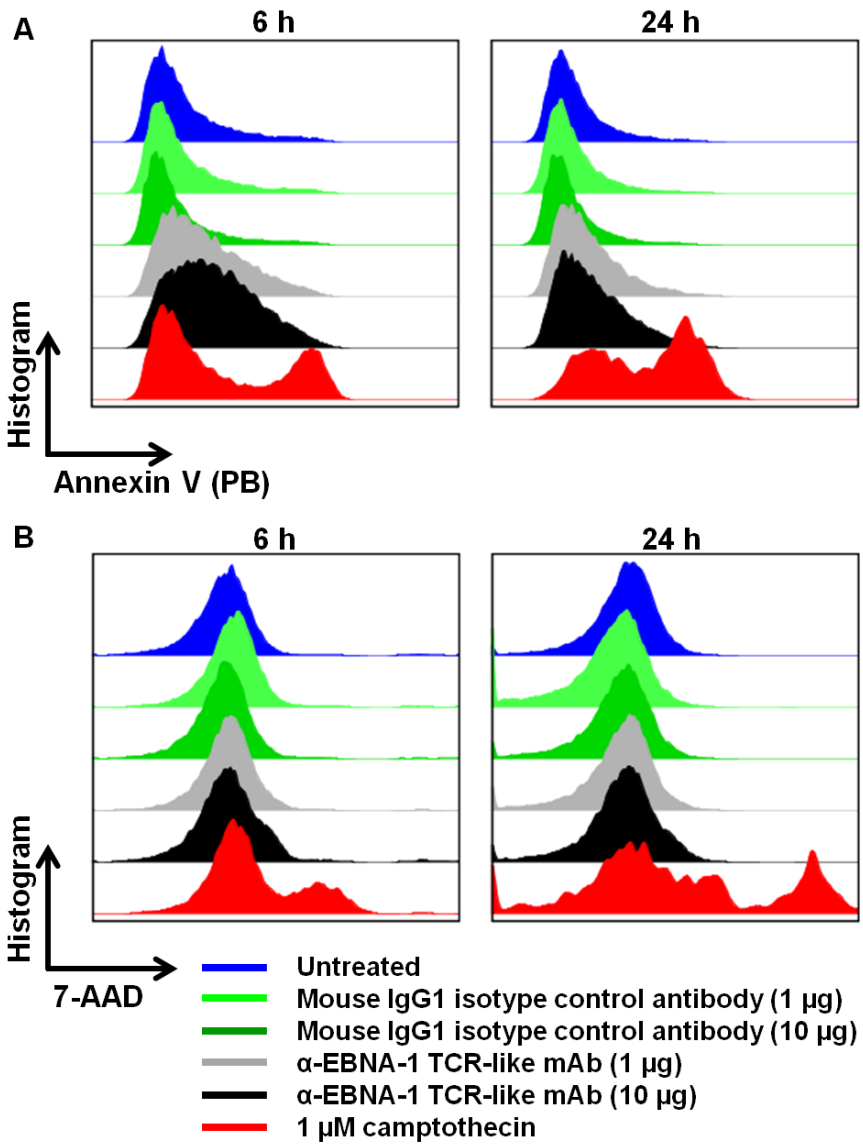

Figure 4.9: Treatment with α-EBNA-1 TCR-like mAb resulted in the induction of early stage apoptosis *in vitro*. To elucidate if α-EBNA-1 TCR-like mAb could elicit direct apoptosis, BLCL was treated with 1 µg and 10 µg of the antibody and harvested 6 h and 24 h later to check for apoptosis. **(A)** Annexin V and **(B)** 7-AAD staining were used as indicators of early and late stage apoptosis respectively. The induction of early stage apoptosis was observed in BLCL treated with α-EBNA-1 TCR-like mAb (1 µg and 10 µg) at both 6 h and 24 h time points. On the other hand, the induction of late stage apoptosis was not observed at both of the assessed time points based on the lack of 7-AAD staining.

4.5 α-EBNA-1 TCR-like mAb promotes the phagocytosis of BLCL *in vitro*

As professional phagocytes of the innate immune system, macrophages have been reportedly capable of phagocytosing tumor cells [219-221]. These cells are present in the NSG mice and have been shown by many to exhibit functional phagocytic activities [219, 222, 223]. To find out if α-EBNA-1 TCR-like mAb could facilitate the phagocytosis of BLCL by macrophages, *in vitro* phagocytosis assay was conducted.

Briefly, BLCL was labeled with CFSE and treated with the antibodies prior to the assay. Macrophages were stained with PE-CD11b for flow cytometric analysis, and PE^+CFSE^+ cells in the second quadrant (Q2) were defined as the successful uptake of CFSE-labeled BLCL by the macrophages. When BLCL was incubated with α-EBNA-1 TCR-like mAb for 3 h prior to phagocytosis, 4.3% of PE^+CFSE^+ cells was observed (**Figure 4.10A**). The enhancement of phagocytosis upon α-EBNA-1 TCR-like mAb treatment was higher than the basal levels of phagocytosis observed when no antibody or mouse IgG1 isotype control antibody was added. Similarly, the enhancement of phagocytosis was also observed when BLCL was pre-incubated with the α-EBNA-1 TCR-like mAb for 24 h prior to the phagocytosis assay (**Figure 4.10B**).

To ensure that the observed PE^+CFSE^+ data acquired on flow cytometry were true phagocytic events and not cell aggregates with non-specific staining, fluorescent microscopy was used to visualize the phagocytosed BLCL within macrophages. As seen in **Figure 4.11**, different phases of phagocytosis such as contact and engulfment were observed with α-EBNA-1 TCR-like mAb treatment.

As an alternative approach to quantify phagocytosis, phagocytic index was used to enumerate phagocytosis based on the manual counting of PE^+CFSE^+ cells. As compared to mouse IgG1 isotype control, the treatment with α-EBNA-1 TCR-like mAb promoted phagocytosis at both 3 h and 24 h time points, consistent with the flow cytometry data (**Figure 4.12**).

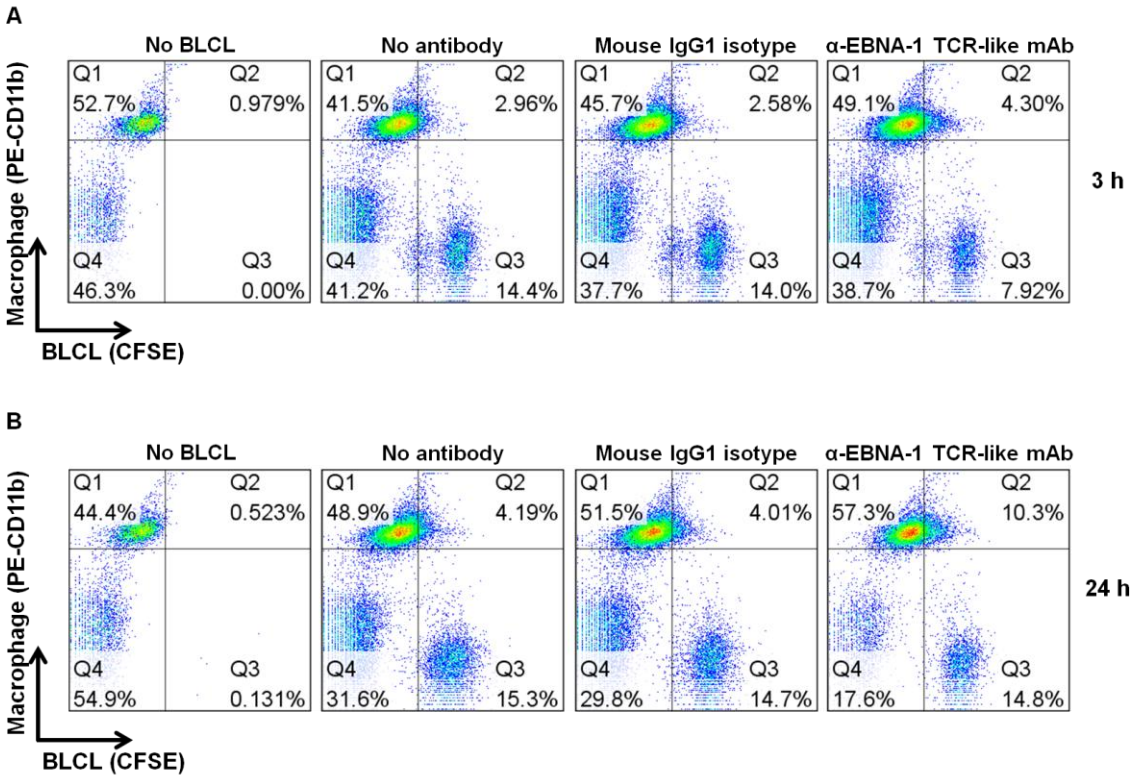

Figure 4.10: α-EBNA-1 TCR-like mAb treatment enhanced the phagocytosis of BLCL (flow cytometry). Flow cytometry was used to elucidate the effects of α-EBNA-1 TCR-like mAb treatment on phagocytosis. Percentage of $CD11b^{+}CFSE^{+}$ cells in quadrant 2 (Q2) denotes successful phagocytosis. Compared to no antibody and mouse IgG1 isotype control treatment, BLCL incubated with α-EBNA-1 TCR-like mAb for **(A)** 3 h and **(B)** 24 h prior to phagocytosis enhanced their uptake by the $CD11b^{+}$ macrophages. Data is representative of two independent experiments.

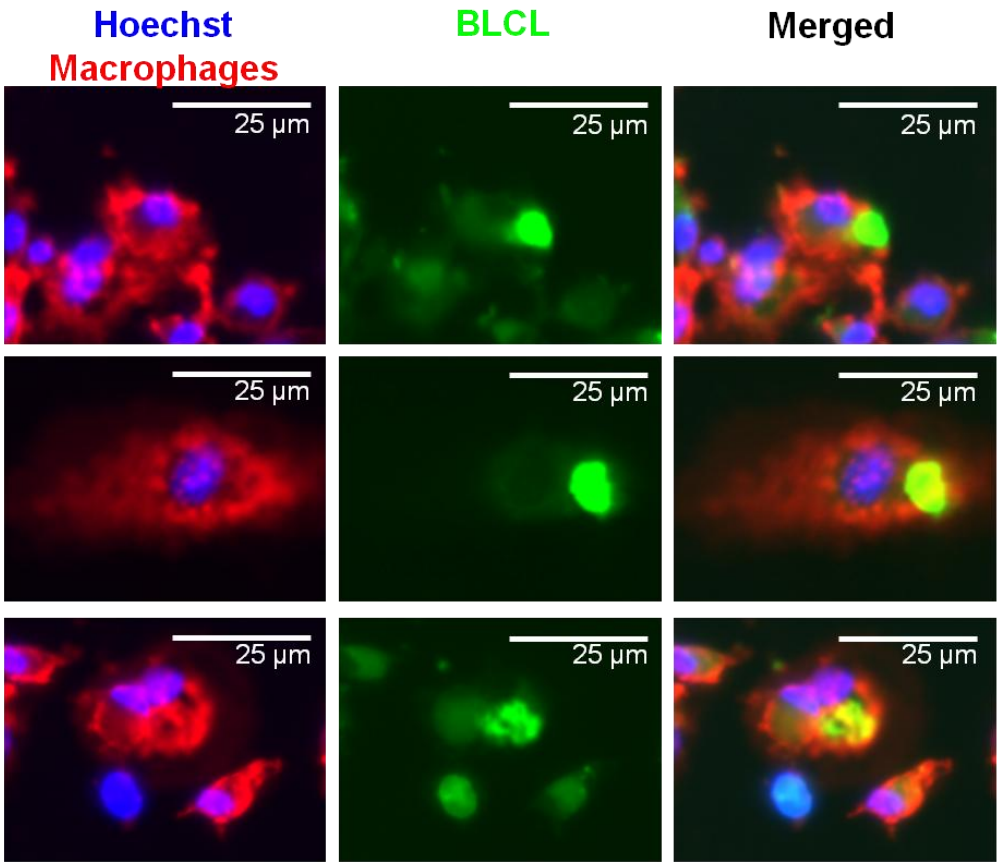

Figure 4.11: Different phases of phagocytosis were observed upon α-EBNA-1 TCR-like mAb treatment. Phagocytosis assay was performed to visualize the ability of α-EBNA-1 TCR-like mAb in facilitating phagocytosis. Immunofluorescent staining showed the engagement and engulfment of BLCL (green) by a macrophage (red) in a phagocytosis assay.

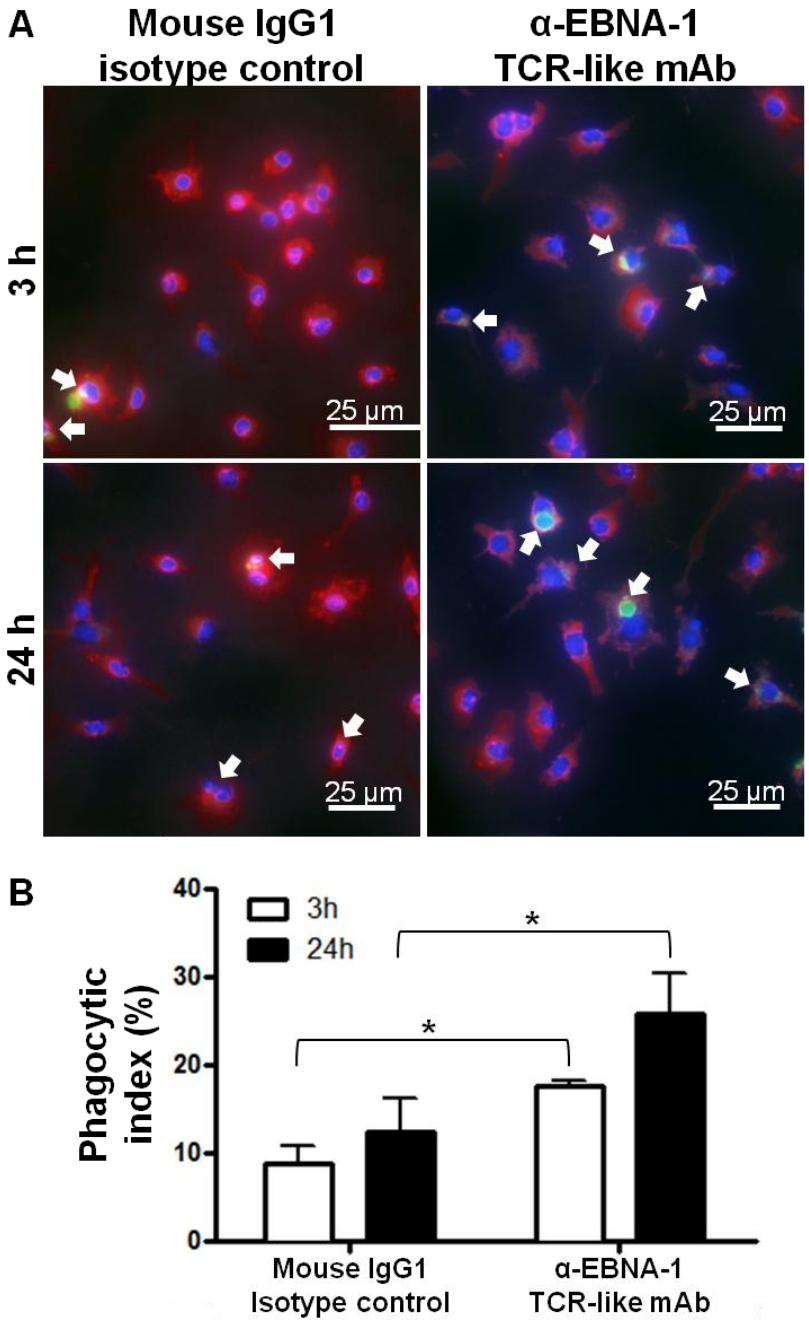

Figure 4.12: α-EBNA-1 TCR-like mAb treatment enhanced the phagocytosis of BLCL (fluorescent microscopy). (A) Immunofluorescent staining was used as an alternative methodology for phagocytosis assay quantification. The enhancement of phagocytosis upon α-EBNA-1 TCR-like mAb treatment was observed at both 3 h and 24 h time points. White arrows were used to indicate the relative amount of phagocytosis. **(B)** Phagocytic index (%) was calculated based on visual scoring of $CD11b^{+}CFSE^{+}$ cells over three FOV. Statistical significances for 3 h and 24 h α-EBNA-1 TCR-like mAb incubation were $p = 0.019$ and $p = 0.0169$ respectively (unpaired Student's *t*-test). Values are expressed as % mean ± SD (*$p < 0.05$).

4.6 Fc-dependent mechanism of α-EBNA-1 TCR-like mAb-mediated phagocytosis

As antibody-mediated phagocytosis requires Fc receptor binding, antibody variant with a mutation in the Fc portion that abrogates Fc receptor binding will abolish phagocytosis. As such, to investigate whether α-EBNA-1 TCR-like mAb-mediated phagocytosis was Fc-dependent, we generated a FcγR-null binding variant of the antibody, denoted as α-EBNA-1 TCR-like mAb (D265A) (**Figure 4.13A**).

As shown in **Figure 4.13B**, the FcγR-null binding variant of α-EBNA-1 TCR-like mAb displayed a similar profile as the unmodified antibody on a SDS-PAGE gel, with a band observed (between 150 kDa to 250 kDa) corresponding to the intact antibody in non-reducing conditions, and two bands corresponding to the heavy (at 50 kDa) and light chains (at 25 kDa) of an antibody under reducing condition. To show that the mutation on α-EBNA-1 TCR-like mAb had no impact on its binding capability, flow cytometric analysis was performed to assess the staining for EBNA-1 pMHC on HLA-A*02 BLCL. Indeed, α-EBNA-1 TCR-like mAb (D265A) demonstrated equivalent binding profile as the unmodified antibody (**Figure 4.13C**).

To assess the functionality of α-EBNA-1 TCR-like mAb (D265A), phagocytosis assay was performed to compare the ability of the FcγR-null binding variant (D265A) and its unmodified antibody in mediating phagocytosis. As seen in **Figure 4.14**, while the unmodified α-EBNA-1 TCR-like mAb had an observed 11.3% $PE^{+}CFSE^{+}$ cells, treatment with the FcγR-null binding variant (D265A) greatly abrogated phagocytosis (4.42%) to levels comparable to the no antibody (5.78%) and mouse IgG1 isotype (6.92%) treatment controls. Taken together, our data validated the capability of the α-EBNA-1 TCR-like mAb in promoting phagocytosis, and further affirmed the involvement of Fc receptor binding in α-EBNA-1 TCR-like mAb-mediated phagocytosis of BLCL.

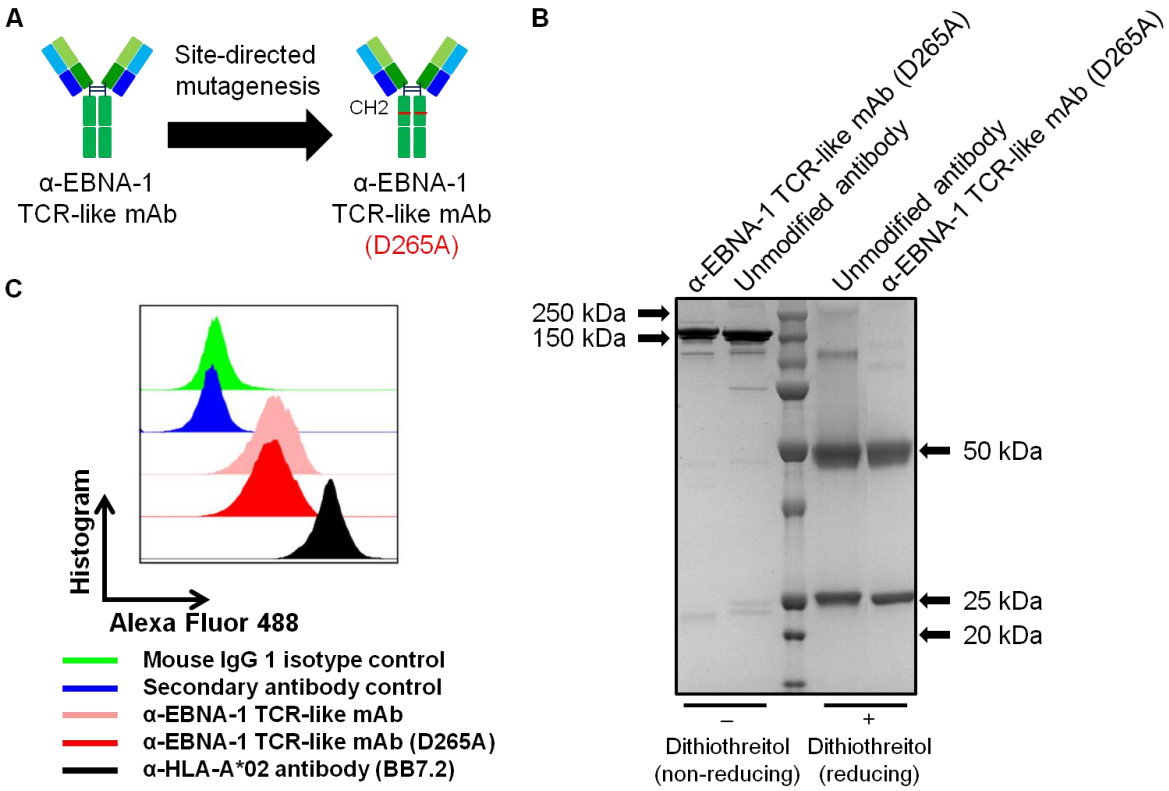

Figure 4.13: Characterization of the FcγR-null binding variant (D265A) of α-EBNA-1 TCR-like mAb. (A) Schematic illustration of the site-directed mutagenesis of aspartic acid at position 265 to alanine in the CH2 domain of the antibody, generating antibody variant incapable of FcγR binding. **(B)** Purified FcγR-null binding variant (D265A) showed no discernible difference from the unmodified α-EBNA-1 TCR-like mAb under both non-reducing and reducing conditions on a SDS-PAGE gel. **(C)** Flow cytometry analysis was performed to compare the binding of FcγR-null binding variant (D265A) with its unmodified α-EBNA-1 TCR-like mAb. Histogram plot showed that both antibodies were similar in their binding to HLA-A*02 BLCL.

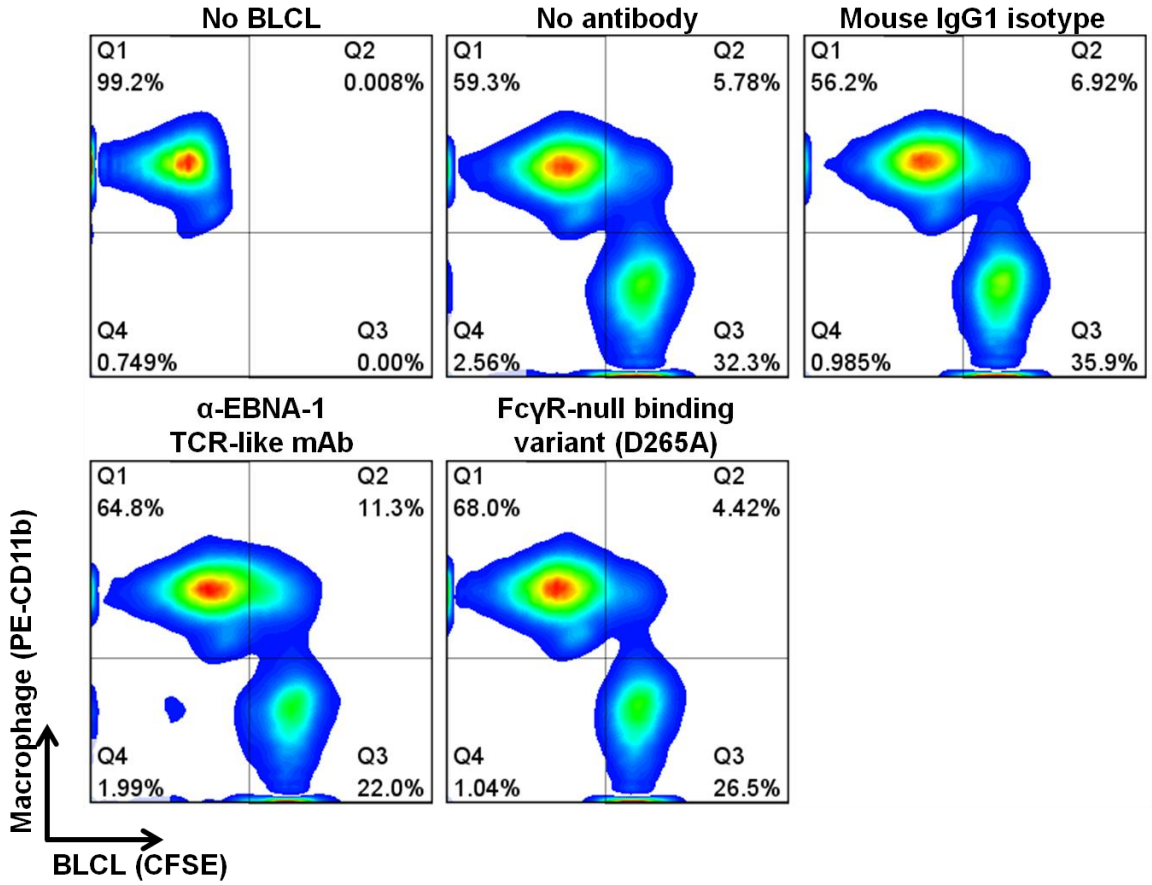

Figure 4.14: **Abolishment of phagocytosis with FcγR-null binding variant (D265A) of the α-EBNA-1 TCR-like mAb.** Phagocytosis assay was performed to confirm the requirement of FcγR in eliciting antibody-mediated phagocytosis. Using the unmodified α-EBNA-1 TCR-like mAb as a positive control, enhanced phagocytosis (11.3%) was observed when compared to no antibody (5.78%) and mouse IgG1 isotype control (6.92%). Phagocytosis was abolished (4.42%) when the FcγR-null binding variant (D265A) of α-EBNA-1 TCR-like mAb was used.

Chapter 5:
Result (III)

5.1 Synopsis

In this chapter, we described the generation of a novel autologous humanized mouse model of EBV-associated disease, which can serve as a potential preclinical model for therapeutic assessment. In this setup, NSG mice were employed to support the reconstitution of a human hematoimmune system. In parallel, autologous BLCLs were generated *in vitro* and injected into NSG mice reconstituted with $CD34^+$ HPCs from the same donor, thereby establishing a syngeneic model. We performed *in vitro* EBV infection with various samples such as cord blood and fetal organs (liver, bone marrow and spleen) to evaluate their ability to generate BLCL for the autologous humanized mouse model. To improve the reconstitution of human immune cells in our system, we further employed HDI of plasmids encoding human cytokines to augment the development of specific immune cell types.

5.2 Establishing a humanized mouse model engrafted with autologous cord blood-derived BLCL

The standard humanized mouse model of EBV infection involves the injection of EBV supernatant to infect *de novo* reconstituted human B cells, supporting EBV infection *in vivo* (**Figure 1.6**). However, this approach poses inconsistency in the efficiency of *in vivo* EBV infection

due to varied numbers of reconstituted human B cells available for infection within each mouse.

To improve the model, we modified the current approach by infecting B cells with EBV *in vitro* using cord blood-derived B cells from the negative fraction of $CD34^+$ selection. Upon the obtainment of stabilized BLCL after six weeks of passaging, we injected a fixed number of BLCL into 12 weeks old humanized mouse reconstituted with matching HPCs from the same donor, establishing an orthotopic and autologous humanized mouse model (**Figure 5.1**). This approach would enable us to inject a precise number of BLCL, achieving the desired disease outcome. In addition, as BLCL was generated *in vitro*, these cells could be thoroughly characterized and tested for their sensitivity to therapeutics *in vitro*.

As per normal *de novo* generation of the human lymphoid immune cells in the humanized mouse, the reconstitution of human immune cells such as CD45, CD3, CD4, CD8, and CD19 were observed (**Figure 5.2**). To delineate the development of human immune cells in this autologous humanized mouse model, weekly facial bleeding was performed for flow cytometric immunophenotyping over the course of 18 weeks.

As seen in **Figure 5.3A**, $hCD45^+$ cells were detected in the peripheral blood of the autologous humanized mice for the entire 18 weeks, albeit with decreasing chimerism over time. Within these $hCD45^+$ cells, a decreasing percentage of $CD19^+$ B cells reconstitution was accompanied by the observed increment in $CD3^+$ T cells (**Figure 5.3B**). In terms of CD4/CD8 T cell ratio, a general trend of increasing $CD4^+$ T cells was observed when compared to $CD8^+$ T cells (**Figure 5.3D-F**).

In humanized mice injected with autologous BLCL, no obvious pathological manifestation was observed upon euthanasia (data not shown). While these mice had larger spleens, they were not significantly larger than those from the non-injected humanized control mice (**Figure 5.4A**). However, mice that were injected with autologous BLCL displayed reduced weight gain over the time course and were therefore suggested to be less healthy than the control mice ($p < 0.0001$) (**Figure 5.4B**).

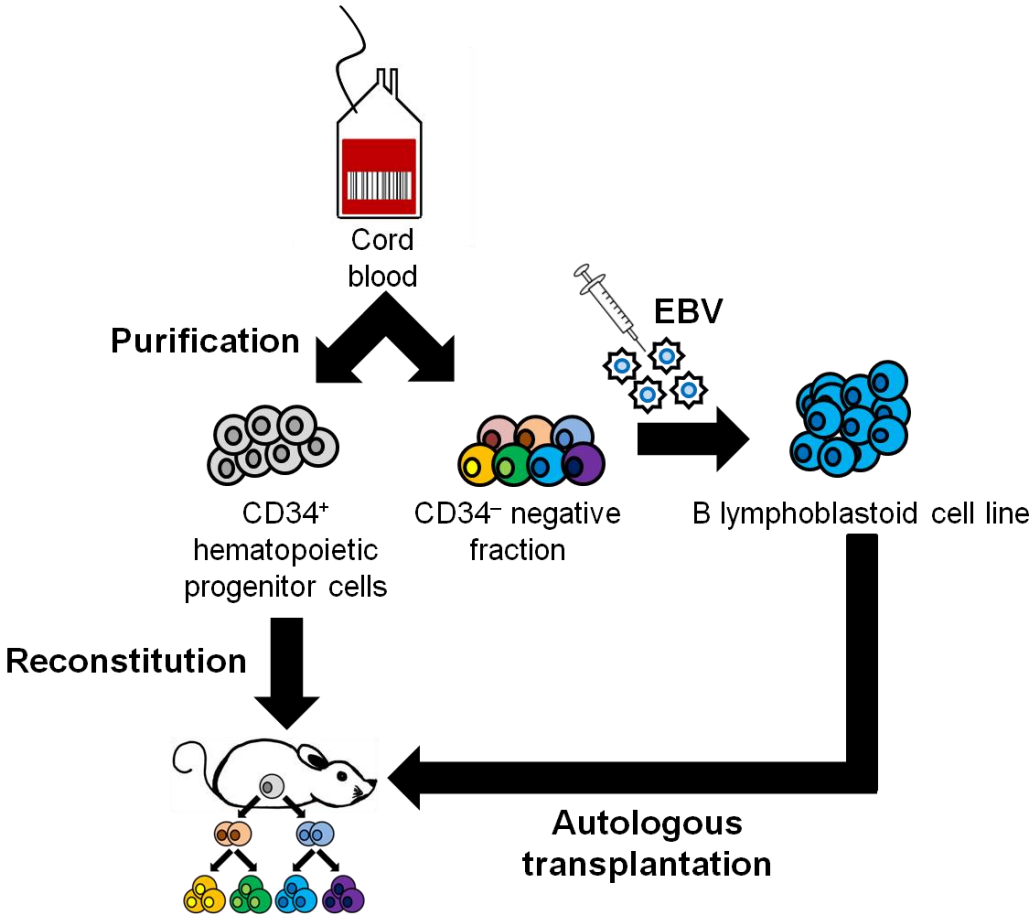

Figure 5.1: **The development of a novel humanized mouse model for preclinical testing.** The current humanized mouse model of EBV-associated diseases involves the injection of EBV supernatant into a humanized mouse, thereby achieving i*n vivo* infection. In our current approach, $CD34^+$ HPCs were purified from the cord blood for the reconstitution of the humanized mouse. In parallel, BLCL was generated from the *in vitro* infection of B cells present in the $CD34^-$ fraction of the same cord blood sample. Upon the successful reconstitution of the human immune cells in the mouse, autologous BLCL was transplanted into its matching humanized mouse to generate a novel humanized mouse model for the evaluation of therapeutics.

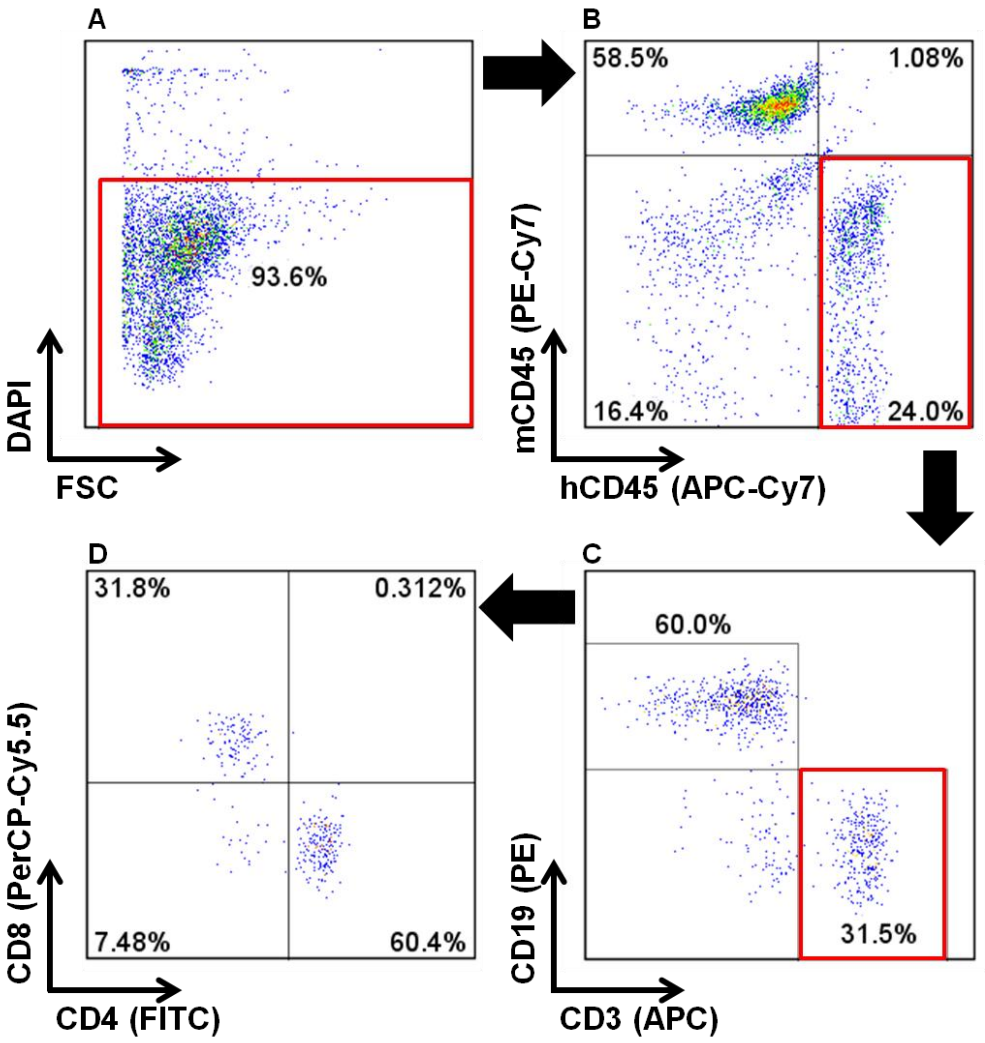

Figure 5.2: The *de novo* generation of human immune cells in the humanized mouse. Upon the injection of $CD34^+$ HPCs from human cord blood, mice were kept for 12 weeks to allow the differentiation of human immune cells. Mice were then bled on week 12 to check for the percentages of chimerism (hCD45 versus mCD45). Human immune cells such as B cells ($CD19^+$) and T cells ($CD4^+$ and $CD8^+$) were detected in the peripheral bloods of these humanized mice.

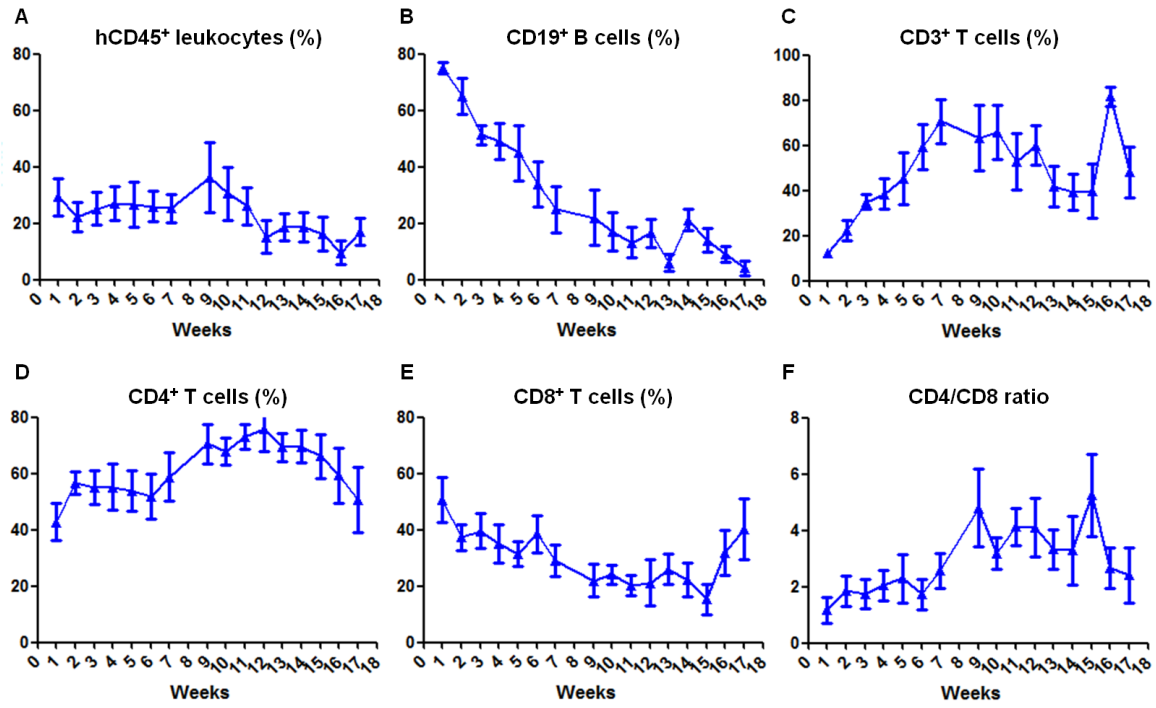

Figure 5.3: Profile of the human immune cells in the humanized mouse. Flow cytometric immunophenotyping was used to profile the reconstitution of human immune cells in the peripheral blood of the humanized mice. Mice were first bled at 12 weeks old (denoted as week 0) for the initial reconstitution check, followed by weekly facial bleeding till the age of 30 weeks old to monitor the changes in the percentages of human immune cells. **(A)** A general trend of declining chimerism (%hCD45$^+$ cells) was observed in all humanized mice. **(B and C)** Within the CD45$^+$ cells, B cells (%) declined inversely to the increased T cells (%). **(D-F)** Rising CD4/CD8 ratio indicated the increasing percentage of CD4$^+$ T cells (over CD8$^+$ T cells) across 18 weeks. Values are expressed as mean ± SD.

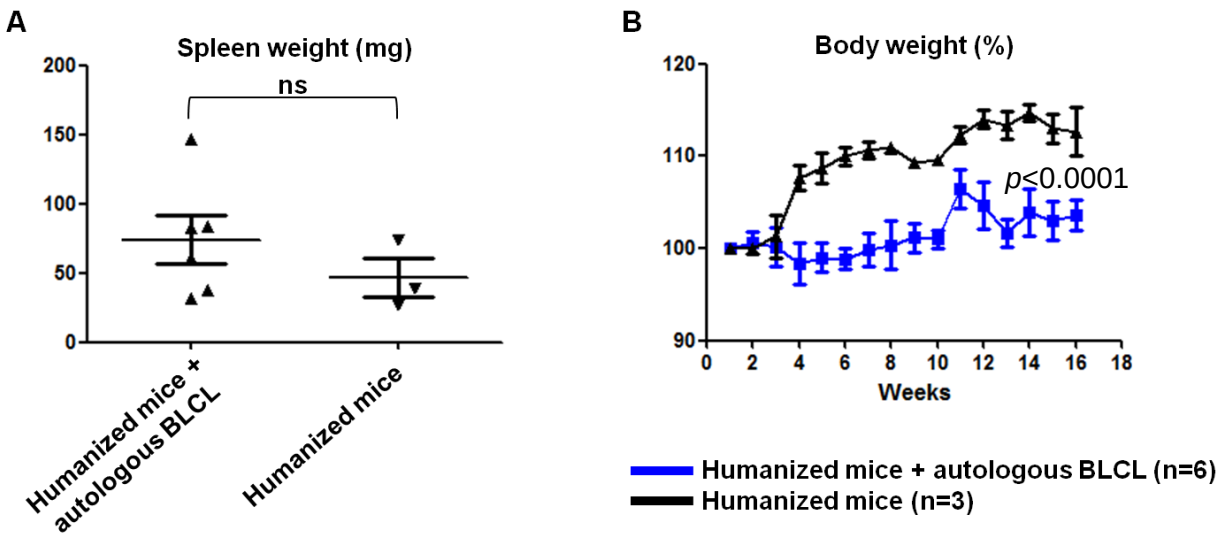

Figure 5.4: Body and spleen weight of humanized mouse injected with autologous BLCL. (A) Mice were euthanized at the end of 18 weeks with spleens harvested and expressed in microgram (mg). No significant (ns) difference in the spleen weight was noted between humanized mice injected with BLCL and its control (p = 0.3362). **(B)** Mice were weighed on a weekly basis. Body weight of mice was expressed as a percentage over the weight on day 1 (current weight/weight on day 1)*100. Humanized mice with autologous BLCL injected displayed lesser weight gain as compared to control mice without BLCL injection (p < 0.0001). Values are expressed as mean ± SD.

5.3 Fetal liver as an alternative source of $CD19^+$ B cells for BLCL generation

With the success of utilizing cord blood to generate an autologous humanized mouse model, we proceeded to recapitulate this model using the fetal liver. This is because the fetal liver can provide a greater number of $CD34^+$ HPCs for the reconstitution of a larger cohort of humanized mice. We employed an identical approach as depicted in **Figure 5.1** to obtain BLCL from $CD34^-$ fraction of the fetal liver. However, *in vitro* EBV infection of this fraction failed to generate any BLCL.

To increase the possibility of establishing BLCL from the fetal liver $CD34^-$ fraction, cells were sorted for CD19 to obtain a highly purified population of B cells for *in vitro* EBV infection. In the $CD19^+$ fraction, cells were positive for CD45 and CD19, but negative for CD3, CD4, and CD8 (**Figure 5.5**, first row). On the other hand, a mixture of B cells and T cells were observed in the unsorted fraction (**Figure 5.5**, last row). Despite the enrichment of $CD19^+$ B cells, the formation of macroscopic cell clumps was not observed and BLCL generation using $CD34^-$ fraction of the fetal liver was unsuccessful.

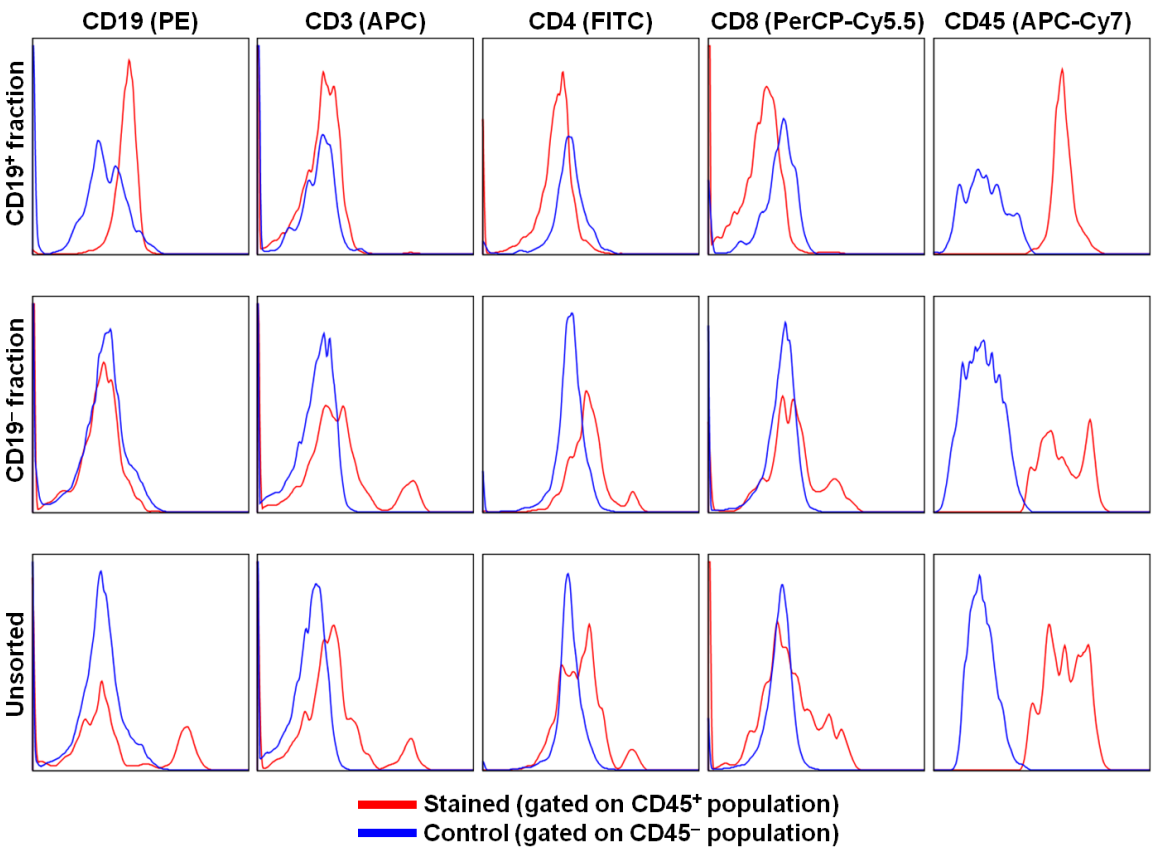

Figure 5.5: CD34$^-$ fraction of fetal liver as a source of B cells for BLCL generation. The CD34$^-$ fraction obtained after CD34$^+$ HPCs isolation process was further sorted for CD19$^+$ B cells (**Top row**). In the CD19$^+$ fraction, cells were confirmed to be positive for CD19 and CD45, but negative for CD3, CD4 and CD8. EBV supernatant was added into each of the three fractions (CD19$^+$ fraction, CD19$^-$ fraction, and unsorted) for BLCL generation.

5.4 Fetal bone marrow and fetal spleen as alternative sources of $CD19^+$ B cells for BLCL generation

With the inability to generate BLCL from the fetal liver $CD34^-$ fraction, we next explored the usage of fetal bone marrow and fetal spleen as alternative sources of B cells for BLCL generation. Based on the CD19 and CD45 staining, the presence of unwanted $CD45^-CD19^-$ cells, which can hinder the efficiency of EBV, was observed to be in excess in all three fetal liver samples (**Figure 5.6**). More importantly, a notably higher percentage of $CD45^+CD19^+$ cells were observed in the fetal bone marrow (16.9% and 51.8%) and fetal spleen (43.4% to 62.1%), indicating a greater abundance of B cells for EBV infection.

As the B cells from fetal bone marrow and fetal spleen are developmentally and immunophenotypically distinct, the characterization of these B cells from these two lymphoid organs was necessary to elucidate their immunophenotypes prior to EBV infection and BLCL generation. As seen in **Figure 5.7A**, an average of 85% and 95% B cell purity was obtained for the CD19-sorted fetal bone marrow and spleen respectively.

Based on the comparison of cell surface markers, we observed distinctive differences in the immunophenotypes of B cells from the fetal bone marrow and fetal spleen (**Figure 5.7A**). A notable higher numbers of $CD34^+$ cells (hematopoietic progenitor cell marker) were

found in the fetal bone marrow, coherent with the presence of HPCs in the bone marrow for hematopoiesis.

When we gated on the $CD19^+$ B cells from fetal bone marrow and fetal spleen, a further distinction in CD10, IgM, and IgD expressions were observed. In the fetal bone marrow, the majority of the $CD19^+$ B cells were $CD10^+IgM^-IgD^-$, exhibiting surface markers of pro- and pre-B cell stage, illustrating the process of early B cell differentiation in the bone marrow. In comparison, a majority of the $CD19^+$ B cells in the fetal spleen, a secondary lymphoid organ, displayed a $CD10^-IgM^+IgD^+$ profile. This observation is in agreement with B cell development, where the loss of CD10 expression is accompanied by the gain of IgM and IgD expressions when B cells mature and migrate into the periphery.

In view of the progressive maturation of B cells, the decline of CD10 expression alongside with the increase of CD20 and CD45 expressions were well-illustrated in the $CD19^+$ B cells of the fetal spleen, displaying a higher expressions of CD20 and CD45 as compared to the $CD19^+$ B cells of the fetal bone marrow (**Figure 5.7B**) [224-226]. Cells from both developmental niches lacked staining for the plasma cell marker CD138.

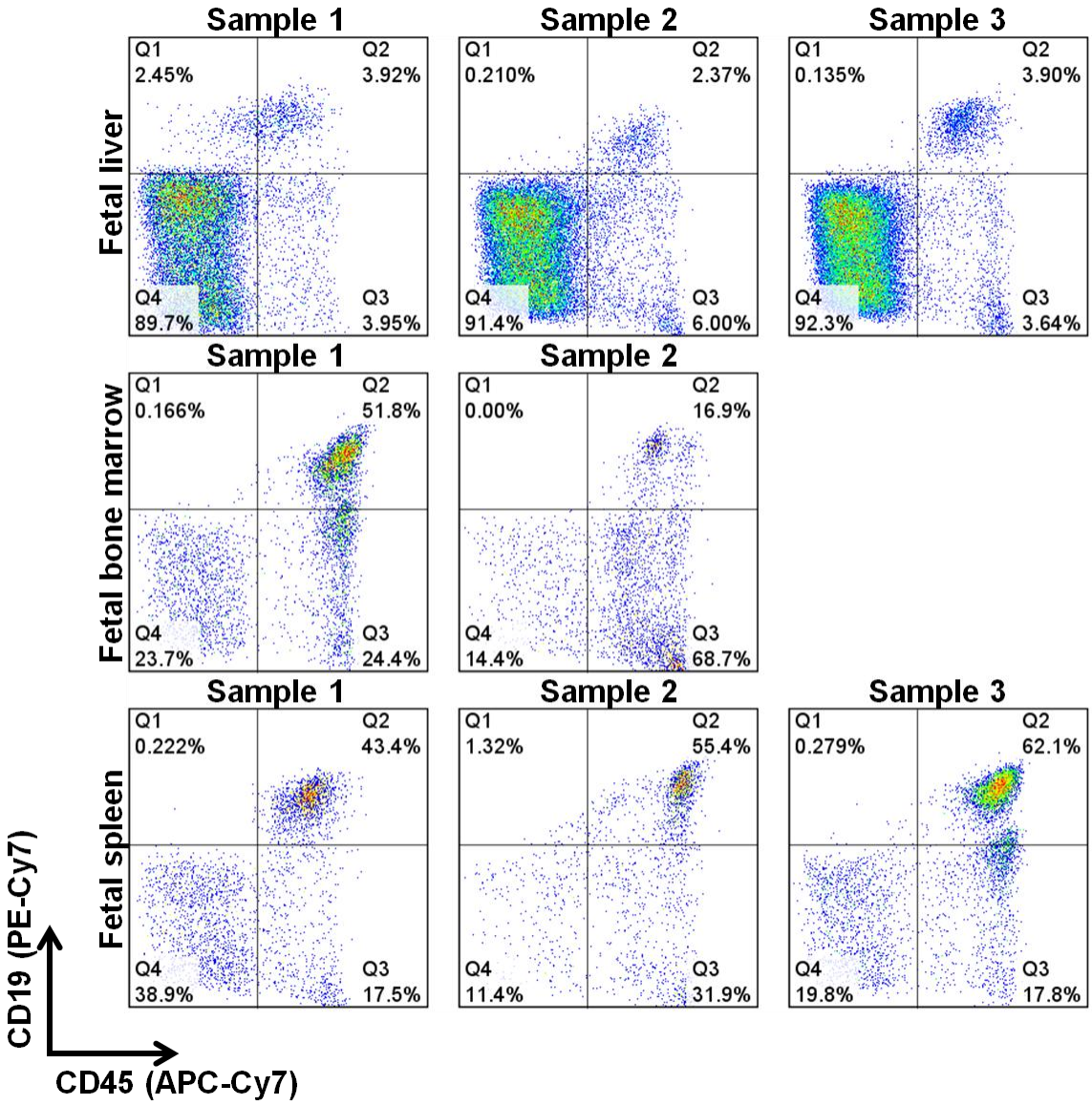

Figure 5.6: Comparison of the $C19^{+}CD45^{+}$ cells between fetal liver $CD34^{-}$ fraction, fetal bone marrow, and fetal spleen. Owing to the inability to generate BLCL from the $CD34^{-}$ fraction of the fetal liver, fetal bone marrow and fetal spleen were explored as alternative sources of B cells. Based on $C19^{+}CD45^{+}$ gating, a low percentage of B cells (2.37% to 3.92%) was observed in the fetal liver. This was in contrast to the fetal bone marrow (16.9% and 51.8%) and fetal spleen (43.4% to 62.1%), which indicated a greater abundance of B cells for BLCL generation.

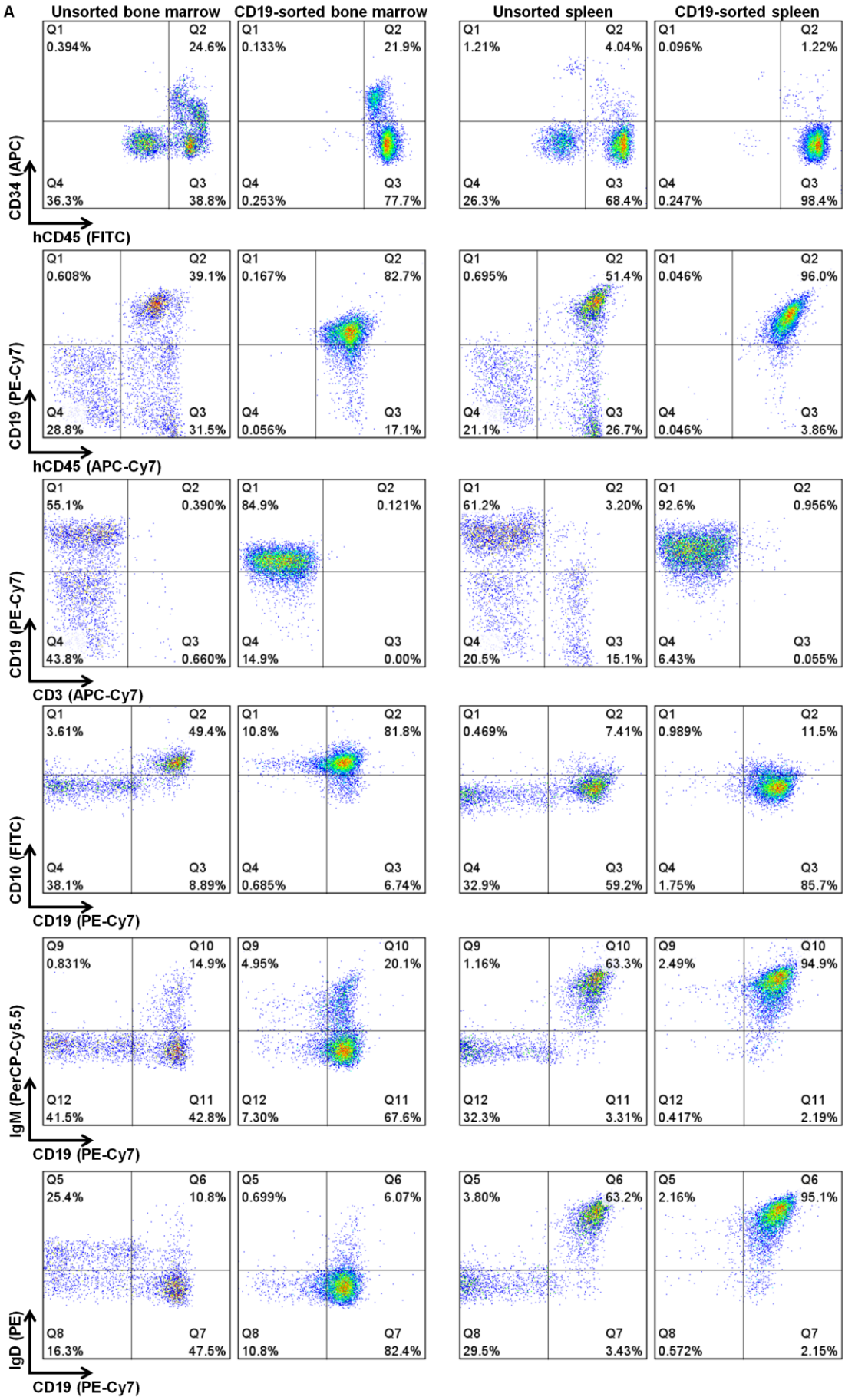
A
Unsorted bone marrow
CD19-sorted bone marrow
Unsorted spleen
CD19-sorted spleen
CD34 (APC)
hCD45 (FITC)
Q1 0.394%
Q2 24.6%
Q4 36.3%
Q3 38.8%
Q1 0.133%
Q2 21.9%
Q4 0.253%
Q3 77.7%
Q1 1.21%
Q2 4.04%
Q4 26.3%
Q3 68.4%
Q1 0.096%
Q2 1.22%
Q4 0.247%
Q3 98.4%
CD19 (PE-Cy7)
hCD45 (APC-Cy7)
Q1 0.608%
Q2 39.1%
Q4 28.8%
Q3 31.5%
Q1 0.167%
Q2 82.7%
Q4 0.056%
Q3 17.1%
Q1 0.695%
Q2 51.4%
Q4 21.1%
Q3 26.7%
Q1 0.046%
Q2 96.0%
Q4 0.046%
Q3 3.86%
CD19 (PE-Cy7)
CD3 (APC-Cy7)
Q1 55.1%
Q2 0.390%
Q4 43.8%
Q3 0.660%
Q1 84.9%
Q2 0.121%
Q4 14.9%
Q3 0.00%
Q1 61.2%
Q2 3.20%
Q4 20.5%
Q3 15.1%
Q1 92.6%
Q2 0.956%
Q4 6.43%
Q3 0.055%
CD10 (FITC)
CD19 (PE-Cy7)
Q1 3.61%
Q2 49.4%
Q4 38.1%
Q3 8.89%
Q1 10.8%
Q2 81.8%
Q4 0.685%
Q3 6.74%
Q1 0.469%
Q2 7.41%
Q4 32.9%
Q3 59.2%
Q1 0.989%
Q2 11.5%
Q4 1.75%
Q3 85.7%
IgM (PerCP-Cy5.5)
CD19 (PE-Cy7)
Q9 0.831%
Q10 14.9%
Q12 41.5%
Q11 42.8%
Q9 4.95%
Q10 20.1%
Q12 7.30%
Q11 67.6%
Q9 1.16%
Q10 63.3%
Q12 32.3%
Q11 3.31%
Q9 2.49%
Q10 94.9%
Q12 0.417%
Q11 2.19%
IgD (PE)
CD19 (PE-Cy7)
Q5 25.4%
Q6 10.8%
Q8 16.3%
Q7 47.5%
Q5 0.699%
Q6 6.07%
Q8 10.8%
Q7 82.4%
Q5 3.80%
Q6 63.2%
Q8 29.5%
Q7 3.43%
Q5 2.16%
Q6 95.1%
Q8 0.572%
Q7 2.15%

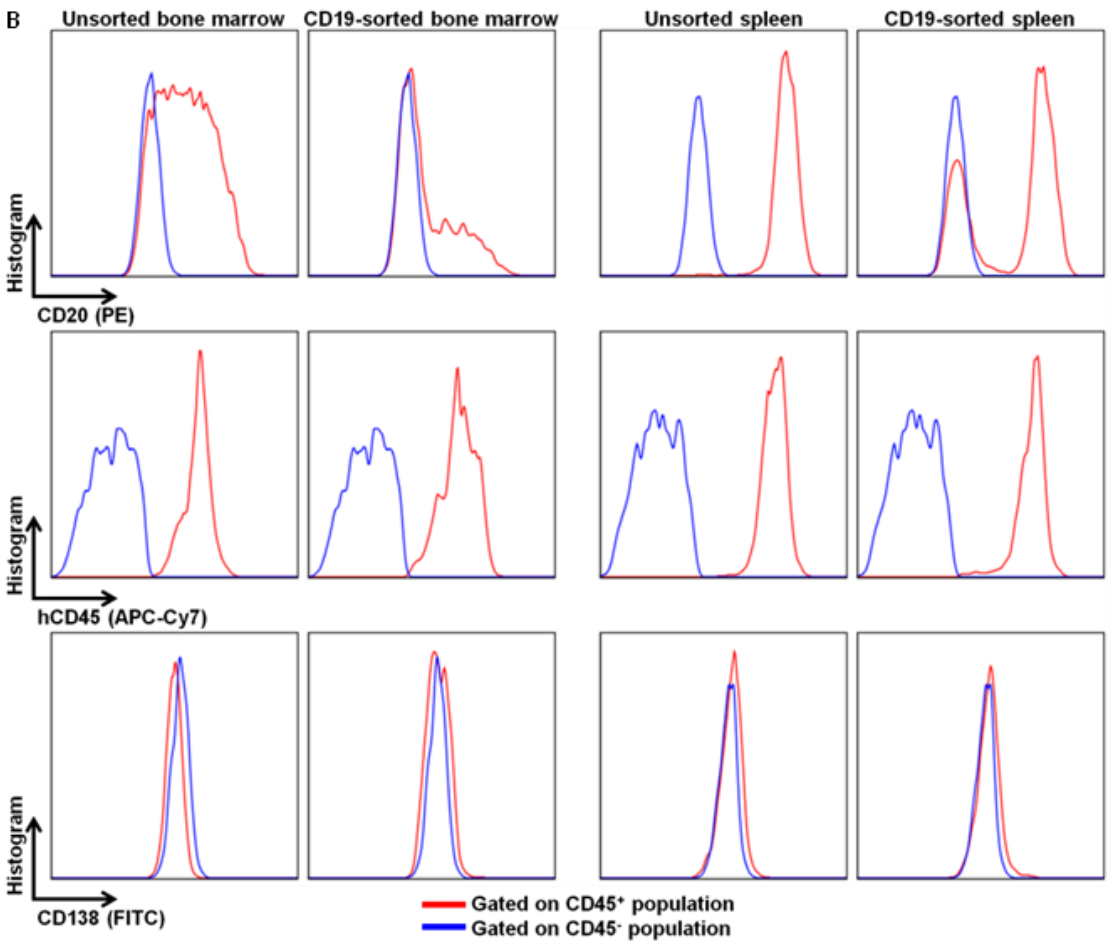

Figure 5.7: Characterization of CD19$^+$ B cells in the fetal bone marrow and fetal spleen. Flow cytometric immunophenotyping of B cells in the fetal bone marrow and fetal spleen was performed prior to *in vitro* EBV infection. A portion of cells from the fetal bone marrow and fetal spleen was further sorted for CD19 and presented alongside. **(A)** The majority of the CD19$^+$ B cells in the fetal bone marrow were CD10$^+$IgM$^-$IgD$^-$, while cells from the fetal spleen were mostly CD10$^-$IgM$^+$IgD$^+$. **(B)** B cells from the fetal spleen displayed higher expression of CD45 and CD20 than those of the fetal bone marrow. All cells were negative for plasma cell marker CD138.

5.5 Characterization of the fetal-derived BLCLs

Regardless of the immunophenotypic differences between $CD19^+$ cells from the fetal bone marrow and fetal spleen, BLCLs were successfully established from both samples. As early as day 29, the formation of macroscopic cell clusters characteristic of B cell immortalization and BLCL establishment were observed in both unsorted and CD19-sorted fetal bone marrow and fetal spleen samples (**Figure 5.8A**). While BLCLs were generated from all the fractions, higher efficiency and faster outgrowth of BLCLs were observed in the unsorted fractions of fetal bone marrow and fetal spleen (**Figure 5.8B**).

Despite the fact that fetal bone marrow and fetal spleen are two different compartments for B cell development, BLCLs generated from these two samples displayed similar immunophenotype. As shown in **Figure 5.9**, fetal-derived BLCL demonstrated negative staining for non-B cell markers such as CD3, CD4, CD8, and CD56 ($CD3^-CD4^-CD8^-CD56^-$). Furthermore, these BLCLs were not stained for developmental-specific B cell markers such as CD5, CD10, CD23, CD27, and CD138 ($CD5^-CD10^-CD23^-CD27^-CD138^-$).

These cells were stained for pan-B cell markers such as CD19 and CD20 ($CD19^+CD20^+$), along with the detection of co-stimulatory markers such as CD40, CD86, and HLA-DR ($CD40^+CD86^+HLA\text{-}DR^+$). Staining revealed that BLCLs generated from the unsorted and CD19-

sorted spleen fractions had indistinguishable immunophenotype (**Appendix F**).

During EBV infection, the upregulation of CD95 is observed on B cells as the result of EBV LMP1 expression [214-216]. Indeed, we observed the expression of CD95 in these fetal-derived BLCLs and immunoblot in **Figure 3.12** further confirmed the presence of EBV latent proteins - EBNA-1, LMP1, and EBNA-2. Importantly, the detection of EBNA-2, which is uniquely found in PTLD patients and BLCLs, confirmed that these fetal-derived BLCLs were expressing the latency III program (**Table 1.1**).

With the successful establishment of BLCLs from the fetal bone marrow and fetal spleen, these cells were tested for their staining with α-EBV TCR-like mAbs. As shown in **Figure 5.10**, staining was observed with α-EBNA-1 TCR-like mAb on HLA-A*02 fetal-derived BLCL but not non-HLA-A*02 fetal-derived BLCL. Modest staining was also seen with α-LMP1 TCR-like mAb, consistent with the observation of EBNA-1 pMHC > LMP1 pMHC as described earlier with the PBMC-derived BLCLs in **Figure 3.13**. These data demonstrated that the fetal-derived BLCLs not only expressed surface markers and EBV latent proteins akin to that of EBV-infected B cells in humans, they also displayed similar staining profile with α-EBV TCR-like mAbs.

A

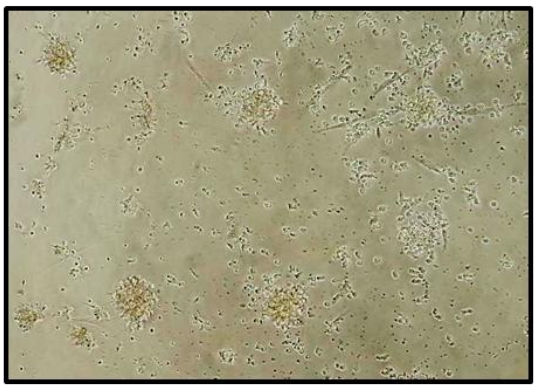

B

Relative outgrowth	Unsorted	CD19-sorted
Fetal bone marrow	+++	+
Fetal spleen	+++	+

Figure 5.8: Establishment of BLCLs from both fetal bone marrow and fetal spleen. Regardless of the immunophenotypic differences between the $CD19^+$ B cells harvested from the fetal bone marrow and fetal spleen, successful BLCL establishment was achieved with both fetal organs. **(A)** The formation of macroscopic colonies was detected at day 29. **(B)** BLCLs established from the unsorted fetal bone marrow and fetal spleen displayed faster outgrowth as compared to those generated from the CD19-sorted fractions. (+) indicates the relative amount of BLCL outgrowth based on microscopy scoring.

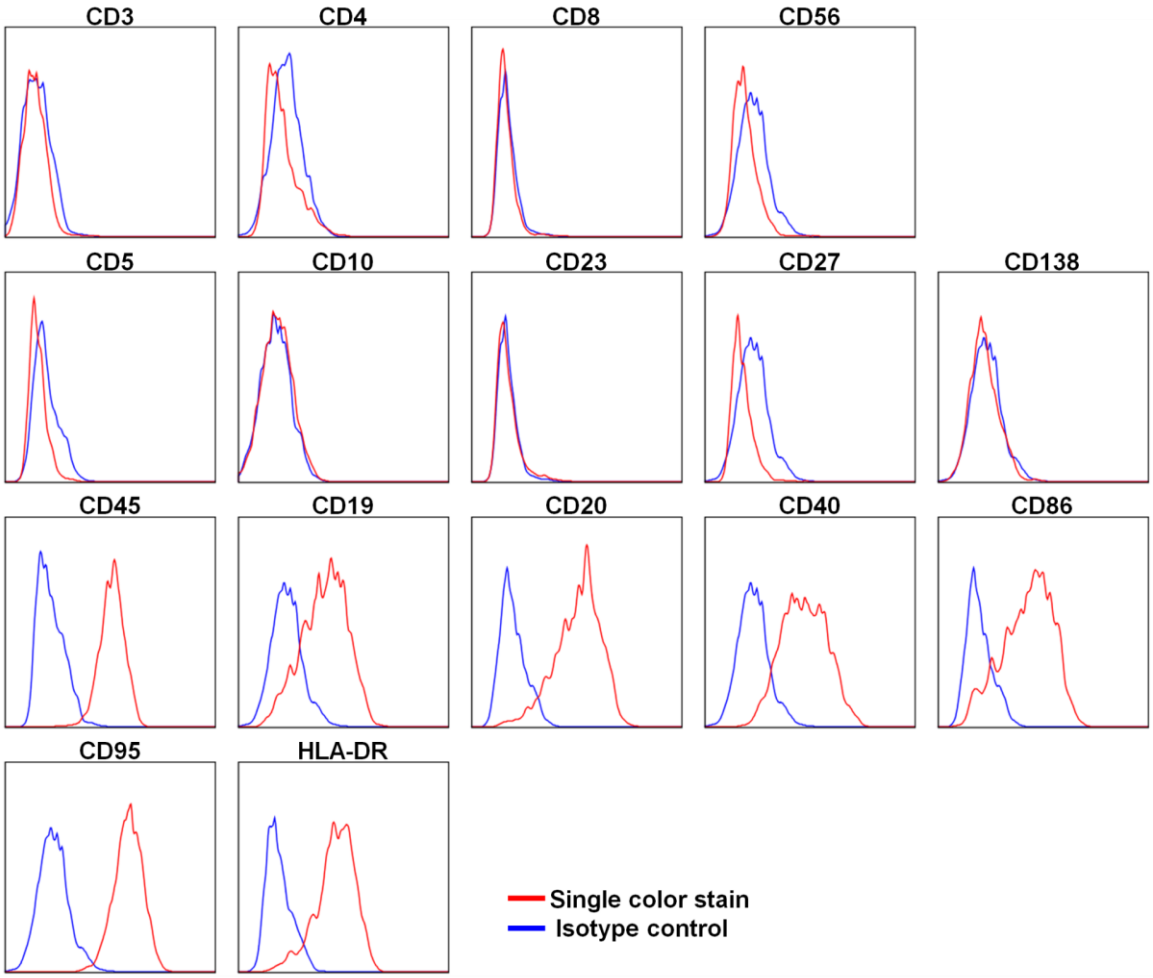

Figure 5.9: Immunophenotype of BLCL generated from fetal samples. Upon *in vitro* EBV infection and immortalization of B cells from the fetal samples (bone marrow and spleen), stable BLCL capable of indefinite proliferation was established. Flow cytometric immunophenotyping was performed to characterize the BLCL based on their expression of surface markers. BLCL generated from fetal bone marrow and fetal spleen expressed similar immunophenotype, with no staining observed for non-B cell markers such as CD3, CD4, CD8, and CD56. B cell differentiation markers such as CD5, CD10, CD23, CD27, and CD138 were also absent. These cells were verified as BLCL based on their surface expression of CD45, CD19, and CD20. The expression of EBV latent proteins (**Figure 3.12)** confirmed the presence of EBV. Additionally, the immunophenotype of BLCL generated from unsorted fraction spleen was also found to be indistinguishable from those generated from the CD19-sorted fraction (**Appendix F**).

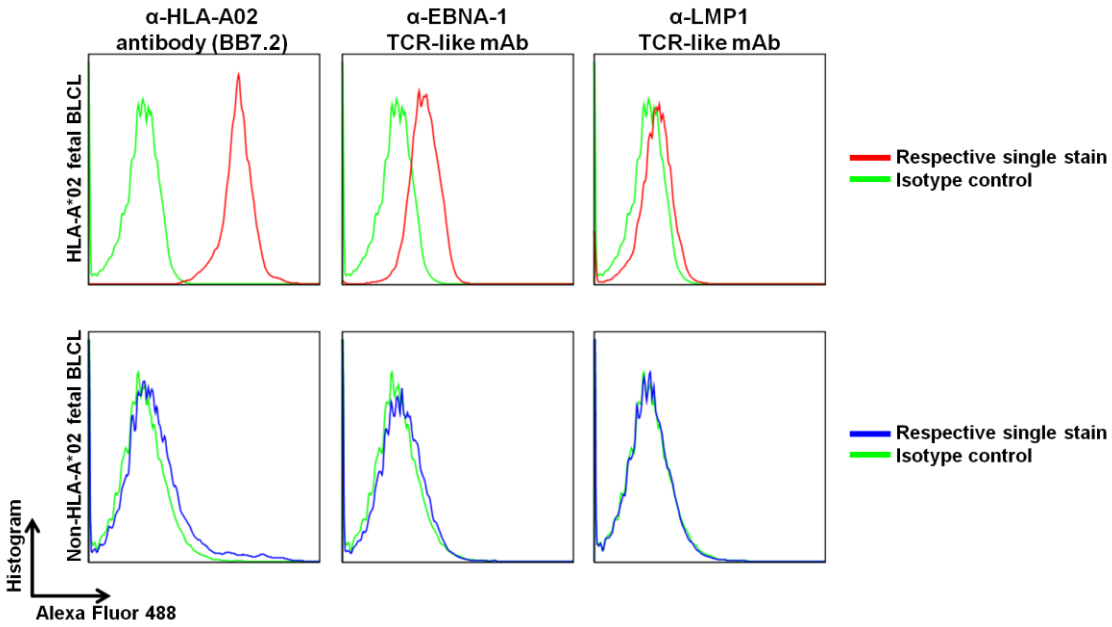

Figure 5.10: Detection of surface EBNA-1 and LMP1 pMHC on BLCLs generated from fetal samples. Staining with α-EBNA-1 TCR-like mAb and α-LMP1 TCR-like mAb were performed on HLA-A*02 and non-HLA-A*02 fetal BLCLs. Staining with both antibodies were observed in HLA-A*02 fetal BLCL but not on the non-HLA-A*02 fetal BLCL. Higher staining was observed with the α-EBNA-1 TCR-like mAb as compared to α-LMP1 TCR-like mAb, consistent with the staining observed with PBMC-derived BLCLs (**Figure 3.13**).

5.6 Improving human immune cells reconstitution in the autologous humanized mouse model

With the successful establishment of an autologous humanized mouse model, this model could serve as a platform to evaluate the therapeutic efficacy and toxicity of novel therapeutics such as α-EBNA-1 TCR-like mAb. This model could further be utilized to elucidate the roles of humoral (antibody) effector cells such as monocytes/macrophages, dendritic cells and NK cells in mediating the therapeutic effects. To enable the determination of antibody treatment effects and mechanisms, we sought to boost the reconstitution of these human immune cells in our autologous humanized mice via HDI of plasmids encoding human IL-15 and FLT3L, a technique employed by Qingfeng et al. (**Figure 5.11**) [198].

Mice were hydrodynamically injected with respective plasmids at week 13 post-humanization and their peripheral blood was checked for human immune cells reconstitution from week 14 to 17. While the increased in $CD11c^+$ a cell (dendritic cells) was observed at weeks 14 and 15, this enhancement was not found to be statistically significant (**Figure 5.12A** and **B**). On the other hand, no augmentation of the $CD14^+$ cells (monocytes/macrophages) reconstitution was noted throughout (**Figure 5.12C** and **D**).

In contrast, the analysis of $CD56^+$ and $NKp46^+$ expression in the peripheral blood revealed an enhancement of NK cell percentages upon HDI (**Figure 5.13**). Representative mice with similar NK cells reconstitution at week 12 were compared to illustrate the augmentation of these $CD56^+NKp46^+$ NK cells (**Figure 5.13A** and **C**). The enhancement of $CD56^+$ and $NKp46^+$ cells reconstitution were observed at weeks 14 and 15, before returning to levels similar to that of untreated humanized mice at week 16 (**Figure 5.13B** and **D**). Taken together, we have demonstrated that HDI can improve the reconstitution of the human NK cells in the autologous humanized mice, providing a means to investigate the role NK cells in antibody treatment.

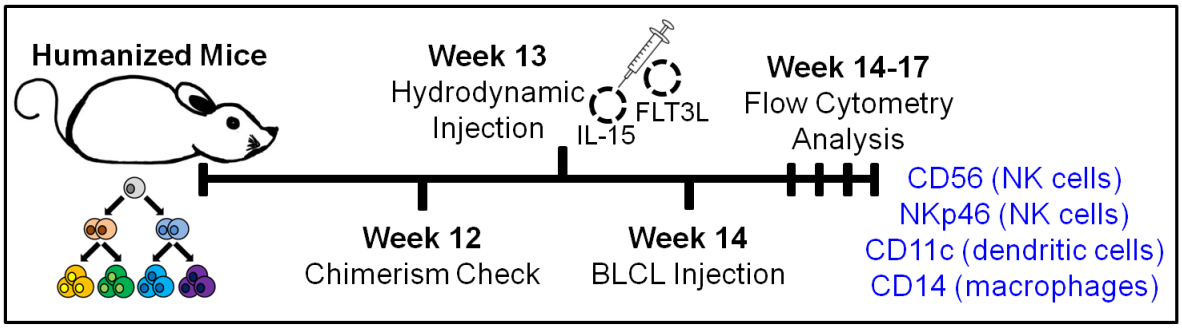

Figure 5.11: Improving the human immune cells reconstitution in the humanized mice. Schematic illustration of using HDI of plasmids encoding human IL-15 and FLT3L to boost the human immune cells reconstitution in the humanized mouse injected with autologous BLCL. Fetal liver $CD34^+$ HPCs-reconstituted humanized mice were bled at week 12 for chimerism check (hCD45 versus mCD45). At week 13, HDI of plasmids encoding IL-15 and FLT3L was performed. Thereafter, weekly facial bleeding was conducted to check for the percentages of CD56, NKp46, CD11c, and CD14 reconstitution in the peripheral blood of mice. The injection of autologous BLCL (established from EBV infection of B cells from the fetal spleen) was carried out on week 14.

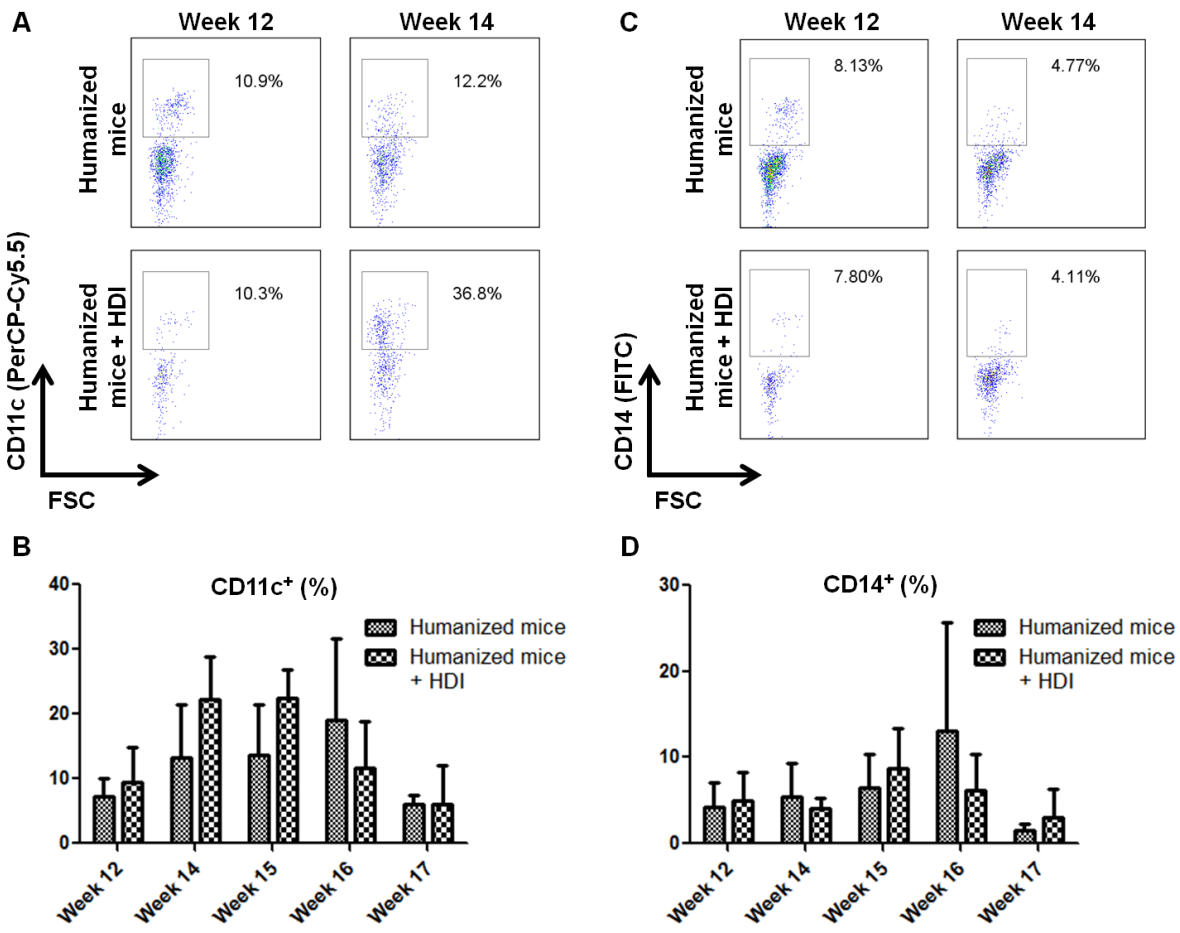

Figure 5.12: Effects of HDI on the reconstitution of CD11c$^+$ and CD14$^+$ cells. Percentages of CD11c$^+$ and CD14$^+$ cells were obtained via multicolour flow cytometric analysis of the mouse peripheral blood. **(A and C)** Flow cytometry plot showing the percentages of CD11c and CD14 before (at week 12) and after (at week 14) hydrodynamic injection of plasmids encoding IL-15 and FLT3L. **(B and D)** CD11c$^+$ (%) and CD14$^+$ (%) from week 12 to 17. Although an increased reconstitution of CD11c$^+$ cells was observed at week 14 and 15, the effect was not statistical significant. No enhancement in CD14$^+$ cells reconstitution was observed. Values are expressed as mean ± SD.

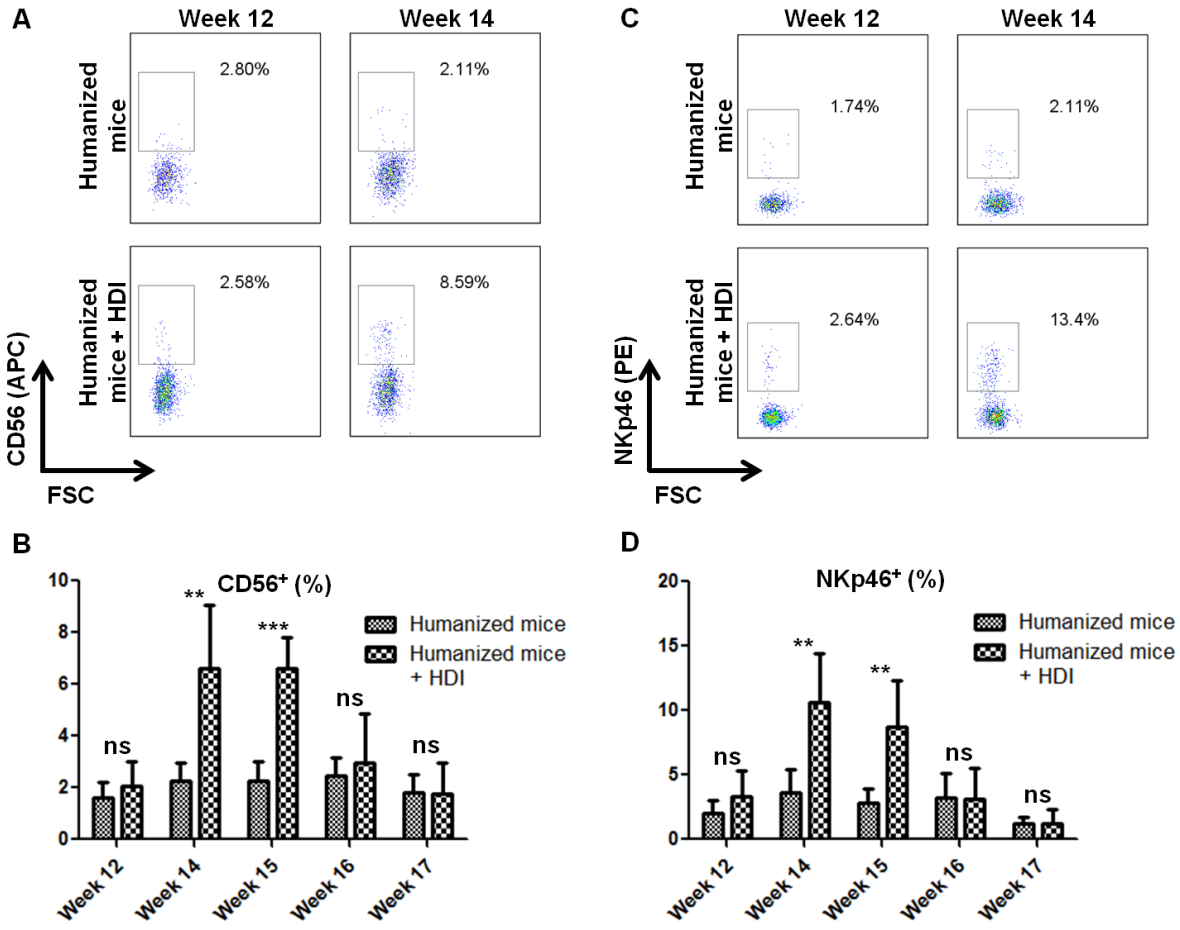

Figure 5.13: Effects of HDI on the reconstitution of CD56$^+$ and NKp46$^+$ cells. Percentages of CD56$^+$ (%) and NKp46$^+$ (%) cells were obtained via multicolour flow cytometric analysis of the mouse peripheral blood. **(A and C)** Flow cytometry plot showing the percentage of CD56 and NKp46 before (at week 12) and after (at week 14) hydrodynamic injection of plasmids encoding IL-15 and FLT3L. **(B and D)** CD56$^+$ (%) and NKp46$^+$ (%) from week 12 to 17. There was a statistical significant enhancement of CD56$^+$ cells reconstitution at week 14 (p = 0.0036) and week 15 (p < 0.0001). A similar observation was also noted for NKp46$^+$ cells reconstitution at week 14 (p = 0.0014) and week 15 (p = 0.0037). ** p < 0.01 and *** p < 0.001. Values are expressed as mean ± SD.

Chapter 6:

Discussion and Future Perspectives

6.1 Discussion

Epstein-Barr virus, the ubiquitous gammaherpesvirus is associated with a large number of human malignancies of epithelial and lymphoid origins. As a common antigen found in both lytic and latent phases of EBV infection, EBNA-1 plays crucial roles in viral genome maintenance, immunoevasion, and possibly EBV-oncogenesis. As such, there has been a long-standing interest in targeting EBNA-1 as a means to attenuate EBV infection and tumorigenesis in EBV-associated diseases. However, targeting EBNA-1 was deemed impractical as various studies in the early 1990s reported that the GAr within the EBNA-1 protein could auto-inhibit its degradation, thereby reducing its peptide presentation to T cells and consequently impairing EBNA-1-specific T cell responses.

Consistent with earlier reports, we showed that the deletion of GAr in E1ΔGA construct resulted in the increased expression of EBNA-1 protein [18, 204]. While previous studies utilized fusion proteins and non-viral epitopes such as ovalbumin (SIINFEKL), GFP, p53 and IκBα as the epitope reporters for EBNA-1 presentation, these read-outs might not reflect how EBNA-1 is naturally processed and presented. This is because these fusion partners can potentially affect the rate and fidelity of EBNA-1 protein synthesis, folding, transport, degradation, and presentation [227]. As an alternative to the usage of fusion partners, we employed the 2A sequences to achieve equimolar

translation of GFP and WT EBNA-1 or E1ΔGA, thereby overcoming the problems associated with the use of fusion proteins. With these constructs, we further confirmed that the presence of GAr not only affected EBNA-1 expression but also reduced GFP synthesis, substantiating the role of GAr in mediating viral evasion mechanism by reducing protein synthesis.

In 2004, three landmark publications reshaped the paradigm of EBNA-1 presentation with the suggestion that EBNA-1-specific T cells could be detected *in vivo* and that, EBNA-1 peptides could be generated for presentation to T cells through defective ribosomal products – erroneous EBNA-1 protein derivatives from the translational machinery [56-58]. The processing and presentation of EBNA-1 protein for T cell priming were further validated based on the detection of both EBNA-1-specific CD4 and CD8 T cells in healthy EBV-seropositive individuals [48, 56, 57, 228, 229]. These studies affirmed that EBNA-1 presentation is indeed naturally occurring.

Based on the observation of EBNA-1-specific T cells, we interrogated the ability of our in-house produced, EBNA-1-specific antibody (α-EBNA-1 TCR-like mAb) to distinguish the presentation of EBNA-1 epitope between WT EBNA-1 and E1ΔGA-transfectants. However, we were unable to detect EBNA-1 peptide (FMVFLQTHI)-MHC complexes in both WT EBNA-1 and E1ΔGA-transfected HEK293T cells with our antibody.

The lack of staining on HEK293T transfectants with α-EBNA-1 TCR-like mAb could be attributed to the inability of the antibody to bind to surface EBNA-1 pMHC or the absence of these surface complexes. However, we have excluded the possibility that our antibody is incapable of staining surface pMHC complexes because its specificity has been verified by various experimental techniques such as pMHC ELISA, peptide pulsing, and direct staining of surface EBNA-1 pMHC on BLCLs. While we did not address why surface EBNA-1 pMHC were not detected in EBNA-1-transfectants, one possibility could be that the forced expression of a non-native EBNA-1 protein in cells (HEK293T and HeLa) which are not the natural hosts of EBV might compromise the natural generation of a processed and unaltered epitope (FMVFLQTHI) detected by α-EBNA-1 TCR-like mAb. Nonetheless, EBNA-1 epitopes could be measured via mass spectrometry-based approaches to evaluate the full profile of presented peptides, though this would require the optimization of surface peptide elution strategies [230, 231]. Still, it is encouraging that α-EBNA-1 TCR-like mAb could detect the presentation of surface EBNA-1 pMHC on the B cells latently infected with EBV (BLCLs), demonstrating the availability of EBNA-1 as a therapeutic target.

With the observation that α-EBNA-1 TCR-like mAb could detect the presentation of the endogenous EBNA-1 epitope on BLCLs, we set out to investigate whether this antibody could be used to target EBV-infected cells. Based on the surface plasmon resonance data

previously reported by our laboratory, and the pMHC ELISA data presented here, we showed that α-EBNA-1 TCR-like mAb has excellent binding characteristics, with affinity and avidity profiles in the nanomolar range [129].

We further demonstrated that staining with α-EBNA-1 TCR-like mAb was only observed on HLA-A*02 BLCLs, but not on PBMC from which this BLCL was generated, highlighting its specificity in detecting surface EBNA-1 pMHC presented by these EBV-infected cells. Equally encouraging, we were able to detect constitutive surface presentation of the EBNA-1 pMHC with α-EBNA-1 TCR-like mAb on several donor-derived BLCLs, illustrating the feasibility of targeting surface EBNA-1 pMHC with our antibody.

We next employed a mouse xenograft model with HLA-A*02 BLCL injected into NSG mice as a means to evaluate the *in vivo* therapeutic effect of α-EBV TCR-like mAb. As NSG mice are devoid of a functional adaptive immune system, the injection of EBV-infected BLCL and their subsequent unrestricted proliferation in mice is analogous to immunosuppressed humans developing B cell lymphoproliferative disorder. As BLCL derived from different donors are heterogeneous in their immunophenotypes and their growth rates, the employment of this mouse xenograft model can potentially capture and reflect individualized response to treatment.

In this model, successful engraftment of BLCL was evident as early as day 7 post-injection of the BLCL. Severe disease manifestations were observed in the spleens, livers, and kidneys when these mice were monitored over a longer period to study disease progression. The administration of α-EBNA-1 TCR-like mAb resulted in delayed weight loss and prolonged survival in these mice. Surprisingly, this therapeutic effect was not observed in mice given the α-LMP1 TCR-like mAb, despite this antibody displaying a higher binding affinity as compared to α-EBNA-1 TCR-like mAb [129].

A possible reason for the therapeutic effect observed with the α-EBNA-1 TCR-like mAb could be due to a greater availability of surface EBNA-1 pMHC for antibody binding, correlating to the flow cytometry data where α-EBNA-1 TCR-like mAb displayed a stronger staining profile compared to the α-LMP1 TCR-like mAb (**Figure 3.13**). This could suggest that, while the binding avidity of an antibody is critical, the surface availability/epitope density might be an equally important factor in determining the therapeutic efficacy of an antibody. The significance of surface epitope density has been illustrated by FDA-approved anti-human epidermal growth factor receptor 2 (HER2) antibody, where patients with a higher score of HER2 overexpression on tumors displayed a better treatment outcome [232]. Therefore, surface availability of pMHC for TCR-like mAb binding has to be included as a factor when designing treatment modalities with this type of antibody.

When organs of the α-EBNA-1 TCR-like mAb-treated mice were examined, amelioration of disease was observed in the livers and spleens but not in the kidneys. Furthermore, an increasing BLCL infiltration was seen in the kidneys at later time points, possibly providing an explanation as to how all the mice succumbed to the disease. To understand the underlying mechanisms of α-EBNA-1 TCR-like mAb treatment, a series of *in vitro* assays were performed. Antibodies have been shown to mediate an array of effector functions such as the direct induction of apoptosis, CDC, and ADCC [123, 125, 132-135]. We showed that α-EBNA-1 TCR-like mAb treatment *in vitro* could trigger early apoptosis and promote antibody-mediated phagocytosis. While the ability to mediate direct apoptosis has been ascribed to similar antibody-based therapeutic modalities [124, 134], our group is the first to provide evidence on the dual functionalities of TCR-like mAbs in promoting early apoptosis, as well as enhancing the phagocytosis of tumor cells. It would be of interest to evaluate whether the α-EBNA-1 TCR-like mAb could additionally perform CDC and ADCC *in vitro* as well as *in vivo*. Nonetheless, the dual functionalities of α-EBNA-1 TCR-like mAb in mediating both immune effector-dependent and -independent functions that we demonstrated here, are favorable to its consideration as a therapeutic candidate.

In the recent years, immunotherapy has gained increasing international attention for its utility in cancer treatment. An example is the successful application of anti-CD20 antibody (rituximab) in PTLD treatment. As

one of the most effective forms of treatment, rituximab clearly demonstrates the feasibility of antibody-based approach in PTLD treatment, but there are unwanted side-effects based on its use in PTLD patients [105, 106]. The use of rituximab has not only been shown to increase the chance of opportunistic infection but also to promote the development of $CD20^{-}$ lymphoma refractory to rituximab treatment [102, 103]. The depletion of healthy CD20-expressing B cells can moreover be detrimental to the already immunosuppressed graft recipients and this outcome is counterproductive as humoral responses are crucial for long-term host immunity.

The α-EBNA-1 TCR-like mAb we present here exhibits the ability to differentiate EBV-infected cells from the uninfected cells, offering an advantage over the pan-B cell depletion engendered by rituximab treatment. At the same time, given the common expression of EBNA-1 in all EBV-associated malignancies of varying latency programs, the use of this antibody might further enable the targeting of EBNA-1-expressing cells in different EBV-associated diseases. As a novel class of immunotherapeutics, the α-EBNA-1 TCR-like mAb we detail here is the first-of-its-kind that has been evaluated for its therapeutic function in a murine model of EBV-PTLD.

In an up-and-coming therapy for PTLD, allogeneic EBV-specific T cells are isolated from donors and injected into PTLD patients [114-120]. However, the generation and employment of adoptive T cell therapy

often involve a significant time delay and require technical expertise. This limits its widespread application and its availability in urgent clinical settings. The prospect of this approach is further complicated by the high degree of stringency required for HLA-compatibility to avoid graft-versus-host disease and the propensity of disease complications arising from donor-derived pathogens such as cytomegalovirus.

The TCR-like mAb we describe here binds to surface EBNA-1 pMHC in a manner similar to how EBV-specific T cells recognize their targets (EBV-infected cells). As an antibody, α-EBNA-1 TCR-like mAb has advantages in that it can be produced in large quantities and utilized in clinical settings where adoptive T cell therapy is not practical. In addition, these antibodies are ‘immune’ to the immunosuppressive tumor microenvironment which can regulate T cell function [132]. Finally, as EBNA-1 is expressed in EBV latency programs I, II and III, the utility of α-EBNA-1 TCR-like mAb is not restricted to latency III-expressing PTLD but can also be extended to treat EBV-associated diseases of other latency programs.

The α-EBNA-1 TCR-like mAb we report here is a mouse-derived antibody, and thus it is not suitable for application in humans in its current form as its administration can lead to the generation of a human anti-mouse antibody response. This response can lead to the development of allergic reactions such as fever, chills, anaphylaxis, urticaria and hypotension [233-237]. Moreover, these human anti-

mouse antibodies can form immune complexes with the mouse-derived antibody, attenuating the therapeutic efficacy of treatment [238-241]. As such, current efforts from our laboratory focus on generating a humanized antibody variant of the α-EBNA-1 TCR-like mAb. While the conversion of mouse-derived α-EBNA-1 TCR-like mAb is underway, we have developed a novel humanized mouse model of EBV-PTLD compatible for the preclinical evaluation of α-EBNA-1 TCR-like mAb.

Our approach is based on the humanized mouse model of EBV infection. In the conventional modeling of EBV infection, EBV supernatant is injected into the humanized mice, establishing an *in vivo* EBV infection of the reconstituted human B cells. Here, we present a novel transplantable tumor model in which autologous BLCL generated *in vitro* is injected into humanized mouse reconstituted with $CD34^+$ HPCs derived from the same donor. In this model, we have validated the expression of latency III program in BLCL before transplanting them into the humanized mice (**Figure 3.12**).

BLCLs are the *in vitro* counterpart of B cells found in EBV-PTLD patients, both bearing the latency III expression pattern, justifying the biological relevance of using BLCL to model EBV-PTLD. The use of BLCL also provides convenience, as cells can be maintained in culture and made readily available. These cells can be characterized and assayed for their responses to therapeutic candidates *in vitro* prior to *in vivo* evaluation. The use of BLCL also offers added advantage over the

injection of virus supernatant in the conventional modeling as the virus titer does not equate to infectivity. In this regard, the employment of BLCL offers a more quantitative control over the desired tumor load, allowing a more precise control of the disease outcome as compared to the use of a virus supernatant.

In terms of establishing an *in vivo* model of EBV-PTLD, our approach encompasses both orthotopic and syngeneic facets of animal modeling. As BLCL is intravenously injected into mice, they are transplanted onto an appropriate anatomical setting similar to that of PTLD in humans. With both BLCLs and HPCs derived from the same donor (autologous), they have the identical genetic background, thus eliminating a possibility of immunological rejection due of HLA-incompatibility.

We have successfully generated an autologous humanized mouse model and delineated the human immune cells that reconstitute using samples derived from human cord blood. However, due to the limited availability of $CD34^+$ HPCs in cord blood, the reconstitution of humanized mice is often restricted to 4-5 mice per single unit of cord blood, leading to the lack of statistical power required for studies. We therefore switched to the usage of the human fetal liver as it provides a greater number of $CD34^+$ HPCs for generating a large cohort of humanized mice. We have further demonstrated that both fetal bone marrow and fetal spleen can provide a good source of B cells for BLCL generation and showed that BLCLs generated from both lymphoid

organs were indistinguishable. Encouragingly, these fetal-derived BLCLs were stained positive for surface EBNA-1 pMHC (**Figure 3.10**), providing an important indication that our autologous humanized mouse model may function as a valuable platform for the future evaluation of α-EBNA-1 TCR-like mAb.

While we have successfully developed an autologous humanized mouse model, this model required additional refinements. This is because cells such as dendritic cells, monocytes/macrophages, and NK cells are poorly reconstituted and not well-studied in the humanized mouse [190-192]. As these cell types are important immune effectors in antibody therapy and the availability of these cells in the humanized mouse would impact the outcome of antibody treatment. It was therefore important to determine and improve the reconstitution of these cells.

To enhance the reconstitution of the relevant immune cells, we performed HDI of plasmids encoding for human IL-15 and FLT3L into humanized mice. While no enhancements of dendritic cells and macrophages were observed, a significant augmentation of NK cells reconstitution was detected for two consecutive weeks (**Figure 5.13**). Here, we have demonstrated that HDI is a practical and cost-effective approach in the transient augmentation of specific immune cells in the autologous humanized mice.

With the information on the specific cell types responding to the HDI as well as the kinetics of the enhancement, subsequent work can be focused on exploring the necessity of a maintenance boost and the utility of other cytokine-expressing plasmids to achieve a more robust platform for antibody evaluation.

6.2 Future perspectives

We have demonstrated that the α-EBNA-1 TCR-like mAb in its native IgG1 format was capable of eliciting an observable therapeutic effect in BLCL-engrafted NSG mice. It would be of interest to evaluate whether different isotypes and subclasses of the antibody can elicit better effector functions. Currently, a humanized variant of the α-EBNA-1 TCR-like mAb is under development, and in due course the evaluation of its therapeutic efficacy, pharmacodynamics, pharmacokinetics or toxicology will be conducted. Additionally, functional analysis of different immune cell types can be studied by using cell-specific immunodepletion to dissect the role of each cell type in the humanized mouse in mediating α-EBNA-1 TCR-like mAb treatment effects.

Besides the humanization of α-EBNA-1 TCR-like mAb, the future modification can encompass the conjugation of recombinant immunotoxins or cytokines to enhance its cytotoxicity in PTLD treatment. Another area that can be further explored to enhance therapeutic efficacy is the conversion of α-EBNA-1 TCR-like mAb into a bispecific T cell engager [242, 243]. These antibodies combine the specificity of two antibodies, with one arm of the antibody specific for the EBNA-1 pMHC, and the other arm specific for $CD3^+$ T cells. In this manner, the bispecific antibody of α-EBNA-1 TCR-like mAb can bind to EBV-infected cells, and at the same time draws T cells into proximity for the killing of the pathological B cells.

Multiple studies have looked into the synergistic effects of combinatory drug therapy in cancer treatments [219, 244]. In particular, rituximab and cyclophosphamide which are used to treat PTLD have demonstrated synergistic effects when delivered as a combinatory treatment in the treatment of other hematological malignancies. Prompted by such observations, the combinatory treatment of α-EBNA-1 TCR-like mAb with current drugs can be investigated. Finally, our laboratory has also generated two other α-EBV TCR-like mAbs targeting LMP1 and LMP2A (α-LMP1 TCR-like mAb and α-LMP2A TCR-like mAb). It would be of interest to determine if a combinatory treatment of all three TCR-like mAbs may engender any form of therapeutic synergism.

Appendix

Appendix A: protein sequences of WT EBNA-1 and E1ΔGA

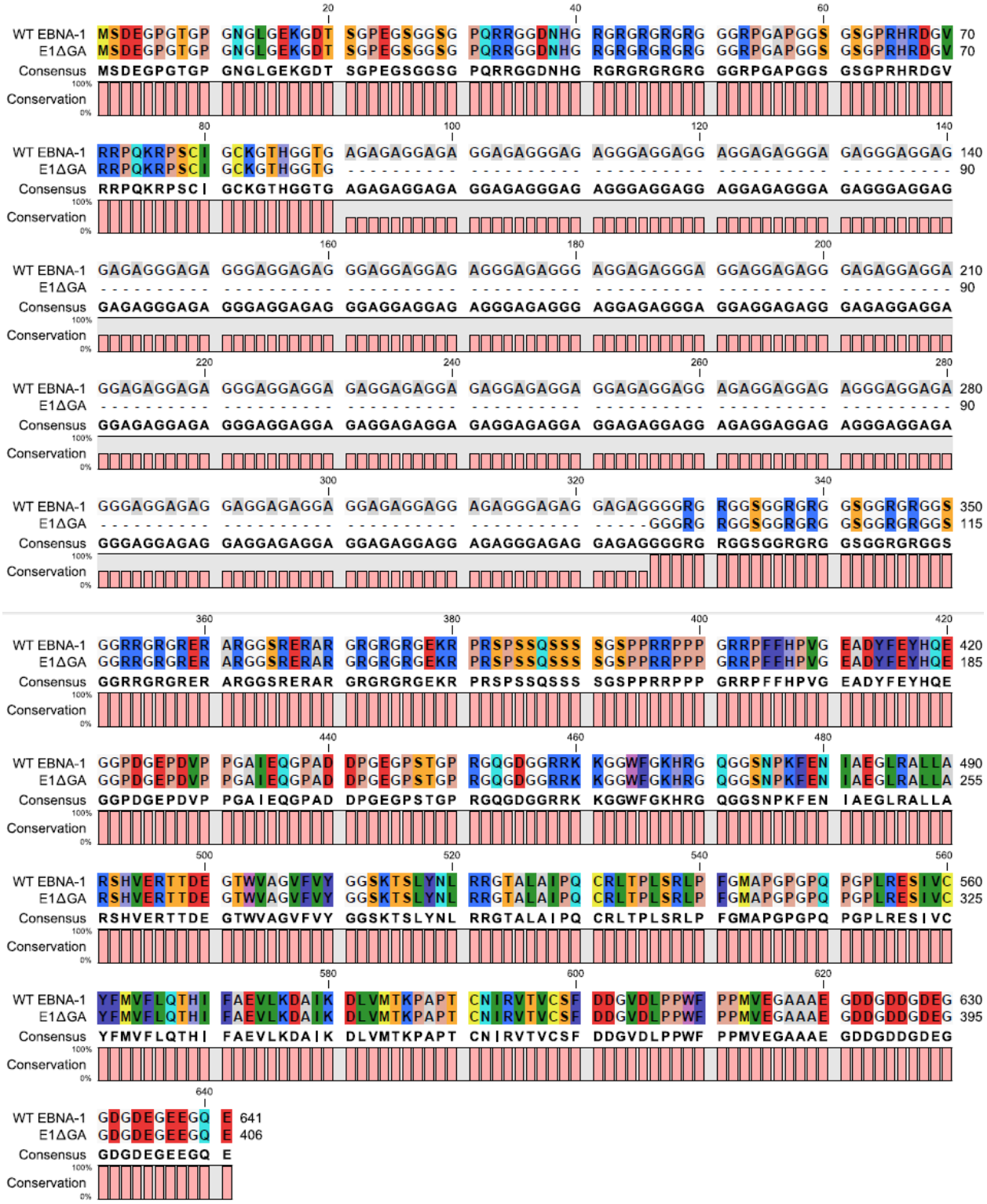

Appendix B: intracellular EBNA-1 staining in HEK293T and CF986 BLCL

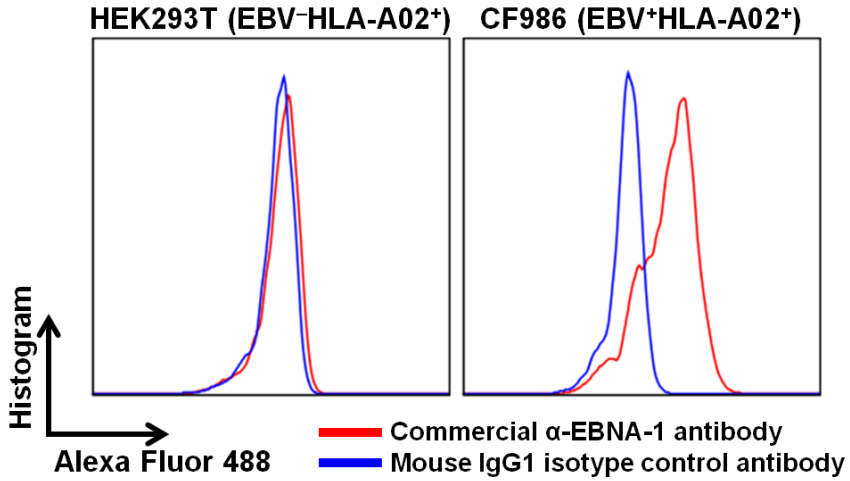

Appendix C: surface staining of EBNA-1 and LMP1 pMHC on HLA-A*02 BLCLs

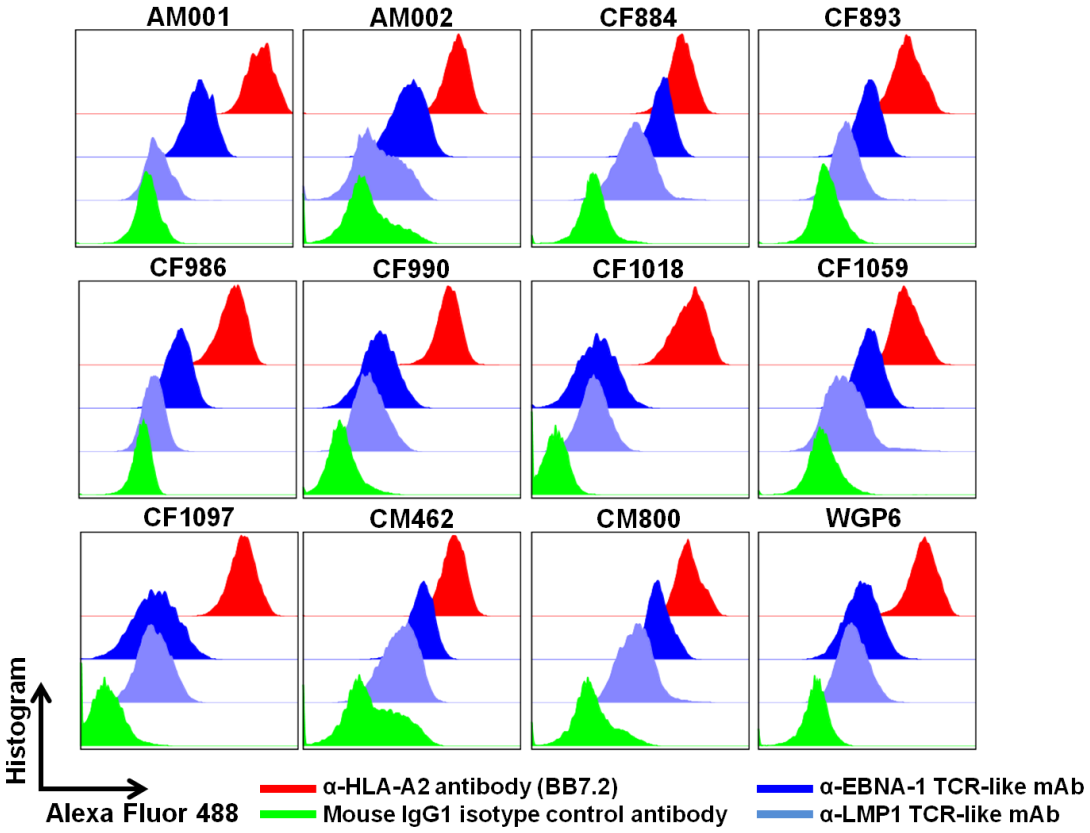

Appendix D: kinetics of surface EBNA-1 pMHC staining

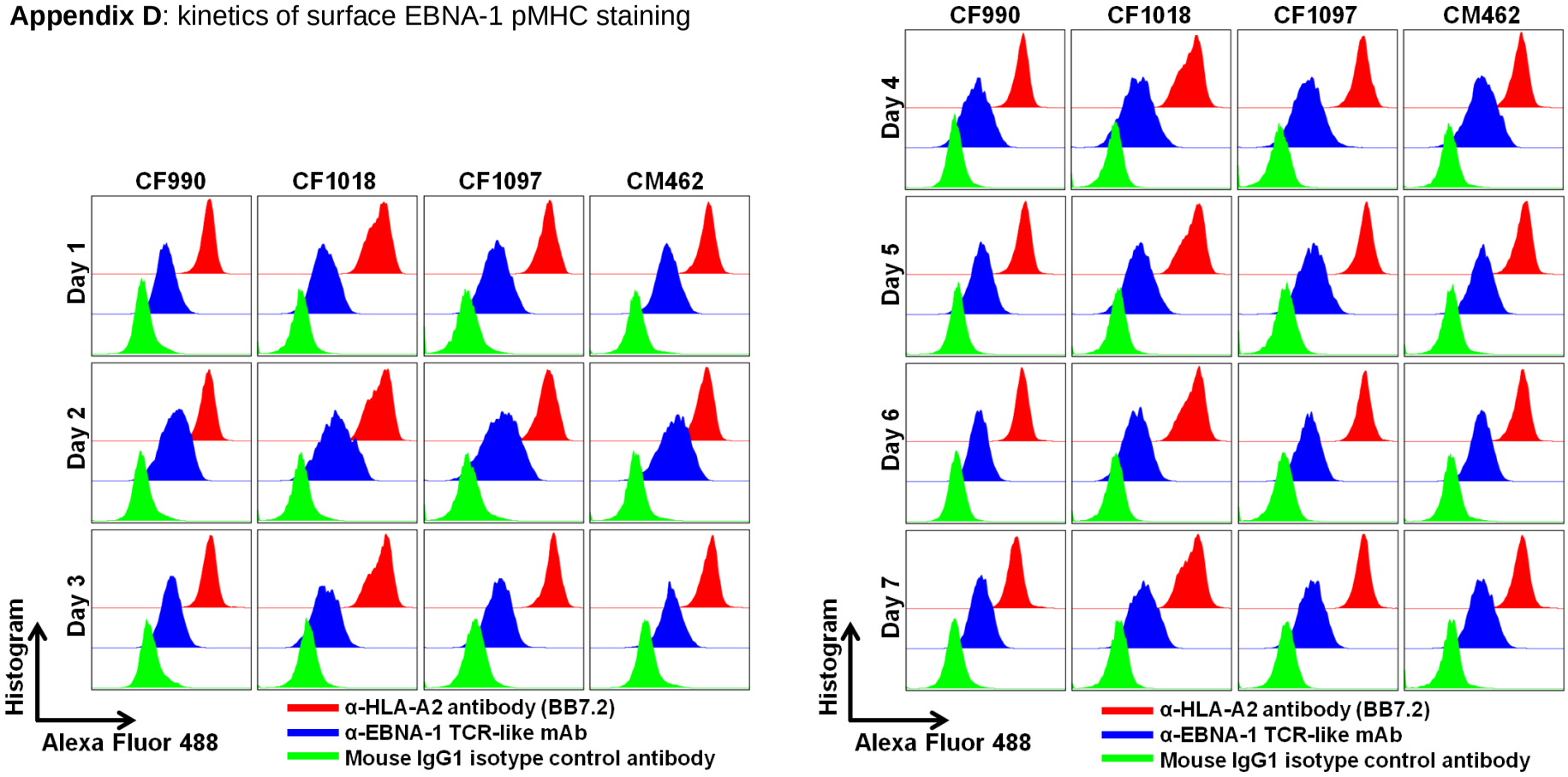

Appendix E: α-EBNA-1 TCR-like mAb ameliorated disease manifestations in the spleens and livers of treated mice.

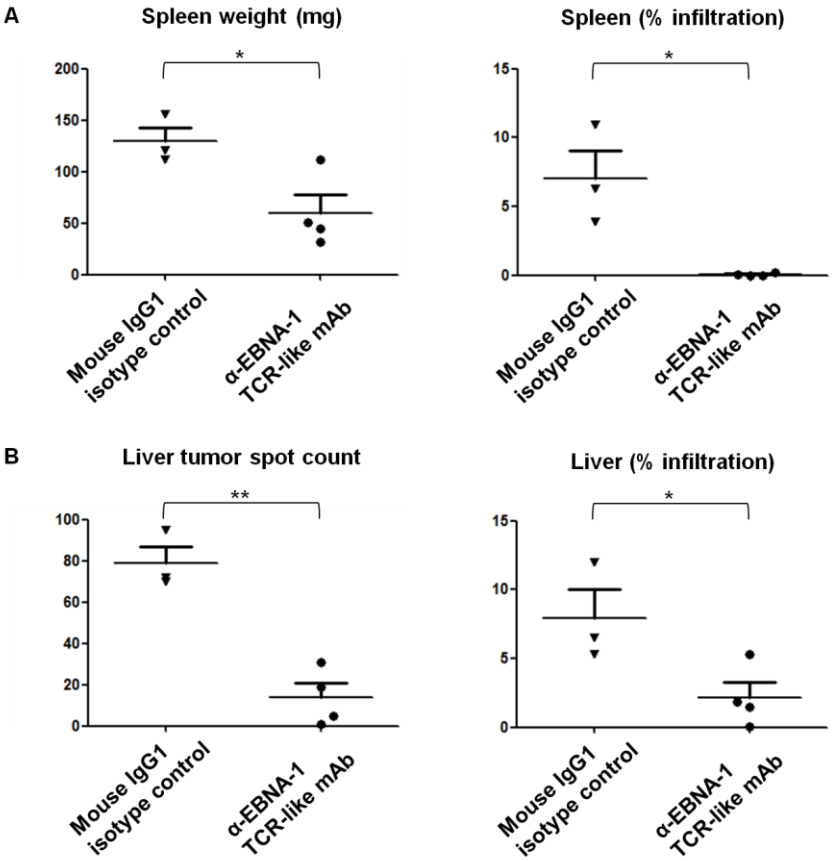

Appendix F: immunophenotype of BLCLs generated from the unsorted and CD19-sorted fractions of fetal spleen

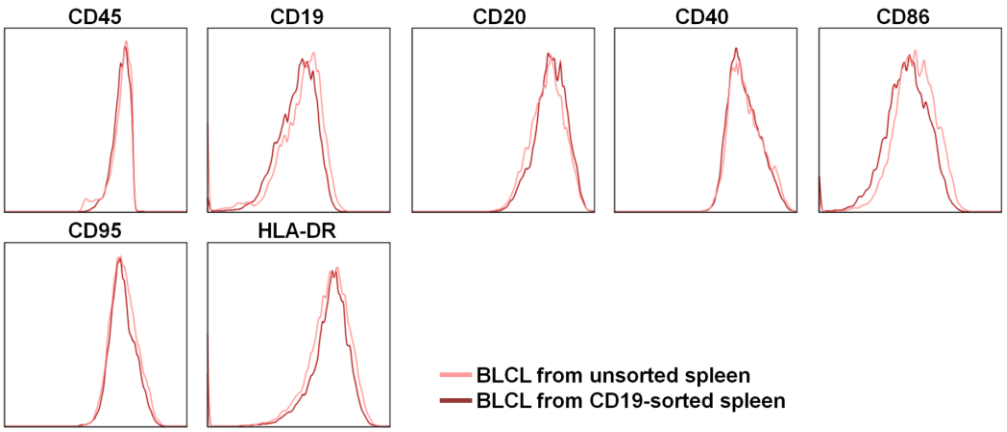

References

References

1. Cohen, J.I., *Epstein-Barr virus infection.* N Engl J Med, 2000. **343**(7): p. 481-92.
2. Lacoste, V., et al., *Genetic diversity and molecular evolution of human and non-human primate Gammaherpesvirinae.* Infect Genet Evol, 2010. **10**(1): p. 1-13.
3. Epstein, M.A., B.G. Achong, and Y.M. Barr, *Virus Particles in Cultured Lymphoblasts from Burkitt's Lymphoma.* Lancet, 1964. **1**(7335): p. 702-3.
4. Delecluse, H.J., et al., *Epstein Barr virus-associated tumours: an update for the attention of the working pathologist.* J Clin Pathol, 2007. **60**(12): p. 1358-64.
5. Fields, B.N., D.M. Knipe, and P.M. Howley, *Fields virology*. Vol. 3rd. 1996, Philadelphia: Lippincott-Raven Publishers.
6. Allday, M.J. and D.H. Crawford, *Role of epithelium in EBV persistence and pathogenesis of B-cell tumours.* Lancet, 1988. **1**(8590): p. 855-7.
7. Sumaya, C.V., *Primary Epstein-Barr virus infections in children.* Pediatrics, 1977. **59**(1): p. 16-21.
8. Adams, A. and T. Lindahl, *Epstein-Barr virus genomes with properties of circular DNA molecules in carrier cells.* Proceedings of the National Academy of Sciences of the United States of America, 1975. **72**(4): p. 1477-1481.
9. Babcock, G.J., et al., *EBV Persistence in Memory B Cells In Vivo.* Immunity, 1998. **9**(3): p. 395-404.
10. Khan, G., et al., *Is EBV persistence in vivo a model for B cell homeostasis?* (1074-7613 (Print)).
11. Falk, K., et al., *The role of repetitive DNA sequences in the size variation of Epstein-Barr virus (EBV) nuclear antigens, and the identification of different EBV isolates using RFLP and PCR analysis.* The Journal of general virology, 1995. **76 (Pt 4)**: p. 779-90.
12. Gutierrez Mi Fau - Raj, A., et al., *Sequence variations in EBNA-1 may dictate restriction of tissue distribution of Epstein-Barr virus in normal and tumour cells.* 1997(0022-1317 (Print)).
13. Dillner, J., et al., *Antibodies against a synthetic peptide identify the Epstein-Barr virus-determined nuclear antigen.* Proc Natl Acad Sci U S A, 1984. **81**(15): p. 4652-6.
14. Yates, J.L., N. Warren, and B. Sugden, *Stable replication of plasmids derived from Epstein-Barr virus in various mammalian cells.* Nature, 1985. **313**(6005): p. 812-5.
15. Lee Ma Fau - Diamond, M.E., J.L. Diamond Me Fau - Yates, and J.L. Yates, *Genetic evidence that EBNA-1 is needed for efficient, stable latent infection by Epstein-Barr virus.* 1999(0022-538X (Print)).

16. Lupton, S. and A.J. Levine, *Mapping genetic elements of Epstein-Barr virus that facilitate extrachromosomal persistence of Epstein-Barr virus-derived plasmids in human cells.* Molecular and cellular biology, 1985. **5**(10): p. 2533-42.
17. Blake, N., et al., *Human CD8+ T cell responses to EBV EBNA1: HLA class I presentation of the (Gly-Ala)-containing protein requires exogenous processing.* Immunity, 1997. **7**(6): p. 791-802.
18. Levitskaya, J., et al., *Inhibition of antigen processing by the internal repeat region of the Epstein-Barr virus nuclear antigen-1.* Nature, 1995. **375**(6533): p. 685-8.
19. Khanna, R., et al., *Isolation of cytotoxic T lymphocytes from healthy seropositive individuals specific for peptide epitopes from Epstein-Barr virus nuclear antigen 1: implications for viral persistence and tumor surveillance.* Virology, 1995. **214**(2): p. 633-7.
20. Chao, M., et al., *The V-val subtype Epstein-Barr virus nuclear antigen 1 promotes cell survival after serum withdrawal.* Oncol Rep, 2015. **33**(2): p. 958-66.
21. Wang, L., et al., *Epstein-Barr virus nuclear antigen 1 (EBNA1) protein induction of epithelial-mesenchymal transition in nasopharyngeal carcinoma cells.* Cancer, 2014. **120**(3): p. 363-72.
22. Gruhne, B., R. Sompallae, and M.G. Masucci, *Three Epstein-Barr virus latency proteins independently promote genomic instability by inducing DNA damage, inhibiting DNA repair and inactivating cell cycle checkpoints.* Oncogene, 2009. **28**(45): p. 3997-4008.
23. Gruhne, B., et al., *The Epstein-Barr virus nuclear antigen-1 promotes genomic instability via induction of reactive oxygen species.* Proc Natl Acad Sci U S A, 2009. **106**(7): p. 2313-8.
24. Wysokenski, D.A. and J.L. Yates, *Multiple EBNA1-binding sites are required to form an EBNA1-dependent enhancer and to activate a minimal replicative origin within oriP of Epstein-Barr virus.* Journal of virology, 1989. **63**(6): p. 2657-66.
25. Yates, J.L., S.M. Camiolo, and J.M. Bashaw, *The minimal replicator of Epstein-Barr virus oriP.* Journal of virology, 2000. **74**(10): p. 4512-22.
26. Reisman, D. and B. Sugden, *trans activation of an Epstein-Barr viral transcriptional enhancer by the Epstein-Barr viral nuclear antigen 1.* Molecular and cellular biology, 1986. **6**(11): p. 3838-46.
27. Sugden, B. and N. Warren, *A promoter of Epstein-Barr virus that can function during latent infection can be transactivated by EBNA-1, a viral protein required for viral DNA replication during latent infection.* Journal of virology, 1989. **63**(6): p. 2644-9.
28. Gahn, T.A. and B. Sugden, *An EBNA-1-dependent enhancer acts from a distance of 10 kilobase pairs to increase expression*

of the Epstein-Barr virus LMP gene. Journal of virology, 1995. **69**(4): p. 2633-6.
29. Wood, V.H., et al., *Epstein-Barr virus-encoded EBNA1 regulates cellular gene transcription and modulates the STAT1 and TGFbeta signaling pathways.* Oncogene, 2007. **26**(28): p. 4135-47.
30. Burnet, M., *Cancer; a biological approach. I. The processes of control.* 1957(0007-1447 (Print)).
31. Roth, G., T. Curiel, and J. Lacy, *Epstein-Barr viral nuclear antigen 1 antisense oligodeoxynucleotide inhibits proliferation of Epstein-Barr virus-immortalized B cells.* Blood, 1994. **84**(2): p. 582-7.
32. Sheu, L.F., et al., *Enhanced malignant progression of nasopharyngeal carcinoma cells mediated by the expression of Epstein-Barr nuclear antigen 1 in vivo.* The Journal of pathology, 1996. **180**(3): p. 243-8.
33. Kube, D., et al., *Expression of epstein-barr virus nuclear antigen 1 is associated with enhanced expression of CD25 in the Hodgkin cell line L428.* Journal of virology, 1999. **73**(2): p. 1630-6.
34. Rock, K.L., et al., *Inhibitors of the proteasome block the degradation of most cell proteins and the generation of peptides presented on MHC class I molecules.* Cell, 1994. **78**(5): p. 761-71.
35. Rock, K.L., I.A. York, and A.L. Goldberg, *Post-proteasomal antigen processing for major histocompatibility complex class I presentation.* Nat Immunol, 2004. **5**(7): p. 670-7.
36. Kloetzel, P.M. and F. Ossendorp, *Proteasome and peptidase function in MHC-class-I-mediated antigen presentation.* Curr Opin Immunol, 2004. **16**(1): p. 76-81.
37. Townsend, A. and J. Trowsdale, *The transporters associated with antigen presentation.* Semin Cell Biol, 1993. **4**(1): p. 53-61.
38. Gil-Torregrosa, B.C., A. Raul Castano, and M. Del Val, *Major histocompatibility complex class I viral antigen processing in the secretory pathway defined by the trans-Golgi network protease furin.* J Exp Med, 1998. **188**(6): p. 1105-16.
39. Howe, C., et al., *Calreticulin-dependent recycling in the early secretory pathway mediates optimal peptide loading of MHC class I molecules.* EMBO J, 2009. **28**(23): p. 3730-44.
40. Cresswell, P., *Antigen processing and presentation.* Immunol Rev, 2005. **207**: p. 5-7.
41. Shastri, N., S. Schwab, and T. Serwold, *Producing nature's gene-chips: the generation of peptides for display by MHC class I molecules.* Annu Rev Immunol, 2002. **20**: p. 463-93.
42. Khanna R Fau - Burrows, S.R., et al., *Localization of Epstein-Barr virus cytotoxic T cell epitopes using recombinant vaccinia: implications for vaccine development.* 1992(0022-1007 (Print)).
43. Trivedi, P., et al., *The epstein-Barr-virus-encoded membrane protein LMP but not the nuclear antigen EBNA-1 induces*

rejection of transfected murine mammary carcinoma cells. Int J Cancer, 1991. **48**(5): p. 794-800.
44. Khanna, R., et al., *Class I processing-defective Burkitt's lymphoma cells are recognized efficiently by CD4+ EBV-specific CTLs.* Journal of immunology, 1997. **158**(8): p. 3619-25.
45. Munz, C., et al., *Human CD4(+) T lymphocytes consistently respond to the latent Epstein-Barr virus nuclear antigen EBNA1.* J Exp Med, 2000. **191**(10): p. 1649-60.
46. Paludan, C., et al., *Epstein-Barr nuclear antigen 1-specific CD4(+) Th1 cells kill Burkitt's lymphoma cells.* Journal of immunology, 2002. **169**(3): p. 1593-603.
47. Nikiforow, S., et al., *Cytolytic CD4(+)-T-cell clones reactive to EBNA1 inhibit Epstein-Barr virus-induced B-cell proliferation.* Journal of virology, 2003. **77**(22): p. 12088-104.
48. Heller, K.N., et al., *Distinct memory CD4+ T-cell subsets mediate immune recognition of Epstein Barr virus nuclear antigen 1 in healthy virus carriers.* Blood, 2007. **109**(3): p. 1138-46.
49. Khanna, R., et al., *Identification of cytotoxic T cell epitopes within Epstein-Barr virus (EBV) oncogene latent membrane protein 1 (LMP1): evidence for HLA A2 supertype-restricted immune recognition of EBV-infected cells by LMP1-specific cytotoxic T lymphocytes.* European journal of immunology, 1998. **28**(2): p. 451-8.
50. Stuber, G., et al., *HLA-A0201 and HLA-B7 binding peptides in the EBV-encoded EBNA-1, EBNA-2 and BZLF-1 proteins detected in the MHC class I stabilization assay. Low proportion of binding motifs for several HLA class I alleles in EBNA-1.* International immunology, 1995. **7**(4): p. 653-63.
51. Levitskaya, J., et al., *Inhibition of ubiquitin/proteasome-dependent protein degradation by the Gly-Ala repeat domain of the Epstein-Barr virus nuclear antigen 1.* Proceedings of the National Academy of Sciences of the United States of America, 1997. **94**(23): p. 12616-21.
52. Heessen, S., et al., *Functional p53 chimeras containing the Epstein-Barr virus Gly-Ala repeat are protected from Mdm2- and HPV-E6-induced proteolysis.* Proc Natl Acad Sci U S A, 2002. **99**(3): p. 1532-7.
53. Dantuma, N.P., et al., *Inhibition of proteasomal degradation by the Gly-Ala repeat of Epstein-Barr virus is influenced by the length of the repeat and the strength of the degradation signal.* Proceedings of the National Academy of Sciences of the United States of America, 2000. **97**(15): p. 8381-8385.
54. Sharipo, A., et al., *A minimal glycine-alanine repeat prevents the interaction of ubiquitinated I kappaB alpha with the proteasome: a new mechanism for selective inhibition of proteolysis.* Nature medicine, 1998. **4**(8): p. 939-44.

55. Zhang, M. and P. Coffino, *Repeat sequence of Epstein-Barr virus-encoded nuclear antigen 1 protein interrupts proteasome substrate processing.* J Biol Chem, 2004. **279**(10): p. 8635-41.
56. Tellam, J., et al., *Endogenous presentation of CD8+ T cell epitopes from Epstein-Barr virus-encoded nuclear antigen 1.* The Journal of experimental medicine, 2004. **199**(10): p. 1421-31.
57. Voo, K.S., et al., *Evidence for the presentation of major histocompatibility complex class I-restricted Epstein-Barr virus nuclear antigen 1 peptides to CD8+ T lymphocytes.* The Journal of experimental medicine, 2004. **199**(4): p. 459-70.
58. Lee, S.P., et al., *CD8 T cell recognition of endogenously expressed epstein-barr virus nuclear antigen 1.* The Journal of experimental medicine, 2004. **199**(10): p. 1409-20.
59. Yoshioka, M., M.M. Crum, and J.T. Sample, *Autorepression of Epstein-Barr virus nuclear antigen 1 expression by inhibition of pre-mRNA processing.* Journal of virology, 2008. **82**(4): p. 1679-87.
60. Apcher, S., et al., *mRNA translation regulation by the Gly-Ala repeat of Epstein-Barr virus nuclear antigen 1.* Journal of virology, 2009. **83**(3): p. 1289-98.
61. Apcher, S., et al., *Epstein Barr virus-encoded EBNA1 interference with MHC class I antigen presentation reveals a close correlation between mRNA translation initiation and antigen presentation.* PLoS pathogens, 2010. **6**(10): p. e1001151.
62. Murat, P., et al., *G-quadruplexes regulate Epstein-Barr virus-encoded nuclear antigen 1 mRNA translation.* Nat Chem Biol, 2014.
63. Tellam, J.T., et al., *mRNA Structural constraints on EBNA1 synthesis impact on in vivo antigen presentation and early priming of CD8+ T cells.* PLoS Pathog, 2014. **10**(10): p. e1004423.
64. Dharnidharka, V.R., et al., *Post-transplant lymphoproliferative disorder in the United States: young Caucasian males are at highest risk.* Am J Transplant, 2002. **2**(10): p. 993-8.
65. Taylor, A.L., R. Marcus, and J.A. Bradley, *Post-transplant lymphoproliferative disorders (PTLD) after solid organ transplantation.* Crit Rev Oncol Hematol, 2005. **56**(1): p. 155-67.
66. Leblond, V., et al., *Lymphoproliferative disorders after organ transplantation: a report of 24 cases observed in a single center.* J Clin Oncol, 1995. **13**(4): p. 961-8.
67. Libertiny, G., et al., *Rising incidence of post-transplant lymphoproliferative disease in kidney transplant recipients.* Br J Surg, 2001. **88**(10): p. 1330-4.
68. Gao, S.Z., et al., *Post-transplantation lymphoproliferative disease in heart and heart-lung transplant recipients: 30-year experience at Stanford University.* J Heart Lung Transplant, 2003. **22**(5): p. 505-14.

69. Finn, L., et al., *Epstein-Barr virus infections in children after transplantation of the small intestine.* Am J Surg Pathol, 1998. **22**(3): p. 299-309.
70. Gottschalk, S., H.E. Rooney Cm Fau - Heslop, and H.E. Heslop, *Post-transplant lymphoproliferative disorders.* (0066-4219 (Print)).
71. Walker, R.C., et al., *Pretransplantation seronegative Epstein-Barr virus status is the primary risk factor for posttransplantation lymphoproliferative disorder in adult heart, lung, and other solid organ transplantations.* J Heart Lung Transplant, 1995. **14**(2): p. 214-21.
72. Hanto, D.W., et al., *Clinical spectrum of lymphoproliferative disorders in renal transplant recipients and evidence for the role of Epstein-Barr virus.* Cancer Res, 1981. **41**(11 Pt 1): p. 4253-61.
73. Young, L., et al., *Expression of Epstein-Barr virus transformation-associated genes in tissues of patients with EBV lymphoproliferative disease.* N Engl J Med, 1989. **321**(16): p. 1080-5.
74. Purtilo, D.T., *Epstein-Barr-virus-induced oncogenesis in immune-deficient individuals.* Lancet, 1980. **1**(8163): p. 300-3.
75. Swinnen, L.J., et al., *Increased incidence of lymphoproliferative disorder after immunosuppression with the monoclonal antibody OKT3 in cardiac-transplant recipients.* N Engl J Med, 1990. **323**(25): p. 1723-8.
76. Newell, K.A., et al., *Posttransplant lymphoproliferative disease in pediatric liver transplantation. Interplay between primary Epstein-Barr virus infection and immunosuppression.* Transplantation, 1996. **62**(3): p. 370-5.
77. Fields, B.N., et al., *Fields' virology*. 2007, Wolters kluwer/Lippincott Williams & Wilkins,: Philadelphia. p. 2 v. ill.
78. Babcock, G.J., et al., *Epstein-barr virus-infected resting memory B cells, not proliferating lymphoblasts, accumulate in the peripheral blood of immunosuppressed patients.* J Exp Med, 1999. **190**(4): p. 567-76.
79. Campo, E., et al., *The 2008 WHO classification of lymphoid neoplasms and beyond: evolving concepts and practical applications.* Blood, 2011. **117**(19): p. 5019-32.
80. Moss, D.J., A.B. Rickinson, and J.H. Pope, *Long-term T-cell-mediated immunity to Epstein-Barr virus in man. I. Complete regression of virus-induced transformation in cultures of seropositive donor leukocytes.* Int J Cancer, 1978. **22**(6): p. 662-8.
81. Misko, I.S., D.J. Moss, and J.H. Pope, *HLA antigen-related restriction of T lymphocyte cytotoxicity to Epstein-Barr virus.* Proc Natl Acad Sci U S A, 1980. **77**(7): p. 4247-50.
82. Thorley-Lawson, D.A., *The transformation of adult but not newborn human lymphocytes by Epstein Barr virus and phytohemagglutinin is inhibited by interferon: the early*

suppression by T cells of Epstein Barr infection is mediated by interferon. The Journal of Immunology, 1981. **126**(3): p. 829-33.
83. Callan, M.F., et al., *Direct visualization of antigen-specific CD8+ T cells during the primary immune response to Epstein-Barr virus In vivo.* J Exp Med, 1998. **187**(9): p. 1395-402.
84. Hislop, A.D., et al., *Epitope-specific evolution of human CD8(+) T cell responses from primary to persistent phases of Epstein-Barr virus infection.* J Exp Med, 2002. **195**(7): p. 893-905.
85. Odumade, O.A., et al., *Primary Epstein-Barr virus infection does not erode preexisting CD8(+) T cell memory in humans.* 2012(1540-9538 (Electronic)).
86. Brunstein, C.G., et al., *Marked increased risk of Epstein-Barr virus-related complications with the addition of antithymocyte globulin to a nonmyeloablative conditioning prior to unrelated umbilical cord blood transplantation.* Blood, 2006. **108**(8): p. 2874-80.
87. Kuzushima, K., et al., *Longitudinal dynamics of Epstein-Barr virus-specific cytotoxic T lymphocytes during posttransplant lymphoproliferative disorder.* J Infect Dis, 2000. **182**(3): p. 937-40.
88. Khatri, V.P., et al., *Endogenous CD8+ T cell expansion during regression of monoclonal EBV-associated posttransplant lymphoproliferative disorder.* J Immunol, 1999. **163**(1): p. 500-6.
89. Thorley-Lawson, D.A. and A. Gross, *Persistence of the Epstein-Barr virus and the origins of associated lymphomas.* N Engl J Med, 2004. **350**(13): p. 1328-37.
90. Dunphy, C.H. and P.T. Cagle, *Molecular Pathology of Hematolymphoid Diseases*. 2010: Springer US.
91. Preiksaitis, J.K., et al., *Quantitative oropharyngeal Epstein-Barr virus shedding in renal and cardiac transplant recipients: relationship to immunosuppressive therapy, serologic responses, and the risk of posttransplant lymphoproliferative disorder.* J Infect Dis, 1992. **166**(5): p. 986-94.
92. Riddler, S.A., M.C. Breinig, and J.L. McKnight, *Increased levels of circulating Epstein-Barr virus (EBV)-infected lymphocytes and decreased EBV nuclear antigen antibody responses are associated with the development of posttransplant lymphoproliferative disease in solid-organ transplant recipients.* Blood, 1994. **84**(3): p. 972-84.
93. Starzl, T.E., et al., *Reversibility of lymphomas and lymphoproliferative lesions developing under cyclosporin-steroid therapy.* Lancet, 1984. **1**(8377): p. 583-7.
94. Danese, M.D., et al., *Estimating the Population Benefits and Costs of Rituximab Therapy in the United States from 1998 to 2013 Using Real-World Data.* Med Care, 2016. **54**(4): p. 343-9.
95. Barth, M.J., et al., *Immunotherapeutic approaches for the treatment of childhood, adolescent and young adult non-Hodgkin lymphoma.* (1365-2141 (Electronic)).

96. Bryan, J. and G. Borthakur, *Role of rituximab in first-line treatment of chronic lymphocytic leukemia.* Therapeutics and Clinical Risk Management, 2011. **7**: p. 1-11.
97. van Vollenhoven, R.F., et al., *Longterm Safety of Rituximab: Final Report of the Rheumatoid Arthritis Global Clinical Trial Program over 11 Years.* (0315-162X (Print)).
98. Beckwith, H. and L. Lightstone, *Rituximab in systemic lupus erythematosus and lupus nephritis.* (1660-2110 (Electronic)).
99. Thorley-Lawson, D.A. and A. Gross, *Persistence of the Epstein-Barr virus and the origins of associated lymphomas.* The New England journal of medicine, 2004. **350**(13): p. 1328-37.
100. Kelesidis, T., et al., *Does rituximab increase the incidence of infectious complications? A narrative review.* Int J Infect Dis, 2011. **15**(1): p. e2-16.
101. Aksoy, S., et al., *Infectious complications of rituximab in patients with lymphoma during maintenance therapy: a systematic review and meta-analysis.* Leuk Lymphoma, 2009. **50**(3): p. 357-65.
102. Duman, B.B., et al., *Loss of CD20 antigen expression after rituximab therapy of CD20 positive B cell lymphoma (diffuse large B cell extranodal marginal zone lymphoma combination): a case report and review of the literature.* Med Oncol, 2012. **29**(2): p. 1223-6.
103. Muramatsu, H., et al., *CD20-negative Epstein-Barr virus-associated post-transplant lymphoproliferative disease refractory to rituximab in a patient with severe aplastic anemia.* Int J Hematol, 2011. **93**(6): p. 779-81.
104. Elstrom, R.L., et al., *Treatment of PTLD with rituximab or chemotherapy.* Am J Transplant, 2006. **6**(3): p. 569-76.
105. Maldonado, N.I., et al., *Successful treatment of a patient with Epstein-Barr virus-positive B-cell lymphoproliferative disorder resembling post-transplant lymphoproliferative disorder using single-agent rituximab.* J Clin Oncol, 2011. **29**(22): p. e658-60.
106. Said-Conti, V., et al., *Successful treatment of central nervous system PTLD with rituximab and cranial radiotherapy.* Pediatr Nephrol, 2013. **28**(10): p. 2053-6.
107. Blaes, A.H., et al., *Rituximab therapy is effective for posttransplant lymphoproliferative disorders after solid organ transplantation: results of a phase II trial.* Cancer, 2005. **104**(8): p. 1661-7.
108. Berney, T., et al., *Successful treatment of posttransplant lymphoproliferative disease with prolonged rituximab treatment in intestinal transplant recipients.* (0041-1337 (Print)).
109. Bonney, D.K., et al., *Sustained response to intrathecal rituximab in EBV associated Post-transplant lymphoproliferative disease confined to the central nervous system following haematopoietic stem cell transplant.* (1545-5017 (Electronic)).
110. Choquet, S., et al., *Efficacy and safety of rituximab in B-cell post-transplantation lymphoproliferative disorders: results of a*

prospective multicenter phase 2 study. Blood, 2006. **107**(8): p. 3053-7.
111. Haque, T., et al., *Reconstitution of EBV-specific T cell immunity in solid organ transplant recipients.* J Immunol, 1998. **160**(12): p. 6204-9.
112. Rooney, C.M., et al., *Infusion of cytotoxic T cells for the prevention and treatment of Epstein-Barr virus-induced lymphoma in allogeneic transplant recipients.* Blood, 1998. **92**(5): p. 1549-55.
113. Smith, C.A., et al., *Production of genetically modified Epstein-Barr virus-specific cytotoxic T cells for adoptive transfer to patients at high risk of EBV-associated lymphoproliferative disease.* J Hematother, 1995. **4**(2): p. 73-9.
114. Rooney, C.M., et al., *Adoptive immunotherapy of EBV-associated malignancies with EBV-specific cytotoxic T-cell lines.* Current topics in microbiology and immunology, 2001. **258**: p. 221-9.
115. Craddock, J. and H.E. Heslop, *Adoptive cellular therapy with T cells specific for EBV-derived tumor antigens.* Update Cancer Ther, 2008. **3**(1): p. 33-41.
116. Heslop, H.E., et al., *Long-term outcome of EBV-specific T-cell infusions to prevent or treat EBV-related lymphoproliferative disease in transplant recipients.* Blood, 2010. **115**(5): p. 925-35.
117. Uhlin, M., et al., *A novel haplo-identical adoptive CTL therapy as a treatment for EBV-associated lymphoma after stem cell transplantation.* Cancer Immunol Immunother, 2010. **59**(3): p. 473-7.
118. Comoli, P., et al., *T cell therapy of Epstein-Barr virus and adenovirus infections after hemopoietic stem cell transplant.* Blood Cells Mol Dis, 2008. **40**(1): p. 68-70.
119. Jones, K., et al., *Expansion of EBNA1-specific effector T cells in posttransplantation lymphoproliferative disorders.* Blood, 2010. **116**(13): p. 2245-52.
120. Doubrovina, E., et al., *Adoptive immunotherapy with unselected or EBV-specific T cells for biopsy-proven EBV+ lymphomas after allogeneic hematopoietic cell transplantation.* Blood, 2012. **119**(11): p. 2644-56.
121. Bollard, C.M., *Improving T-cell therapy for epstein-barr virus lymphoproliferative disorders.* J Clin Oncol, 2013. **31**(1): p. 5-7.
122. Icheva, V., et al., *Adoptive Transfer of Epstein-Barr Virus (EBV) Nuclear Antigen 1-Specific T Cells As Treatment for EBV Reactivation and Lymphoproliferative Disorders After Allogeneic Stem-Cell Transplantation.* Journal of clinical oncology : official journal of the American Society of Clinical Oncology, 2013. **31**(1): p. 39-48.
123. Dao, T., et al., *Targeting the intracellular WT1 oncogene product with a therapeutic human antibody.* Sci Transl Med, 2013. **5**(176): p. 176ra33.

124. Jain, R., et al., *Antitumor activity of a monoclonal antibody targeting major histocompatibility complex class I-Her2 peptide complexes.* J Natl Cancer Inst, 2013. **105**(3): p. 202-18.
125. Sergeeva, A., et al., *An anti-PR1/HLA-A2 T-cell receptor-like antibody mediates complement-dependent cytotoxicity against acute myeloid leukemia progenitor cells.* Blood, 2011. **117**(16): p. 4262-72.
126. Sastry, K.S., et al., *Targeting hepatitis B virus-infected cells with a T-cell receptor-like antibody.* J Virol, 2011. **85**(5): p. 1935-42.
127. Biddison, W.E., et al., *Tax and M1 peptide/HLA-A2-specific Fabs and T cell receptors recognize nonidentical structural features on peptide/HLA-A2 complexes.* J Immunol, 2003. **171**(6): p. 3064-74.
128. Makler, O., et al., *Direct visualization of the dynamics of antigen presentation in human cells infected with cytomegalovirus revealed by antibodies mimicking TCR specificity.* Eur J Immunol, 2010. **40**(6): p. 1552-65.
129. Sim, A.C., et al., *Defining the expression hierarchy of latent T-cell epitopes in Epstein-Barr virus infection with TCR-like antibodies.* Sci Rep, 2013. **3**: p. 3232.
130. Bernardeau, K., et al., *Assessment of CD8 involvement in T cell clone avidity by direct measurement of HLA-A2/Mage3 complex density using a high-affinity TCR like monoclonal antibody.* Eur J Immunol, 2005. **35**(10): p. 2864-75.
131. Denkberg, G., et al., *Direct visualization of distinct T cell epitopes derived from a melanoma tumor-associated antigen by using human recombinant antibodies with MHC- restricted T cell receptor-like specificity.* Proc Natl Acad Sci U S A, 2002. **99**(14): p. 9421-6.
132. Dahan, R. and Y. Reiter, *T-cell-receptor-like antibodies - generation, function and applications.* Expert reviews in molecular medicine, 2012. **14**: p. e6.
133. Verma, B., et al., *TCR mimic monoclonal antibody targets a specific peptide/HLA class I complex and significantly impedes tumor growth in vivo using breast cancer models.* J Immunol, 2010. **184**(4): p. 2156-65.
134. Wittman, V.P., et al., *Antibody targeting to a class I MHC-peptide epitope promotes tumor cell death.* J Immunol, 2006. **177**(6): p. 4187-95.
135. Verma, B., et al., *TCR mimic monoclonal antibodies induce apoptosis of tumor cells via immune effector-independent mechanisms.* J Immunol, 2011. **186**(5): p. 3265-76.
136. Cohen, M. and Y. Reiter, *T-Cell Receptor-Like Antibodies: Targeting the Intracellular Proteome Therapeutic Potential and Clinical Applications.* Antibodies, 2013. **2**(3): p. 517.
137. Chang, A.Y., et al., *Opportunities and challenges for TCR mimic antibodies in cancer therapy.* Expert Opin Biol Ther, 2016: p. 1-9.
138. Dubrovsky, L., et al., *T cell receptor mimic antibodies for cancer therapy.* Oncoimmunology, 2016. **5**(1): p. e1049803.

139. Mosier, D.E., et al., *Transfer of a functional human immune system to mice with severe combined immunodeficiency.* Nature, 1988. **335**(6187): p. 256-9.
140. Shultz, L.D., et al., *Human lymphoid and myeloid cell development in NOD/LtSz-scid IL2R gamma null mice engrafted with mobilized human hemopoietic stem cells.* J Immunol, 2005. **174**(10): p. 6477-89.
141. Eastwood, D., et al., *Monoclonal antibody TGN1412 trial failure explained by species differences in CD28 expression on CD4+ effector memory T-cells.* Br J Pharmacol, 2010. **161**(3): p. 512-26.
142. Suntharalingam, G., et al., *Cytokine storm in a phase 1 trial of the anti-CD28 monoclonal antibody TGN1412.* N Engl J Med, 2006. **355**(10): p. 1018-28.
143. Attarwala, H., *TGN1412: From Discovery to Disaster.* J Young Pharm, 2010. **2**(3): p. 332-6.
144. Weissmuller, S., et al., *TGN1412 Induces Lymphopenia and Human Cytokine Release in a Humanized Mouse Model.* PLoS One, 2016. **11**(3): p. e0149093.
145. Cannon, M.J., et al., *Epstein-Barr virus induces aggressive lymphoproliferative disorders of human B cell origin in SCID/hu chimeric mice.* J Clin Invest, 1990. **85**(4): p. 1333-7.
146. Tosato, G., et al., *Abnormally elevated frequency of Epstein-Barr virus-infected B cells in the blood of patients with rheumatoid arthritis.* J Clin Invest, 1984. **73**(6): p. 1789-95.
147. Yang, J., et al., *Characterization of Epstein-Barr virus-infected B cells in patients with posttransplantation lymphoproliferative disease: disappearance after rituximab therapy does not predict clinical response.* Blood, 2000. **96**(13): p. 4055-63.
148. Bosma Gc Fau - Custer, R.P., M.J. Custer Rp Fau - Bosma, and M.J. Bosma, *A severe combined immunodeficiency mutation in the mouse.* 1983(0028-0836 (Print)).
149. Rowe, M., et al., *Epstein-Barr virus (EBV)-associated lymphoproliferative disease in the SCID mouse model: implications for the pathogenesis of EBV-positive lymphomas in man.* J Exp Med, 1991. **173**(1): p. 147-58.
150. Mosier, D.E., et al., *Studies of HIV infection and the development of Epstein-Barr virus-related B cell lymphomas following transfer of human lymphocytes to mice with severe combined immunodeficiency.* Curr Top Microbiol Immunol, 1989. **152**: p. 195-9.
151. Murphy, W.J., et al., *Human-mouse lymphoid chimeras: host-vs.-graft and graft-vs.-host reactions.* Eur J Immunol, 1992. **22**(6): p. 1421-7.
152. Johannessen, I., et al., *Epstein-Barr virus, B cell lymphoproliferative disease, and SCID mice: modeling T cell immunotherapy in vivo.* J Med Virol, 2011. **83**(9): p. 1585-96.
153. Linnerbauer, S., et al., *Virus and autoantigen-specific CD4+ T cells are key effectors in a SCID mouse model of EBV-*

associated post-transplant lymphoproliferative disorders. PLoS Pathog, 2014. **10**(5): p. e1004068.
154. Lacerda, J.F., et al., *Human Epstein-Barr virus (EBV)-specific cytotoxic T lymphocytes home preferentially to and induce selective regressions of autologous EBV-induced B cell lymphoproliferations in xenografted C.B-17 scid/scid mice.* J Exp Med, 1996. **183**(3): p. 1215-28.
155. Ricciardelli, I., et al., *Towards gene therapy for EBV-associated posttransplant lymphoma with genetically modified EBV-specific cytotoxic T cells.* Blood, 2014. **124**(16): p. 2514-22.
156. Merlo, A., et al., *Virus-specific cytotoxic CD4+ T cells for the treatment of EBV-related tumors.* J Immunol, 2010. **184**(10): p. 5895-902.
157. McCune, J.M., et al., *The SCID-hu mouse: murine model for the analysis of human hematolymphoid differentiation and function.* Science, 1988. **241**(4873): p. 1632-9.
158. Vormoor, J., et al., *Immature human cord blood progenitors engraft and proliferate to high levels in severe combined immunodeficient mice.* Blood, 1994. **83**(9): p. 2489-97.
159. Hesselton, R.M., et al., *High levels of human peripheral blood mononuclear cell engraftment and enhanced susceptibility to human immunodeficiency virus type 1 infection in NOD/LtSz-scid/scid mice.* J Infect Dis, 1995. **172**(4): p. 974-82.
160. Shultz, L.D., et al., *Multiple defects in innate and adaptive immunologic function in NOD/LtSz-scid mice.* J Immunol, 1995. **154**(1): p. 180-91.
161. Ito, M., et al., *NOD/SCID/gamma(c)(null) mouse: an excellent recipient mouse model for engraftment of human cells.* Blood, 2002. **100**(9): p. 3175-82.
162. Cao, X., et al., *Defective lymphoid development in mice lacking expression of the common cytokine receptor gamma chain.* Immunity, 1995. **2**(3): p. 223-38.
163. Yahata, T., et al., *Functional human T lymphocyte development from cord blood CD34+ cells in nonobese diabetic/Shi-scid, IL-2 receptor gamma null mice.* J Immunol, 2002. **169**(1): p. 204-9.
164. Traggiai, E., et al., *Development of a human adaptive immune system in cord blood cell-transplanted mice.* Science, 2004. **304**(5667): p. 104-7.
165. Strowig, T., et al., *Transgenic expression of human signal regulatory protein alpha in Rag2-/-gamma(c)-/- mice improves engraftment of human hematopoietic cells in humanized mice.* Proc Natl Acad Sci U S A, 2011. **108**(32): p. 13218-23.
166. Libby, S.J., et al., *Humanized nonobese diabetic-scid IL2rγ(null) mice are susceptible to lethal Salmonella Typhi infection.* Proceedings of the National Academy of Sciences of the United States of America, 2010. **107**(35): p. 15589-15594.
167. Smith, M.S., et al., *Granulocyte-colony stimulating factor reactivates human cytomegalovirus in a latently infected*

humanized mouse model. Cell Host Microbe, 2010. **8**(3): p. 284-91.
168. Mota, J. and R. Rico-Hesse, *Dengue virus tropism in humanized mice recapitulates human dengue fever.* PLoS One, 2011. **6**(6): p. e20762.
169. Baenziger, S., et al., *Disseminated and sustained HIV infection in CD34+ cord blood cell-transplanted Rag2-/-gamma c-/- mice.* Proc Natl Acad Sci U S A, 2006. **103**(43): p. 15951-6.
170. Boss, I.W., et al., *A Kaposi's sarcoma-associated herpesvirus-encoded ortholog of microRNA miR-155 induces human splenic B-cell expansion in NOD/LtSz-scid IL2Rgammanull mice.* J Virol, 2011. **85**(19): p. 9877-86.
171. Dandri, M., et al., *Repopulation of mouse liver with human hepatocytes and in vivo infection with hepatitis B virus.* Hepatology, 2001. **33**(4): p. 981-8.
172. Mercer, D.F., et al., *Hepatitis C virus replication in mice with chimeric human livers.* Nat Med, 2001. **7**(8): p. 927-33.
173. Yajima, M., et al., *A new humanized mouse model of Epstein-Barr virus infection that reproduces persistent infection, lymphoproliferative disorder, and cell-mediated and humoral immune responses.* The Journal of infectious diseases, 2008. **198**(5): p. 673-82.
174. Strowig, T., et al., *Priming of protective T cell responses against virus-induced tumors in mice with human immune system components.* The Journal of experimental medicine, 2009. **206**(6): p. 1423-34.
175. Sato, K., et al., *A novel animal model of Epstein-Barr virus-associated hemophagocytic lymphohistiocytosis in humanized mice.* Blood, 2011. **117**(21): p. 5663-73.
176. Lee, E.K., et al., *Effects of lymphocyte profile on development of EBV-induced lymphoma subtypes in humanized mice.* Proc Natl Acad Sci U S A, 2015.
177. Ma, S.D., et al., *A new model of Epstein-Barr virus infection reveals an important role for early lytic viral protein expression in the development of lymphomas.* Journal of virology, 2011. **85**(1): p. 165-77.
178. White, R.E., et al., *EBNA3B-deficient EBV promotes B cell lymphomagenesis in humanized mice and is found in human tumors.* J Clin Invest, 2012. **122**(4): p. 1487-502.
179. Kuwana, Y., et al., *Epstein-Barr virus induces erosive arthritis in humanized mice.* PLoS One, 2011. **6**(10): p. e26630.
180. Antsiferova, O., et al., *Adoptive Transfer of EBV Specific CD8+ T Cell Clones Can Transiently Control EBV Infection in Humanized Mice.* PLoS Pathog, 2014. **10**(8): p. e1004333.
181. Matsuda, G., et al., *Cellular immunotherapy with ex vivo expanded cord blood T cells in a humanized mouse model of EBV-associated lymphoproliferative disease.* Immunotherapy, 2015. **7**(4): p. 335-41.

182. Heuts, F., et al., *T Cells Modulate Epstein-Barr Virus Latency Phenotypes During Infection of Humanized Mice.* J Virol, 2014.
183. Ma, S.D., et al., *PD-1/CTLA-4 Blockade Inhibits Epstein-Barr Virus-Induced Lymphoma Growth in a Cord Blood Humanized-Mouse Model.* PLoS Pathog, 2016. **12**(5): p. e1005642.
184. Chen, L. and X. Han, *Anti-PD-1/PD-L1 therapy of human cancer: past, present, and future.* J Clin Invest, 2015. **125**(9): p. 3384-91.
185. Watanabe, Y., et al., *The analysis of the functions of human B and T cells in humanized NOD/shi-scid/gammac(null) (NOG) mice (hu-HSC NOG mice).* Int Immunol, 2009. **21**(7): p. 843-58.
186. Namikawa, R., et al., *Infection of the SCID-hu mouse by HIV-1.* Science, 1988. **242**(4886): p. 1684-6.
187. Denton, P.W., et al., *Antiretroviral pre-exposure prophylaxis prevents vaginal transmission of HIV-1 in humanized BLT mice.* PLoS Med, 2008. **5**(1): p. e16.
188. Sun, Z., et al., *Intrarectal transmission, systemic infection, and CD4+ T cell depletion in humanized mice infected with HIV-1.* J Exp Med, 2007. **204**(4): p. 705-14.
189. Melkus, M.W., et al., *Humanized mice mount specific adaptive and innate immune responses to EBV and TSST-1.* Nat Med, 2006. **12**(11): p. 1316-22.
190. Tanaka, S., et al., *Development of mature and functional human myeloid subsets in hematopoietic stem cell-engrafted NOD/SCID/IL2rgammaKO mice.* J Immunol, 2012. **188**(12): p. 6145-55.
191. Huntington, N.D., et al., *IL-15 trans-presentation promotes human NK cell development and differentiation in vivo.* J Exp Med, 2009. **206**(1): p. 25-34.
192. Gille, C., et al., *Monocytes derived from humanized neonatal NOD/SCID/IL2Rgamma(null) mice are phenotypically immature and exhibit functional impairments.* Hum Immunol, 2012. **73**(4): p. 346-54.
193. Nicolini, F.E., et al., *NOD/SCID mice engineered to express human IL-3, GM-CSF and Steel factor constitutively mobilize engrafted human progenitors and compromise human stem cell regeneration.* Leukemia, 2004. **18**(2): p. 341-7.
194. Rathinam, C., et al., *Efficient differentiation and function of human macrophages in humanized CSF-1 mice.* Blood, 2011. **118**(11): p. 3119-28.
195. Rongvaux, A., et al., *Human thrombopoietin knockin mice efficiently support human hematopoiesis in vivo.* Proc Natl Acad Sci U S A, 2011. **108**(6): p. 2378-83.
196. Lapidot, T., et al., *Cytokine stimulation of multilineage hematopoiesis from immature human cells engrafted in SCID mice.* Science, 1992. **255**(5048): p. 1137-41.
197. van Lent, A.U., et al., *IL-7 enhances thymic human T cell development in "human immune system" Rag2-/-IL-2Rgammac-/- mice without affecting peripheral T cell homeostasis.* J Immunol, 2009. **183**(12): p. 7645-55.

198. Chen, Q., M. Khoury, and J. Chen, *Expression of human cytokines dramatically improves reconstitution of specific human-blood lineage cells in humanized mice.* Proc Natl Acad Sci U S A, 2009. **106**(51): p. 21783-8.
199. O'Connell, R.M., et al., *Lentiviral vector delivery of human interleukin-7 (hIL-7) to human immune system (HIS) mice expands T lymphocyte populations.* PLoS One, 2010. **5**(8): p. e12009.
200. Rongvaux, A., et al., *Development and function of human innate immune cells in a humanized mouse model.* Nat Biotechnol, 2014. **32**(4): p. 364-72.
201. Suda, T. and D. Liu, *Hydrodynamic gene delivery: its principles and applications.* Mol Ther, 2007. **15**(12): p. 2063-9.
202. Li, Y., et al., *Induction of functional human macrophages from bone marrow promonocytes by M-CSF in humanized mice.* J Immunol, 2013. **191**(6): p. 3192-9.
203. Chen, Q., et al., *GM-CSF and IL-4 Stimulate Antibody Responses in Humanized Mice by Promoting T, B, and Dendritic Cell Maturation.* Journal of immunology, 2012.
204. Yin, Y., B. Manoury, and R. Fahraeus, *Self-inhibition of synthesis and antigen presentation by Epstein-Barr virus-encoded EBNA1.* Science, 2003. **301**(5638): p. 1371-4.
205. Misteli, T. and D.L. Spector, *Applications of the green fluorescent protein in cell biology and biotechnology.* Nat Biotechnol, 1997. **15**(10): p. 961-4.
206. Michaelson, D. and M. Philips, *The use of GFP to localize Rho GTPases in living cells.* Methods Enzymol, 2006. **406**: p. 296-315.
207. Szymczak, A.L., et al., *Correction of multi-gene deficiency in vivo using a single 'self-cleaving' 2A peptide-based retroviral vector.* Nat Biotechnol, 2004. **22**(5): p. 589-94.
208. Tang, W., et al., *Faithful expression of multiple proteins via 2A-peptide self-processing: a versatile and reliable method for manipulating brain circuits.* J Neurosci, 2009. **29**(27): p. 8621-9.
209. Sugawara, S., T. Abo, and K. Kumagai, *A simple method to eliminate the antigenicity of surface class I MHC molecules from the membrane of viable cells by acid treatment at pH 3.* J Immunol Methods, 1987. **100**(1-2): p. 83-90.
210. Khan, G., et al., *Is EBV persistence in vivo a model for B cell homeostasis?* Immunity, 1996. **5**(2): p. 173-9.
211. Rose, C., et al., *Detection of Epstein-Barr virus genomes in peripheral blood B cells from solid-organ transplant recipients by fluorescence in situ hybridization.* J Clin Microbiol, 2002. **40**(7): p. 2533-44.
212. Wagner, H.J., et al., *Characteristics of viral protein expression by Epstein-Barr virus-infected B cells in peripheral blood of patients with infectious mononucleosis.* Clin Diagn Lab Immunol, 1995. **2**(6): p. 696-9.

213. Wang, D., et al., *Epstein-Barr virus latent infection membrane protein alters the human B-lymphocyte phenotype: deletion of the amino terminus abolishes activity.* J Virol, 1988. **62**(11): p. 4173-84.
214. Le Clorennec, C., et al., *EBV latency III immortalization program sensitizes B cells to induction of CD95-mediated apoptosis via LMP1: role of NF-kappaB, STAT1, and p53.* (0006-4971 (Print)).
215. Ohshima, K., et al., *CD95 (Fas) ligand expression of Epstein-Barr virus (EBV)-infected lymphocytes: a possible mechanism of immune evasion in chronic active EBV infection.* (1320-5463 (Print)).
216. Durandy, A., et al., *Sensitivity of Epstein-Barr virus-induced B cell tumor to apoptosis mediated by anti-CD95/Apo-1/fas antibody.* Eur J Immunol, 1997. **27**(2): p. 538-43.
217. Rickinson, A.B., L.S. Young, and M. Rowe, *Influence of the Epstein-Barr virus nuclear antigen EBNA 2 on the growth phenotype of virus-transformed B cells.* J Virol, 1987. **61**(5): p. 1310-7.
218. Rowe, M., et al., *Three pathways of Epstein-Barr virus gene activation from EBNA1-positive latency in B lymphocytes.* J Virol, 1992. **66**(1): p. 122-31.
219. Chao, M.P., et al., *Anti-CD47 antibody synergizes with rituximab to promote phagocytosis and eradicate non-Hodgkin lymphoma.* Cell, 2010. **142**(5): p. 699-713.
220. Tseng, D., et al., *Anti-CD47 antibody-mediated phagocytosis of cancer by macrophages primes an effective antitumor T-cell response.* Proc Natl Acad Sci U S A, 2013. **110**(27): p. 11103-8.
221. Majeti, R., et al., *CD47 is an adverse prognostic factor and therapeutic antibody target on human acute myeloid leukemia stem cells.* 2009(1097-4172 (Electronic)).
222. Hu, Z., N. Van Rooijen, and Y.G. Yang, *Macrophages prevent human red blood cell reconstitution in immunodeficient mice.* Blood, 2011. **118**(22): p. 5938-46.
223. Hu, Z. and Y.G. Yang, *Full reconstitution of human platelets in humanized mice after macrophage depletion.* Blood, 2012. **120**(8): p. 1713-6.
224. Wintrobe, M.M. and J.P. Greer, *Wintrobe's clinical hematology*. 12th ed. 2009, Philadelphia: Wolters Kluwer/Lippincott Williams & Wilkins Health.
225. Paul, W.E., *Fundamental immunology*. 6th ed. 2008, Philadelphia: Lippincott Williams & Wilkins. xviii, 1603 p.
226. Uchida, J., et al., *Mouse CD20 expression and function.* Int Immunol, 2004. **16**(1): p. 119-29.
227. Wei, J., et al., *Ubiquitous Autofragmentation of Fluorescent Proteins Creates Abundant Defective Ribosomal Products (DRiPs) for Immunosurveillance.* J Biol Chem, 2015. **290**(26): p. 16431-9.
228. Long, H.M., et al., *CD4+ T-cell responses to Epstein-Barr virus (EBV) latent-cycle antigens and the recognition of EBV-*

transformed lymphoblastoid cell lines. Journal of virology, 2005. **79**(8): p. 4896-907.
229. Tellam, J., et al., *Influence of translation efficiency of homologous viral proteins on the endogenous presentation of CD8+ T cell epitopes.* The Journal of experimental medicine, 2007. **204**(3): p. 525-32.
230. Croft, N.P., et al., *Kinetics of antigen expression and epitope presentation during virus infection.* PLoS Pathog, 2013. **9**(1): p. e1003129.
231. Purcell, A.W., N.P. Croft, and D.C. Tscharke, *Immunology by numbers: quantitation of antigen presentation completes the quantitative milieu of systems immunology!* Curr Opin Immunol, 2016. **40**: p. 88-95.
232. Slamon, D.J., et al., *Use of chemotherapy plus a monoclonal antibody against HER2 for metastatic breast cancer that overexpresses HER2.* N Engl J Med, 2001. **344**(11): p. 783-92.
233. Abramowicz, D., A. Crusiaux, and M. Goldman, *Anaphylactic shock after retreatment with OKT3 monoclonal antibody.* N Engl J Med, 1992. **327**(10): p. 736.
234. Dillman, R.O., et al., *Toxicities and side effects associated with intravenous infusions of murine monoclonal antibodies.* J Biol Response Mod, 1986. **5**(1): p. 73-84.
235. van der Linden, E.F., M.J. van Kroonenburgh, and E.K. Pauwels, *Side-effects of monoclonal antibody infusions for the diagnosis and treatment of cancer.* Int J Biol Markers, 1988. **3**(3): p. 147-53.
236. Murray, J.L., et al., *Phase I trial of murine monoclonal antibody 14G2a administered by prolonged intravenous infusion in patients with neuroectodermal tumors.* J Clin Oncol, 1994. **12**(1): p. 184-93.
237. Rettenbacher, L. and G. Galvan, *[Anaphylactic shock after repeated injection of 99mTc-labeled CEA antibody].* Nuklearmedizin, 1994. **33**(3): p. 127-8.
238. Mountain, A. and J.R. Adair, *Engineering antibodies for therapy.* Biotechnol Genet Eng Rev, 1992. **10**: p. 1-142.
239. Shawler, D.L., et al., *Human immune response to multiple injections of murine monoclonal IgG.* J Immunol, 1985. **135**(2): p. 1530-5.
240. Hosono, M., et al., *Human/mouse chimeric antibodies show low reactivity with human anti-murine antibodies (HAMA).* Br J Cancer, 1992. **65**(2): p. 197-200.
241. Sakahara, H., et al., *In vitro complex formation and biodistribution of mouse antitumor monoclonal antibody in cancer patients.* J Nucl Med, 1989. **30**(8): p. 1311-7.
242. Dao, T., et al., *Therapeutic bispecific T-cell engager antibody targeting the intracellular oncoprotein WT1.* Nat Biotechnol, 2015. **33**(10): p. 1079-86.

243. Nagorsen, D. and P.A. Baeuerle, *Immunomodulatory therapy of cancer with T cell-engaging BiTE antibody blinatumomab.* Exp Cell Res, 2011. **317**(9): p. 1255-60.
244. Pallasch, C.P., et al., *Sensitizing protective tumor microenvironments to antibody-mediated therapy.* Cell, 2014. **156**(3): p. 590-602.